INSTITUTO SUPERIOR DE ENGENHARIA DO PORTO
MESTRADO EM ENGENHARIA MECÂNICA




Integration of piezoelectric elements in the injection moulding process for active metamaterial production

DAVID JOSÉ PEREIRA ALMEIDA
outubro de 2025

POLITÉCNICO
DO PORTO

ISEP INSTITUTO SUPERIOR DE ENGENHARIA DO PORTO

Integration of piezoelectric elements in the injection moulding process for active metamaterial production

David José Pereira Almeida

Dissertation to fulfil the requirements to obtain the Master degree in Mechanical Engineering, with a specialisation in Mechanical Constructions

Supervisor: Raul Duarte Salgueiral Gomes Campilho
Co-supervisor: Francisco José Gomes da Silva
Jury:
President:
Armando José Vilaça de Campos
Vowels:
Raul Duarte Salgueiral Gomes Campilho
Pedro Miguel Rebelo Resende

Porto, september 2025

Acknowledgments

I want to express my gratitude to my supervisors at my home institution, Dr. Raul Campilho and Dr. Francisco Silva, for their support and for sharing their vast experience in mechanical engineering that allowed me to grow as a professional. In addition, my appreciation for their insightful contributions to this thesis.

A special thanks and gratitude to my supervisors in the receiving institution (KU Leuven), Dr. Elke Deckers and Phd candidate Stefan Jassen. Regarding Dr. Elke Deckers, my appreciation and gratitude for depositing trust in me and accepting me as a student at KU Leuven, and for the sharing of knowledge. With respect to Stefan Janssen, a special thanks for guiding me and being always available to support me through this journey, with his expertise and friendship. Moreover, I want to acknowledge all the colleagues at LMSD- Diepenbeek Campus (Kristof, Yves, Tim, Jordy, Victor, Gert-Jan, Jarne, Alara, Mathijs, Maedeh, Femke, Tim and Koen) for kindly welcoming me and being always available for a brainstorm around my research topic. Dankuwel!

To Simon from the LMSD workshop, thanks for the ideas and work on the mould milling.

A special thanks to my friends and family for always supporting me through my Academic journey.

Abstract

The global population, subjected to continuous exposure to noise sources in the workplace, can lead to effects such as hearing loss, burnout symptoms, and overall health deterioration. In industrial contexts, vibrations, also a source of noise, not only affect human health but can also reduce equipment performance and shorten service life. Traditional solutions, such as applying insulating materials or adding mass to systems, are often insufficient to significantly reduce noise and vibration, particularly at frequencies below 1000 Hz. Moreover, these approaches may also compromise equipment efficiency due to added mass and negatively affect aesthetics. Acoustic metamaterials have emerged as a superior alternative, as they can create a stop-band effect, are lighter, and, when incorporating piezoelectric elements, can be actively tuned to target specific frequency ranges. Nevertheless, metamaterials are commonly manufactured through additive manufacturing processes, which restricts their use in large-scale applications. The present study addresses this limitation by developing an approach to over-mould piezoelectric elements using injection moulding to produce active metamaterials. Through numerical simulations, a piezoelectric element was selected with the optimal dimensions (36 x 20 x 0.22 mm^3) to achieve the best possible vibrational performance when over-moulded in the hosting part. Following an iterative process, a set of injection tests using acrylonitrile butadiene-styrene (ABS), was conducted, successfully fulfilling the objective of over-moulding the piezo and its electrical components using a validated solution that mimics the two-shot injection moulding process. Furthermore, it was determined that polymer shrinkage is the primary factor causing defects in the piezo, as the contraction forces induce a bending curvature, ultimately leading to its fracture. The two-shot injection solution mitigated this behaviour due to the piezo's full encapsulation, which prevents the piezo from bending under shrinkage. From the set of tests performed, it was concluded that injection pressure, cooling time, and melting temperature do not determine the survival of the piezo during cavity filling. Instead, the decisive factor is the mould design, which ensures stabilisation during injection, together with the two-shot injection concept.

Keywords: Injection moulding; Piezoelectric over-moulding; Active metamaterials; Locally resonant metamaterials; Numerical simulation; Finite Element Method.

Resumo

A população global, sujeita à exposição contínua a fontes de ruído no local de trabalho, pode sofrer efeitos como perda auditiva, sintomas de esgotamento e deterioração geral da saúde. Em contextos industriais, as vibrações, também uma fonte de ruído, não só afetam a saúde humana, como também podem reduzir o desempenho dos equipamentos e encurtar a sua vida útil. Soluções tradicionais, como a aplicação de materiais isolantes ou a adição de massa aos sistemas, muitas vezes são insuficientes para reduzir significativamente o ruído e a vibração, especialmente em frequências abaixo de 1000 Hz. Além disso, estas abordagens também podem comprometer a eficiência dos equipamentos devido à massa adicionada e afetar negativamente a aparência. Os metamateriais acústicos surgiram como uma alternativa superior, pois podem criar um efeito de *stop-band effect*, são mais leves e, quando incorporam elementos piezoelétricos, podem ser ativamente ajustados para atingir faixas de frequência específicas. No entanto, os metamateriais são comumente fabricados por meio de processos de fabrico aditivo, o que restringe seu uso em aplicações em grande escala. O presente estudo aborda esta limitação, ao desenvolver uma abordagem para sobremoldar elementos piezoelétricos usando moldação por injeção para produzir metamateriais ativos. Através de simulações numéricas, foi selecionado um elemento piezoelétrico com as dimensões ideais (36 x 20 x 0,22 mm^3) para alcançar o melhor desempenho vibracional possível quando sobremoldado na peça de suporte. Após um processo iterativo, foi realizado um conjunto de testes de injeção utilizando acrilonitrila butadieno estireno (ABS), o que permitiu cumprir com sucesso o objetivo de sobremoldar o piezoelétrico e seus componentes elétricos utilizando uma solução validada que imita o processo de moldagem por injeção de duas etapas. Além disso, determinou-se que a contração do polímero é o principal fator que causa defeitos no piezoelétrico, uma vez que as forças de contração induzem uma curvatura de flexão, levando à sua fratura. A solução de injeção de duas etapas mitigou este comportamento devido ao encapsulamento total do piezoelétrico, que impede a curvatura devido à contração. A partir do conjunto de testes realizados, concluiu-se que a pressão de injeção, o tempo de arrefecimento e a temperatura de fusão não são os fatores mais determinantes para a sobrevivência do piezoelétrico durante o preenchimento da cavidade. De facto, o fator decisivo é o design do molde, que garante a estabilização durante a injeção, juntamente com o conceito de injeção de duas etapas.

Palavras-chave: Moldação por injeção; Embebimento de elementos piezoelétricos; Metamateriais ativos; Metamateriais localmente ressonantes; Simulação numérica; Método de elementos finitos.

Index

Figures Index

Tables Index

Acronyms and Symbols

Acronyms

ABS	Acrylonitrile butadiene styrene
CAD	Computer Aided Design
Cp	Specific heat
ISEP	*Instituto Superior de Engenharia do Porto*
IM	Injection moulding
L/D	Length/diameter
LMSD	Mecha(tro)nic System Dynamics
LCP	Liquid crystal polymer
P.Porto	*Instituto Politécnico do Porto*
PBT	Polybutylene terephthalate
PC	Polycarbonate
PET	Polythylene terephthalate
PI	Polymide
PLA	Polyactic acid
PM	Piezoeletric material
PMMA	Polymethyl methacrylate
PP	Polypropylene
PVDF	Polyvinylidene fluoride

Symbols

A	Area	m^2
Y	Distance	m
F	Force	N
m	Mass	kg
T	Temperature	$^{\circ}\mathrm{C}$
V	Velocity	$\mathrm{m/s}$
η	Viscosity	$\mathrm{Pa.s}$

1. Introduction

1.1. Contextualization

The world's population is daily exposed to various elements from the surrounding environment, some of which have the potential to impact quality of life. When in the form of noise, continuous exposure in the workplace can lead to effects such as hearing loss, burnout symptoms, and an overall decline in health [1]. Therefore, efforts are being pursued in noise control and mitigation, stimulated by increasingly stringent regulations regarding the quietness of systems in private/public spaces and the public expectations [2]. Moreover, in industrial contexts, besides being a noise source, vibration can degrade performance and shorten equipment lifespan, which increases significant costs in maintenance and energy inefficiencies. To overcome the vibrations issue, traditional solutions are often implemented with the use of techniques such as adding mass or using absorptive materials. However, these solutions often prove inadequate for low-frequency noise and vibrations, since they require substantial isolation material volumes or adding mass to the structure, thus compromising energy efficiency and product design. Solutions involving the implementation of metamaterials can mitigate this problem due to their unique engineered properties, which are not found in natural materials. For this purpose of vibration/noise control, metamaterials are designed to be locally resonant or create a Bragg scattering phenomenon, which imposes a stop band effect.

Acoustic metamaterials are divided into two categories, passive and active, meaning that the range of the stop band effect is pre-defined and cannot change due to the design established during its production (passive), or by incorporating piezoelectric elements into the material, allowing for real-time reconfiguration of the range of the stop band effect (active), enhancing applications where noise/vibration sources have a wide frequency spectrum emission. Nevertheless, despite the advantages of metamaterials over traditional solutions, their implementation in industrial contexts faces challenges due to being fabricated by additive manufacturing, because it is a process characterised by processing limitations in mass scale production, raising production costs and difficulties in attending to high demands [3]. Therefore, the study proposed in this thesis, entitled *Integration of piezoelectric elements in the injection moulding process for active acoustic metamaterial production*, can mitigate the limitations of the current manufacturing process in metamaterial production. Using the injection mould process to over-mould a piezoelectric element into a hosting structure with clamping features that allow for the assembly of a panel provides a solution where a structure exhibits active metamaterial properties and can be applied in general applications to control

vibration and noise. This solution contributes to the market needs in this matter, without limitations regarding mass-scale production.

1.2. Objectives

The thesis's main objective is to over-mould a piezoelectric element using injection moulding, to permit the mass-scale production of a locally resonant metamaterial structure capable of creating a stop band effect in the audible spectrum range. To pursue this objective, a polymer part with connection claws is used as a hosting body to over-mould the piezo, to ultimately form a panel structure with a stop band effect. Therefore, a framework of objectives is defined according to the main objective and the research viability:

- Integration of the piezoelectric element on the host structure without changing the features that allow each hosting part to be assembled into a panel;
- The hosting part's first vibration mode must fall in the audible spectrum range;
- Finding the ideal piezo dimensions that allow for the higher modal coupling effect between the piezo and the hosting part, to enhance vibration performance;
- Incorporate the piezo together with the hosting part, wires and connectors to allow the over-mould piezo connection with an external inductance circuit to actively tune the frequency range of the stop band effect;
- Develop an insert-mould solution capable of holding the piezo and its electric components during cavity filling, and demoulding it without damage;
- The insert-mould design developed to over-mould the piezo must not produce alterations on the components of the mould that accommodate the insert mould;
- Understand which and the degree of influence that the injection parameters have on the outcomes of over-moulding the piezo;
- Ensure the production process of over-moulding the piezo remains efficient, to enhance the mass-scale characteristic.

1.3. Structure

The present thesis is divided into four sections. The first one is the Introduction, where the objectives and the interest of conducting this study are presented, along with the thesis's structure.

The second section outlines information regarding injection moulding, metamaterials, and mould design based on a literature review. This information serves as a starting point for the work developed in the next sections, and as knowledge support for the decisions implemented in the development of solutions to fulfil the objectives established in the first section.

Next, in the third section, which constitutes the main body of work, the best piezo dimensions that suit the hosting part are selected along with the best mould design to over-mould the piezo

by injection moulding. From this selection, a set of tests is carried out, and their results are analysed based on empirical and software engineering simulations, to draw conclusions that allow for a development process that ultimately converges on a viable solution to over-mould the piezo by injection moulding.

The fourth and last section is a compilation of the main conclusions taken from the work developed, and of ideas for future work regarding the integration of piezoelectric elements in injection moulding, to expand knowledge on this research topic.

1.4. Host institution

This thesis was carried out under the Erasmus+ program at KU Leuven University within the research group Mecha(tro)nic System Dynamics (LMSD) at the Diepenbeek campus. LMSD focuses on understanding, monitoring, and controlling the dynamic behaviour of mechatronic systems, covering motion, vibration, and acoustics, throughout their entire life cycle, from design and manufacturing to operation. Their research spans methodologies such as model-based system design, system identification, noise and vibration control, diagnostics, and prognostics, supported by theoretical foundations in model order reduction, signal processing, uncertainty quantification, and machine learning. Applications include powertrains, vehicles, machines, lightweight assembled systems, and aerospace. LMSD unites researchers and specialized professors whose expertise drives knowledge creation with strong industrial relevance, reinforced by the group's close collaboration with industry.

During the development of this thesis at LMSD, the work was supervised by Prof. Dr. Elke Deckers, Professor at KU Leuven, and PhD candidate ir. Stefan Janssen. Their guidance was essential, both in sharing scientific knowledge and in providing access to the necessary equipment to conduct the research. Furthermore, the work carried out is closely connected to Stefan Janssen's PhD thesis, which focuses on the development of novel piezoelectric metamaterials and their manufacturing using injection moulding.

2. State of the art

2.1. Injection moulding

IM is a process that is used worldwide to produce polymer objects. This process was invented by the Hyath brothers in 1872. Since that time, IM has continuously developed to become the most used process to produce polymer parts, since it has the great advantage of being a very economical method of mass production [4].

2.1.1. Process characterisation

The process is characterised by the melted plastic small grains. In the plasticisation cylinder of the IM machine. That is kept at the same temperature as the process temperature, and then it is injected into a mould, which stays cold enough for demoulding the plastics, in case of thermoplastics, or warm enough for crosslinking, for thermosets. The obtained parts can have tight tolerances, and the process is characterised by high cadence. To be more specific, we can divide the process into four steps, in this order [4,5]:

- **Plasticisation**, the material is fed by a material hopper into the cylinder of the injection machine and a screw in rotation is squeezing and pushing the material into the front of the screw, while the material is heated to the process temperature. The polymer flowing speed to the front of the screw depends on the speed of the screw, material rheology, barrel temperature, and back pressure. When the material is being pushed, a large amount of energy is released because of the friction caused by the screw narrowing down. After the material is pushed to the front of the screw, it remains in the zone of applied heat and waiting for the next step [4];
- **Injection**, the material is injected into the mould cavity by the screw, filling the mould. In this step, the material is pushed not by the rotation of the screw, but by a linear movement. The injection speed needs to be properly configured because this parameter will affect the quality of the object produced. The object thickness will influence injection speed, since thinner sections generally need faster injection speeds than thick-walled parts, mainly due to the decreased importance of the relationship between mould filling time and cooling time with a thicker section [4,5];
- **Packing** after the material has been injected into the mould, an amount of material is again injected to compensate for the decrease in volume due to temperature reduction

during mould refrigeration. Packing depends on the process parameters, such as mould refrigeration temperature and packing time [4];

- **Ejection** takes place when the material reaches a certain temperature that can be handled. Under these conditions, the mould opens, and the part is extracted from the mould.

2.1.2. Equipment

Manufacturing parts by IM is quite complex, demanding industrial equipment. To achieve this purpose, an IM machine is composed of the injection system, the clamping mould mechanism, a hydraulic system, an electrical system, and auxiliary equipment. These systems work together to assure the quality of the product.

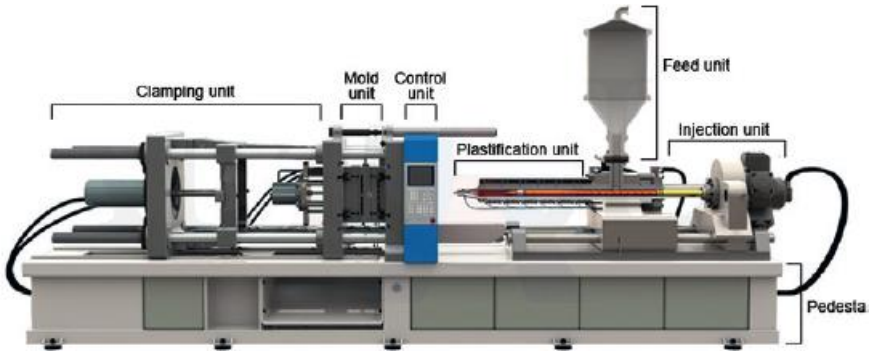

Figure 1- IM machine [6]

As described, the first step of the process is the plasticisation, made possible by the injection system. This system is responsible for melting and plasticising in an even way the polymer grains and ultimately applying pressure to the plasticised material (injection). This process occurs inside the **cylinder**, which is a metal-based component surrounded by heating resistances that heat the polymer. The inner walls of the cylinder should be as smooth as possible to avoid dead angles, gaps, and uneven surfaces. Within the cylinder stays the **screw** that is responsible for plasticising and pressurising the polymer, providing the needed material dosage to fill the mould. Therefore, the screw is divided into three different parts [4,6].

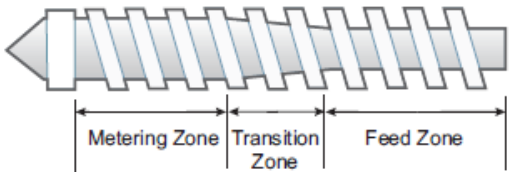

Figure 2- Injection screw [6]

The first part is the **feed zone** (Figure 2), where the grains of polymer enter on the cylinder to initiate the pre-heating and are pushed by the screw in rotation. When reaching the end of it, the polymer already starts to melt. The next section is the **transition zone** (Figure 2), where the depth of the threads gradually diminishes, compressing the plastic, leading to complete melt and mixing of the polymer. After, the polymer moves to the **metering zone** (Figure 2) in which the threads are fixed and are responsible for keeping the melted polymer pressurised and at

the same temperature, stabilising the flow. In terms of screw design, the gap between the screw and the cylinder is kept small to maximise the heat produced by the material shearing, and the heat provided by the resistances can be conducted easily to the material, since polymeric materials have a low conduction coefficient [4,6].

At the tip of the screw, a non-return valve is installed to prevent material backflow during the melting and injection phases. The design of the non-return valve varies depending on the material used in the injection process. However, the valve's primary function is to effectively prevent backflow while ensuring a non-disruption of the melted flow. Proper valve design is crucial to maintain process efficiency and not interfere with the flow behaviour [4].

In some IM machines, the screw system inside the barrel is replaced by a piston unit. In this setup, the material is dosed by an external system that delivers the exact amount of material needed for the process. After, the piston gradually moves the material toward the injection nozzle, heating it to the required processing temperature. Once the material reaches this temperature, the injection occurs, driven by the pressure created as the piston compresses the material. However, this system has a significant drawback compared to the screw-based system. The material remains in the cylinder for an extended period, as it takes longer to reach a fully melted state. This makes the piston system unsuitable for heat-sensitive materials, such as thermosets and rigid polyvinyl chloride (PVC), which can degrade under prolonged heat exposure. In contrast, the screw system offers several advantages. It melts the material faster due to the heat generated by shear stress during the screw's rotational motion. This not only accelerates the process but also ensures a more uniform melting state, resulting in lower material viscosity. Additionally, the screw system experiences less wear and tear compared to the piston system, making it more durable and efficient for various applications [4].

Another crucial element of the injection machine is the **clamping system**, providing the force required to keep the mould halves closed. The dynamics of the system are simple, as it consists of fast linear movement during the opening and the closing of the mould, ensuring a fast cycle and providing the strength required. However, in the final moments during closing, the movement is smooth to avoid damage to the mould surfaces [7].

Two types of clamping systems are available: the direct clamping unit and the toggle-type. The latest is the most used, since it can produce a lighter clamping force due to its smart geometry. In opposition to direct clamping, in the toggle clamping-type, the clamping force is not exerted by the piston that gives motion to the system, but by four metal-based bars connected to the moving plate. Thus, when the mould opens, they move to a V position, and when it closes, the bars keep straight working as a locking mechanism. Preventing the piston from continuously applying pressure to the system. Compared to direct clamping, the biggest disadvantage is the more difficult control of the velocity and closing force [4-8].

As mentioned in section 2.1.1, the system responsible for feeding the injection machine with polymer is the **material hopper**. The pouring of material by the hopper in the injection machine can be due to the action of gravity or using a screw that is directly connected to the plasticisation zone. The solution to be chosen depends on the brand of the hopper and the material used. Inside the hopper are filters and magnets to prevent contaminants and metal

fragments from getting inside the cylinder. Connected to the hopper, normally, there is a dryer to keep the moisture out of the material and to preheat the material [4,6].

2.1.3. Plastics used in injection moulding

Although the advances in materials used in IM, plastics are the most commonly used raw material. Since they have the property of being very versatile and easily worked to produce a complex shape object. These two properties are crucial to produce acoustic metamaterials (as described later in section 2.2).

Plastics are polymers made of chains of monomers connected due to a polymerisation process. What ensures the connection is the action of intermolecular forces between the monomers and covalent bonds between atoms. In contrast, the Van der Walls forces serve as a bonding force between two polymeric chains when they come to interact together [4,9]. According to the literature, there is no formal limit to the number of monomers forming a polymer [4]. Nevertheless, it is consensual that its existence must be high enough not to change the phycochemical properties in cases where equal monomers bond together with chains that already form made plastic. Engineering polymers usually have between 200 and 2000 monomers [4].

The heat-conforming ability of plastics arises from the chemical connections, because intermolecular forces between monomers are weaker than the covalent bonds holding atoms. As a result, when a plastic is heated, the intermolecular forces are ruptured and the monomers become loose, turning the plastic into a viscous state, enabling the conformation of the melted plastic in the desired shape. Next, after a temperature drop, exists the regeneration of intermolecular forces (polymerisation) and the plastic becomes solid again in the desired shape. However, there are some particularities in polymers regarding the differences in the architecture of the molecular chain in the pre-heating state. Thus, the type of polymer used will influence the possibility of reprocessing the material and the final mechanical properties of the manufactured part [6]. In this way, in material sciences, polymers are divided into three categories:

- **Thermoplastics** when compared to other polymers, can be reprocessed by reheating due to a small amount of crosslinking between molecular chains after the process of cure, which can occur by UV light or heat. Regarding the organisation of the molecular chains in the solid state, thermoplastics are divided into **semi-crystalline and amorphous** [10]:

  Semicrystalline polymers are characterised by the higher organisation of their polymeric chains, achieved through the parallel alignment of these chains in the solid state. The degree of this organisation depends on factors such as the cooling rate and the molecular morphology. Greater organisation results in stiffer, denser, and stronger material properties. Additionally, this higher degree of organisation gives an opaque appearance to the material, which arises from the progressive alignment of polymeric chains during the cooling process [4,10]. In semi-crystalline plastics, shrinkage caused

by the material cooling is higher than in thermosets, because of the increasing proximity between polymeric chains in the process of crystallisation. Therefore, since the crystallisation is influenced by the cooling rate, to control the level of shrinkage in the resulting part, the cooling rate of the mould is amplified to reduce the crystallisation. However, this solution produces inferior mechanical properties in the resulting plastic parts [4];

In contrast to semicrystalline polymers, the molecular chains in **Amorphous** plastics are not organised in the solid state, enabling the material to have a low level of contraction compared to semicrystalline plastics. This feature gives the advantage of manufacturing objects with higher tolerances more easily and economically. Considering process temperatures, in amorphous plastics, the melting and glass transition temperatures are the same. However, the cooling phase is bigger compared to semi-crystalline plastics. Thus, the parts take more time to turn into the solid state, and over a wider range of temperatures. From the visual aspect, the amorphous material is transparent like glass [4]. An important aspect to be taken into consideration is the closing pressure of the mould, which should be low to prevent stress concentration on the resulting plastic part, due to the large elastic deformation between the solid point and the melting point [10].

- The other category of plastics is **Thermosets**. In contrast to thermoplastics, these materials cannot be reprocessed due to the higher degree of cross-linking. After manufacturing, if heat is applied to the thermoset plastic, even if it reaches the melting temperature, the material will not flow, and after a moment, it starts to degrade. Despite this disadvantage, higher crosslinking degrees give mechanical properties like stiffness and durability. Other important properties are heat resistance, mechanical strength, durability and chemical resistance [4];

  Processing thermosets is different compared to thermoplastics, since hot moulds are used to improve the curing process to induce cross-linking. Also, the moulds need to have escape channels to let gases formed in the process escape, since thermosets tend to produce more gases. Otherwise, the gases can stay trapped in the plastic, causing quality problems. Additionally, not every thermoset can be processed by IM, since additional attention is needed due to the polymeric chemical reactions. In this case, a fast plasticisation process is required, and the machine must widthstand the high abrasiveness of the material, that's why, traditionally, it is a plastic processed by compression moulding. Usually, when a thermoset is processed, fillers are added, such as fibreglass, organic fibres, ceramics and boron, to improve the properties of the plastic [4,11];

- **Elastomers** may be, natural and synthetic. To be processed by IM the machine requires a mould blow unit to push the material against the walls of the mould to give the pretended geometry, and a special cylinder for elastomers and a dosage delay mechanism [4].

2.1.4. Polymers properties

To effectively manufacture a plastic part, it is important to have present the characteristics and properties of this type of material. With the knowledge of polymers' behaviour, it will be possible to adjust the process parameters and ensure the quality of the final product. Thus, it is primer to know the chemical transformations suffered during the plasticisation and cooling phase, and the thermodynamics during the process.

The general properties of plastics are explained in this section, and they can be divided into mechanical properties, rheological properties and thermal properties.

Mechanical properties of plastics describe their behaviour when subjected to stress. A plastic, in general, can be defined as a ductile material, i.e. it can deform plastically under stress before rupture. When strain/stress curve of a plastic is determined, the conclusions drawn are: for low-stress amplitudes, the strain is also low and the curve behaves linearly (elastic part), and when more stress is applied, the curve already has non-linear behaviour and presents high strain [6].

The stress applied to materials can be normal (tensile stress) or parallel to the surface (shear stress). When processing a polymer by injection moulding, shear stress requires particular attention, since high levels of it can lead to the degradation of the plastic by damaging the polymeric chains, which normally occurs when the polymer fills the mould cavity [4]. This stress phenomenon arises from the high strain that the material suffers when the hot material contacts the cold mould. To avoid it, relaxation of the plastic must be ensured when it reaches the glass transition temperature, with the application of slow cooling that enhances stress relief to the point of becoming residual in the final product [6,12].

Other properties of polymers are the **Rheological properties,** which impact IM considerably, because visco-elastic materials change their viscosity due to stress variations. A plastic in the melted state is a material that behaves differently compared to other fluids, because of the polymeric nature of its composition. Thus, in this forward section of the thesis, the focus is to understand the influence of stress on the strain of the melted material, and the influence of temperature and pressure on the viscosity of the plastic. Knowing these aspects, it is possible to predict with some certainty how the melted plastic will flow and fill the mould [4,6].

A melted plastic is a non-Newtonian fluid, meaning that the viscosity is influenced by the shear rate. When the shear rate increases, the viscosity will decrease due to the rupture of the interaction between polymeric chains. However, since plastic is an elastic material, it has the ability to return to its original shape after the applied stress [13].

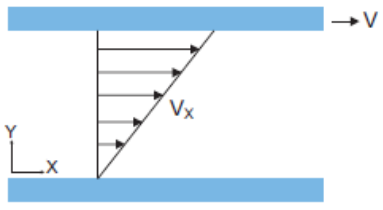

Figure 3- Flow between two slabs [6]

Figure 3 shows two parallel walls, with the upper wall being movable and the other fixed. If a force is applied, the upper wall will move in a constant velocity, inducing shear stress in the fluid. As seen in Figure 3, the velocity is not the same along the flow, due to the resistance of the fluid with the wall, a property called **viscosity (η)**. This property of the fluid can be calculated by the fraction between the shear stress applied on the plate and the shear rate of the fluid (equation *1*) [6,13].

$$\eta = \frac{F/A}{V/Y} \qquad 1$$

Besides the shear rate, other properties influence the viscosity of the melted plastic, such as the molecular weight. By choosing a plastic with a higher **molecular weight**, the material presents a higher viscosity because a higher molecular weight means that the polymeric chains are bigger, which enhances entanglement of the molecules, offering flow resistance[6]. In mathematical terms, it is possible to model the variance in viscosity, also known as shear-thinning. The nature of this equation is a power law (equation*2*) that relates the shear rate in the fluid with a factor K that represents the consistency index, and the exponent n. In case of pseudoplastics, the exponent varies between 0 and 1, because of the nature of the variance of the viscosity with shear stress [13,14].

$$\eta = K\dot{\gamma}^{n-1} \qquad 2$$

It is important to retain that a melted plastic is a non-Newtonian fluid that behaves like a pseudoplastic fluid, meaning that by increasing the shear stress, the viscosity (calculated by equation *2*) diminishes. This is explained at the macromolecular level as a result of the rupture of some of the polymeric chains when the shear rate increases (Figure 4), which facilitates movement between chains and consequently promotes an easy flow of the fluid [6].

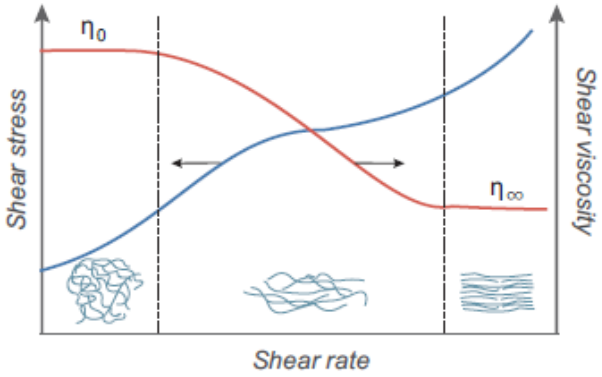

Figure 4- Shear viscosity and shear stress vs. shear rate [6]

Temperature is one of the most manipulated parameters to induce viscosity variations in fluids during manufacturing processes like IM. The viscosity-temperature relation in plastics is similar to most fluids: the viscosity reduces with increasing temperature. On the other hand, **Pressure** does not have much influence on the viscosity in IM, due to the relatively lower pressures used in the process, only having some influence when the process involves fast injection [6].

As observed by Weissenberg [13,15], when a melted polymer flows through a tube or a closed space, the shear stress caused by the interaction fluid-wall creates a normal stress differential between the flow direction and the normal direction to it, resulting in **rod-climbing**. This effect can be noticed when a rod provided with rotational motion is immersed in melted plastic and the plastic starts to ascend in the rod wall. This phenomenon is explained by the pressure difference in the upward direction created by the shear stress of the rod. At the macrolevel, while the rod is spinning, the polymeric chains close to the rod become aligned with the circular shape of it, and by counter reaction of the chains, they try to return to the original shape by pulling the surrounding polymeric chains in the direction of rod [13,16]. This pull movement creates a pressure difference that induces the plastic to go up the rod. Another example of the influence of shear stress in plastics is **extrudate swell**. Being characterised by the quick expansion of melted plastics at high pressure while exiting a constrained space [6,13].

Thermal properties are critical in IM, since the material is subjected to varying temperature gradients. Understanding these gradients is essential to tune process parameters and selecting the appropriate equipment. The property that most influences temperature gradients is the specific heat capacity (Cp). Specific heat quantifies the amount of heat required to raise or lower the temperature of a material by one unit. Typically, Cp varies with temperature. In the case of polymers, Cp increases with temperature and reaches its maximum value during the solid-to-melt phase transition [6].

During a phase change, materials exhibit a distinct variation in enthalpy. For crystalline materials, an endothermic heat flow peak is observed during heating (melting point), as a significant amount of energy is absorbed to break down the crystal structure. Conversely, during cooling, an exothermic peak occurs (crystallisation temperature) due to the release of energy as the material re-forms its crystalline structure.

When discussing the temperatures associated with melting, crystallisation, and glass transition, the peak or average temperature of each phase is typically considered. In polymers, due to the high energy and increased motion of the polymeric chains, these phase transformations occur over a range of temperatures. In contrast, amorphous materials, lacking a structured arrangement, do not exhibit sharp peaks during phase changes. Instead, these show a gradual temperature transition without a distinct melting peak [6,17].

2.1.5. Parameters of the process

As described in the previous sections, IM is a complex manufacturing process due to plastic being influenced by multiple factors that impact its properties. These properties significantly affect the quality and mechanical characteristics of the final product. By carefully controlling machine parameters, including temperature, pressure, and injection velocity, it is possible to optimise the final mechanical properties and ensure the quality of the resulting products.

The **cylinder temperature** is adjusted based on the type of plastic being used. Material suppliers typically provide the recommended temperature settings for their products. As an alternative, standard temperatures are defined directly on the machine. While it is possible to set the temperature of the electrical heaters, it is also essential to account for the heat generated by

friction between the screw and the polymer within the chamber. The cylinder typically features six zones for temperature adjustment. Depending on the material being processed, different temperature profiles can be applied. For thermosets with reinforcements, or when fast and uniform heating of the material is required and a short cycle time is necessary, all zones are set to the same temperature (horizontal pattern). On the other hand, an ascending temperature profile is used for materials sensitive to heat variations, as it minimises viscosity variations and ensures proper material flow. A descending profile may also be used, although it is recommended only for specific and special cases. The temperature at the **nozzle** area has a smaller impact on the remaining areas, and it should only be enough to compensate for the thermal loss when the material flows through this area. Generally, the temperature should be high as possible without degrading the molecular chains, which improves the relaxation of the polymer, reduces the internal stress after cooling and improves the final quality [4,6].

Injection speed should be as high as possible to prevent defects in the resulting product. By increasing injection speeds, big variations of temperature are prevented while the material is filling the mould, which avoids an uneven filling of the mould, and consequently prevents high residual stress when the plastic solidifies. Injection speed is usually higher for parts with thin walls, rather than wide walls to ensure that the filling is made by the front of the melted flow. However, injection speed also influences the orientation of the polymeric chains on the melted plastic, starting when the melted plastic starts to flow. At this moment, the molecules adopt the direction of injection, and by increasing the filling speed more shear stress is generated, which leads to well-oriented molecules that cause anisotropy and uneven shrinkage when the plastic solidifies [4,6]. Thus, the injection speed needs to be calibrated to prevent an uneven filling while avoiding extremely oriented polymer molecules.

To diminish the problem of increasing the filling speed, since the value should be as high as possible to reduce the variation of temperature and pressure, it is advised to change the temperature. Increasing the temperature of the cylinder and the mould reduces the viscosity of the flow and therefore the shear stress of the melted plastic, which lowers the orientation of the polymeric chains [4,6].

Pressure and time of injection are related to each other to guarantee the quality of the final product. Injection pressure is the pressure exerted by the screw pushing the melted flow to fill the mould. The amount of required pressure must be sufficiently high to fill the mould fast, but not too high to prevent residual stresses on the ejected part. The duration of the exerted pressure is the injection time. The duration of the pressure is regulated to balance quality and efficiency of the process, must be short enough to give time for the material to solidify in the gate to prevent reflow, and to maximise the cycle time. For amorphous thermoplastics, the injection pressure and the time cannot be excessively high to prevent residual stress and defects when ejecting the manufactured product. However, for crystalline thermoplastics, the pressure and time need to be higher to help the crystallisation process [4,6].

Screw speed is crucial and varies depending on the material used. Manufacturers provide recommended rpm ranges to help operators achieve ideal processing conditions. The optimal speed effectively mixes the plastic without causing excess friction, which could damage it through the heat produced by the shear stress of the screw. An excessive speed can cause

overheating, reduce melted plastic uniformity, and increase wear on the screw [18]. When no specific data on screw speed is available, matching it to the cooling time is a practical approach. By selecting a speed that finishes melting just before the mould is ready to open, idle time at the screw tip is minimised, ensuring efficient and stable processing [6].

2.2. Acoustic metamaterials

In engineering, acoustics is the field that studies the behaviour of mechanical waves, known as sound. The focus around this field is the manipulation of sound and its propagation using the materials available in nature. However, when developing a device to manipulate sound, engineers face considerable challenges due to the limitations of natural materials. In that way, a new research field was created to study alternative solutions and improvements in natural materials, resulting in the development of metamaterials [19].

2.2.1. Basic principle and characteristics

Metamaterials are engineered materials that exhibit properties superior to traditional materials found in nature. They are composed of meta-atoms, which are small structural units typically arranged periodically in a host material. In the case of acoustic metamaterials, these structures, referred to as resonators, are specifically designed to influence the behaviour of mechanical waves propagating through the material. Unlike conventional materials, metamaterials interact with waves more effectively, resulting in absorption and vibration damping, a phenomenon known as the stop band effect. This effect can be achieved using phononic crystals or structures locally resonant [19-21].

When considering properties of resonators and their capabilities to create zones of no free wave propagation, it is important to look to their degrees of freedom and their influence when an acoustic wave passes through them. By which, resonator affected properties are the **elastic coefficient and mass** [22,23]. To have an insightful notion of these concepts, Figure 5 illustrates the types of degrees of freedom present on a resonator.

From dynamics, each degree of freedom on a body can be represented by a spring-mass system. Figure 5 represents three combinations of these systems that will induce the properties that enable metamaterials to cause a stop band effect. Figure 5 a) is a system representing the equivalent mass and spring stiffness of the tree combinations b),c) and d), by which, its clearly that: $m_1 > m_2 > m_3$ and $m_{eff} = m_1 + m_2 + m_3$; Applied to the system, are two parameters in function of time: a force ($F(t)$) that gives motion to the system and the resulting displacement ($x(t)$). Considering the Hooke's law and as described by Haberman and Guild [22], in the system $m_{eff} = F(t)/\ddot{x}(t)$ and $K_{eff} = F(t)/x(t)$.

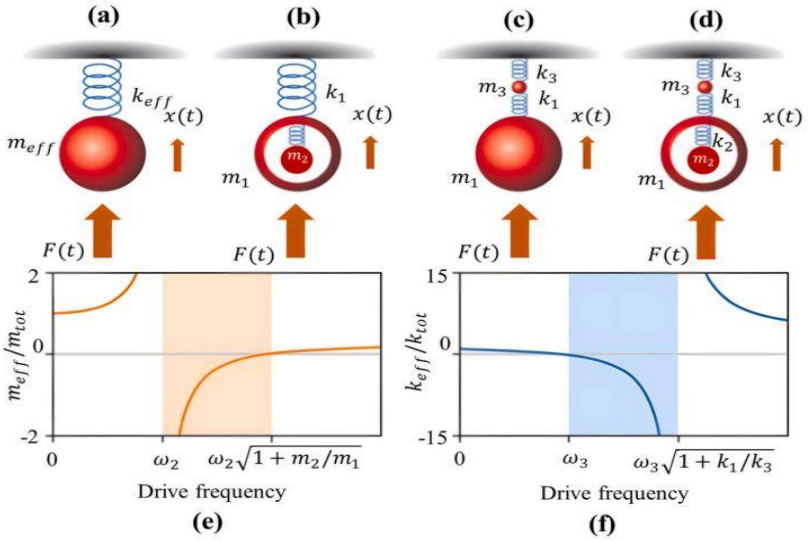

Figure 5- a) general spring-mass system, b) negative mass, c) negative spring stiffness, d) negative mass and stiffness, e) results regarding system b), results regarding system c) [22]

When an acoustic wave is imposed and its frequency is modified over time, the system exhibits negative values in terms of vector direction, mass (Figure 5 b) and stiffness (Figure 5 c) at the resonance frequency. Giving the material properties that enable a stop band effect. More specifically, as the frequency transitions through resonance, the phase of the effective mass's motion relative to the applied acoustic force shifts by 180°. Consequently, the orientation of the acoustic wave shifts in relation to the acceleration or displacement of the resonator, enabling the stop band effect by countering the applied acoustic wave. This stop band effect can be visible in Figure 5 e) and Figure 5 f), in the orange and blue regions respectively [22].

Considering the tree combinations, the system b) corresponds to negative mass, c) to negative stiffness and d) to the combination of negative mass and stiffness [22,24]. These principles govern the fundamental physics underlying the construction of metamaterials. The concept that will be analysed throughout this section 2.2.

2.2.2. Phononic crystals

As evidenced in section 2.2.1, the stop band effect can be caused by resonators. On the other hand, the stop band effect can also be replicated by placing repetitively and in the same sequence, designed structures (each named phononic crystal) on a host structure. In the host structure, the distance between the phononic crystals must be equal to half of the wavelength of the imposed wave, creating the phenomenon known as Bragg scattering. In which individual waves are reflected by the phononic crystal, causing interference between the waves. This interference significantly reduces the transmission of the propagating wave (stop band effect). However, these types of structures are unfeasible for small frequency ranges, because for waves with low frequencies, the distance between phononic crystals is inherently high, resulting in non-viability for applications with restricted dimensions [20,25].

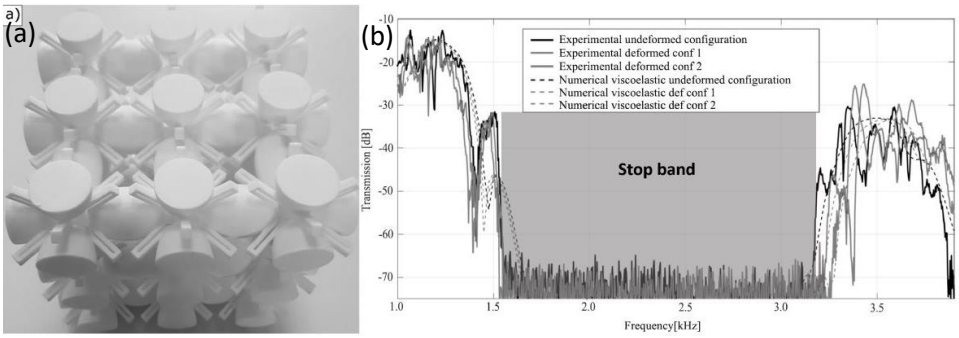

Figure 6- Phononic crystal realisation using 3D printing a) and its vibration transmission measurement and prediction in 3 different configurations (b) [20]

2.2.3. Locally resonant metamaterials

As explained in section 2.2.1, a way of achieving the stop band effect is by inserting resonators in a host material. Here, the principle differs from the Bragg scattering effect and focuses on the resonance properties of the resonator. In a simple way, a resonator can be defined as an object with well-characterised characteristics that resonates at a specific level of frequency. Therefore, placing resonators on a host material and applying a wave on the metamaterial at the resonance frequency of the resonators, the response will be radiation of the waves in an opposite phase by the resonators, causing destruction of the input wave [20,27].

Over the years, multiple approaches have been developed to implement the concept of a local resonator. One idea called Helmholtz resonator, involves using a defined volume of air trapped within a precisely measured spherical compartment. This configuration functions effectively as a resonator due to its well-defined and controlled structure, since by knowing the exact volume of air, it is possible to calculate the resonance frequency of the air cavity with precision, enabling the filtration of acoustic waves at that specific frequency. [28].

A first proposal of this concept was developed by Fang et al [29] in 2006, by placing multiple Helmholtz resonators in series to create a stop band effect by negative elastic coefficient. By testing it, it was concluded that, when an acoustic wave is induced on the resonance frequency of each resonator, the response projected by each Helmholtz resonator through the entry of the cavity is in the opposite phase of the acoustic wave, causing the stop band effect [28,29]. Years later, in 2018, Yu et al. [30] took another approach to improve the potential of the concept proposed by Fang et al [29]. The author Yu et al. [30] conducted an experiment to understand if the stiffness of the material that Helmholtz resonators are made haves influence on the stop band effect. Revealing that if the top panel of the Helmholtz resonator is made from an elastic material, the stop band effect occurs for lower frequencies. Concluding that the critical parameter to calculate the resonance frequency is the material properties of the top panel on the resonator, leading to the disregard of the cavity size (Figure 7) [28,30]. With the findings of Yu et al.[30] the application of metamaterials based on Helmholtz resonators will be wider, since it can be produced in a smaller size for applications with limited space and still create a stop band effect without compromising the work frequencies (Figure 7).

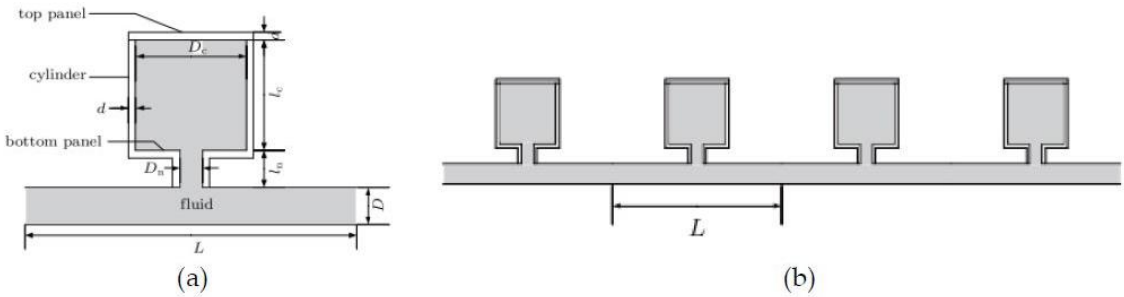

Figure 7- a) Sketch of an elastic Helmholtz resonator, b) sketch of an infinite periodic pipe with elastic Helmholtz resonators [30]

Another concept of a local resonator was proposed by Liu et al. [31], which involves the implementation of sonic crystals. In this work, a composite material was built consisting of a cube made of 15.5 mm diameter lead balls equally spaced embedded in silicone rubber. In the experiment, one face of the cube was submitted to a sound with frequency modulation that ranged from 250Hz to 1600Hz, and on the opposite side of the cube was a sound detector to register the results [31]. The stop band effect was registered at 500Hz due to the resonance of the balls inside the cube due to the phenomenon of Fano-type interference [20,27].

In the last two concepts shown in the present section (Helmholtz resonator and sonic crystal), the solutions were based on a specific sequenced and designed structure, although other concepts of local resonators were developed that do not depend on its design. The concept is called membrane acoustic metamaterial, and it consists of placing an elastic membrane under tension by a rigid frame. This tension applied to the membrane is to guarantee a reaction against the vibrations, but also to adjust the resonance properties by tuning the membrane tension. Although, the common approach to adjust the resonance properties is by placing a selected weight on the centre of the membrane to work as a spring-mass system. A metamaterial acoustic membrane normally works for frequencies ranging from 50Hz to 2000Hz [32]. When studying the effectiveness of this type of solution, the focus is **on the normal displacement of the membrane and its modes of vibration**. According to an experiment by Yang et al. [33], when a metamaterial membrane is submitted to an acoustic wave, the behaviour produced can be seen in Figure 8.

a) b)

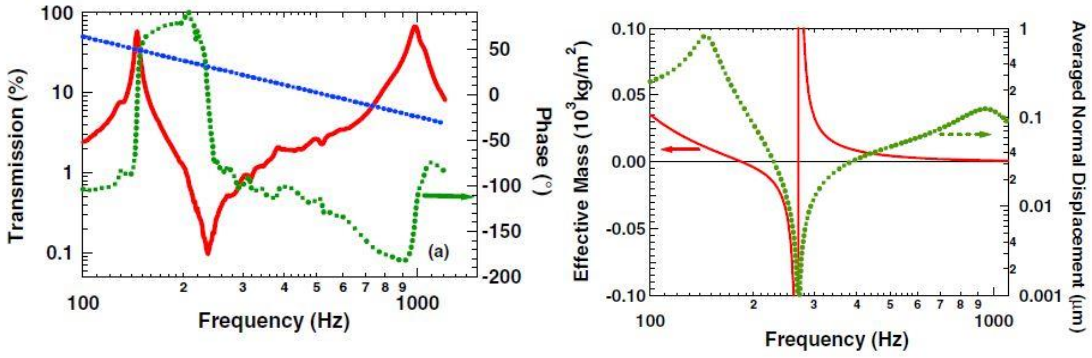

Figure 8- Dynamic response of metamaterial acoustic membrane [33]

Analysing Figure 8 a), in the red curve that represents the transmission amplitude of the membrane, it's possible to see that there are two maximum points where the transmission reaches the maximum rate, and therefore correspond to the two vibration modes of the membrane. The first occurs at 145Hz, when the attached mass presents vertical displacement and consequently the membrane also experiences motion, and the second mode is recorded at 984Hz and corresponds to the immobility of the mass at the centre of the membrane and the normal displacement of the membrane. However, what is important to register is the drop in transmission recorded at 237Hz, visible in Figure 8 b) [33]. At this frequency, the acoustic wave in is most part is reflected, due to the antiresonance condition that occurs when an induced frequency is between the values of two modes of vibration. Which leads to the response of each mode in asymmetric phases between them, cancelling the wave by negative mass effectiveness [32,33]. Property that is represented by the red curve in Figure 8 b).

According to Ma and Sheng [32], membrane acoustic metamaterials, the vibration modes registered at low frequencies (below 1000Hz) are symmetric due to the lower thickness of the membrane, giving only the property of negative mass density. To overcome single negativity mass density and give the material the property of negative modulus, the membrane also needs to have an asymmetric vibration mode at lower frequencies. Thus, another membrane was added to the frame, resulting in a double membrane metamaterial with double negativity, since it combines symmetric and asymmetric modes. Giving also the ability to produce a stop band effect for frequencies above 1000Hz [32].

2.2.4. Locally active metamaterials

Until section 2.2.3, the basis and principles of metamaterials were covered, as well as their types and ways of creating the stop band effect. However, it was shown that this type of engineered material only functions for some very specific frequencies due to the design or properties of the components involved. To change this paradigm, engineers try to develop another type of metamaterials based on the same basic principles but making it possible to change the acoustic properties in real time, leading to active metamaterials. To achieve the objective, one of the solutions followed is the integration of piezoelectric elements in its composition. **Piezoelectric materials (PM)** are characterised by having electro-mechanical properties. This means that, by applying electricity, the strain of the PM will change (inverse piezoelectric action) and if the PM is deformed the voltage will change [34].

In active metamaterials, PM are embedded in a typical resonator and due to the electro-mechanical coupling between the PM and the resonator, it is possible to tune in real time the frequency gap of the stop band effect by adjusting the voltage given to the PM. Because if the voltage is adjusted, the PM strain changes, and by mechanical principle, it conditions the stiffness of the resonator's surface, and consequently, the resonance frequency. Taking into account this behaviour, and the engineered properties present in a metamaterial (negative bulk modulus and negative mass), it is possible to change the frequency range where the metamaterial presents stop band effect, although this is only possible if the electric circuit connected to the PM has **negative capacitance** [34-36].

Taking the same principle of a PM with negative capacitance, but with a hybrid concept, Dalela et al. [37] applied piezoelectric membranes made of PVDF, with weights attached, in a host material. Therefore, the range of the stop band effect can be tuned by giving different input voltages to the piezoelectric membrane, resulting in the variation of its stiffness, which causes the membrane to resonate in multiple frequencies [37,38]. In a different study made by Hu et al. [39], two piezoelectric components are used, each one placed in a local resonator, and connected in the same circuit with negative capacitance. The objective of this configuration is to couple the two resonators like a spring connection, and by adjusting the capacitance of the circuit, the stiffness of the connection is changed. It was demonstrated that this system works, enabling the tunability of the band gap of the stop band effect in low frequency spectrum [39].

Another approach, and the more common, is to use a PM as a resonator by connecting it to a **synthetic inductance circuit,** to enable a stop band effect. The configuration of the active metamaterial is possible because the electrical inductance of the circuit can be tuned, leading to the control of the electrical resonance of the PM and consequently matching with the resonance of the acoustic wave. So, when a wave is induced in the host structure, the PM will have a dynamic response and resonate in the opposite phase of the wave. Due to its piezoelectric property, the strain of the PM is transformed into an electric current, cancelling the acoustic propagation.

In a study, Silva et al [40] demonstrated that by using PM shunted to a synthetic inductance circuit, there is the possibility of generating a wider stop band effect(between 93Hz and 405Hz), due to the ability of auto-tuning the circuit, by using a digital potentiometer and microcontroller unit. When an acoustic wave is induced on the system, due to the dynamic response of the PM, an output voltage is created and read by the microcontroller unit, which calculates the frequency of the acoustic wave. Having this information, it is possible for the microcontroller to calculate the right resistance that the potentiometer should present to adjust the inductance of the circuit so that the PM resonates in the wave frequency [40].

As shown, the two possible concepts to tune the range of the stop band effect are either by adjusting the stiffness of a local resonator with a PM or by using a PM as a resonator. Following these two principles, Rodrigues and Oliveira [41] proposed a combination of the two methods to exploit the results. In this work, a local mechanical resonator of the cantilever type was used, in which the mechanical resonator has two weights on the tips. On each side of the resonator, two piezoelectric discs are placed and adjusted so that they do not resonate at the frequency of the mechanical resonator, so that the sound that was not absorbed by the local resonator is absorbed by the piezoelectric disc, allowing a larger stop band effect. This concept was applied to an automobile firewall to reduce the noise transmitted from the engine to the passenger. In this application, the peak of the transmission noise is at 200Hz, leading to the mechanical resonator being defined to resonate at that specific frequency to damp the sound. However, in the surroundings of 200Hz, there are other peaks of noise transmission. Thus, by tuning the piezoelectric discs in a wider frequency range around 200Hz the peaks, the sound transmission can be absorbed. In total, a 30dB reduction was possible between 180Hz and 220Hz [41].

2.2.5. Applications

The potential of the metamaterials is huge when considering the achievements that can be produced in the acoustic fields. One of the possible application fields is **underwater acoustic absorption for submarines**. A study was made by RADULOVIĆ et al [42], to study the viability of using metamaterials with the principle of acoustic cloaking to enable a submarine to avoid sonar detection. A very useful characteristic for military purposes. In the study, it was proven by calculus and acoustic pressure maps that, for cylindrical shapes (characteristic shape of a submarine) with 50 layers of acoustic cloaking metamaterial, it is possible to avoid detection in the working frequencies of sonars, covering infrasound and audible sound. In the same field, but with a different type of acoustic metamaterial, Zou S. [43] planned theoretically the use of PM integrated in a viscoelastic local resonator that works actively to cancel and absorbing, respectively, the sound that is emitted to the submarine. In the case presented by RADULOVIĆ et al [42], the effect produced is the guiding of the acoustic waves without changing their properties, giving the effect of the absence of the submarine. Which differs from the second case Zou S. [43] since the metamaterial theoretically avoids detection of the submarine by not reflecting the acoustic waves.

A major field of application is the **automobile industry**. In terms of comfort, the most critical spectrum of noise is high frequencies. However, this problem can be solved by applying vibration dampers in the structure. On the other hand, when considering low frequency noises and the metal sheets that propagate the noises through the car, the most critical aspects are driving safety and the reliability of the car components. Since it is hard to damp low frequencies noises and the existing methods can add a significant weight to the car, acoustic metamaterials can mitigate this limitation. To prove the liability of acoustic metamaterials in vehicles, Liao et al [44] concluded that local resonators can perfectly reduce low frequencies noises in metal sheets used in cars. Moreover, it was possible to verify a high longevity of the designed local resonators for long service time periods [44]. The study by Rodrigues and Oliveira [41] presented in section 2.2.4 was also a successful application of metamaterials on reducing wave propagation in a car structure.

In **housing and construction**, one of the aspects that has a huge influence on the market value of the final building is the acoustic isolation, since sound deeply impacts human comfort. When considering noise sources like highways, railways, busy streets and airports, buildings next to these infrastructures are subjected to low frequency noises. Since materials used in construction have their natural limitations in terms of sound isolation, according to Arjunan et al. [45], it gives a great application field to acoustic metamaterials. In the research conducted by Arjunan et al. [45], numerous solutions of acoustic metamaterials that are in development by other authors to be applied in buildings were summarised. One of the most promising in terms of cost-effectiveness is the use of acoustic metamaterial plates. This concept presents viability, since it has an extended service life without maintenance actions, good for architecture applications where the weight and volume of the isolation needs to be reduced, and freedom of design in the host surface, since the orientation of the metamaterial plate don't need to be a specific one [45-48]. The author Arjunan et al. [45] globally consider that the

acoustic metamaterials in construction are the future and outperform traditional isolation materials. In is perspective, an application that will bring a great advance in construction is the sound isolation of air conducts, ventilation systems and windows by using metamaterials. Existing already solutions where acoustic metamaterials perform air renovation with the exterior environment and at the same time isolate the sound that comes from the exterior of the building [49]. Described by Arjunan et al. [45], the most significant problem in the application of metamaterials in building is the mass-scale achievement. It still takes a considerable time to produce a structure based on metamaterials, since the most used method is addictive manufacturing or a process that requires a considerable time for construction. An obstacle that is proposed to be solved in this thesis by trying to implement IM (fast manufacturing process) in the production of acoustic metamaterials.

2.2.6. State of the art of injection moulding in acoustic metamaterials

In Table 1 is represented the latest studies to understand the viability of producing resonators by IM, with the final purpose of being applied in acoustic metamaterials.

Table 1- Production of resonators by IM

Bibliographic reference	**Description**
Steijvers et al. [50]	This study researches the viability of the production of resonators by IM, with focus on dynamic performance and geometric quality of the final part. Thus, multiple injection tests were carried out to assess the influence of the injection spot on the final characteristics of the resonator. Moreover, two shapes were designed, a cantilever type and a circlet type with a weight on the top edge, with both injected using PP and ABS. After scaling the samples, it was concluded that manufacturing resonators by IM is possible, both showing repeatability in the results. The beam resonator made of ABS, a deviation of 1.5 and 5.6 mg was registered, and using PP, 19.1mg and 10,7mg (low mass deviations). For the circlet type, the deviation between PP samples is higher compared to the ABS samples. Considering dynamic tests, the range of the stop band effect is situated on the gap of 200Hz to 600Hz. To notice that in the dynamic tests, the deviation for the PP resonators is also higher, due to the higher shrinkage of PP compared to ABS.

Table 1- Production of resonators by IM (continued)

Steijvers et al. [51]	This research made in 2023, is based on the previous research by K. Steijvers et al. [47]**,** where, besides the two already described resonators (cantilever and circlet type) with the same design and material specifications for IM, a third one is used, a double beam resonator. This new study focuses on using programs of IM simulation, like Moldex3D 2022, to see the filling flow behaviour of the polymer, possible defects and the influence of the injection process parameters. In order to understand the influence of the IM process on the dynamic response of the resonator, and therefore have better predictions of the stop band effect using the data from the IM simulations. After testing and comparing the results, it was concluded that the use of Moldex3D 2022 to predict the influence of the IM process leads to lower deviations in terms of the mass and geometry of the resonator, and consequently a better prediction of the stop band effect. Since it can be seen in the simulation, effects like shrinking, warpage, density distribution and final mass. And therefore, adjust the process parameters to avoid such defects resulting in a better prediction of the stop band effect frequency, since the mass and geometry affect the resonance frequency.
Steijvers et al. [52]	This study describes the investigation of the impact of manufacturing a cantilever beam resonator with a washer insert. Since, in some cases exists the need to apply an object to a local resonator, to adjust its mass. The materials used were ABS and PP to embed the washer, with the objective of understanding the impact of amorphous and semi-crystalline respectively, on resonator manufacturing. Therefore, it was concluded similarly to tests performed previously by the author, that amorphous polymers have better repeatability and dynamic characteristics for manufacturing resonators. In addition, it was also demonstrated that the use of inserts in the process does not affect the prediction of the stop band effect compared with not using the metal insert. Last, by assembling the resonators with the washers in an aluminium plate, it was measured that the resonator with the insert has a stop band effect of 53Hz wide around 395Hz, and without the insert, the width was 48.5Hz at 538.25Hz. As expected, putting an insert on the resonator, the point of the stop band effect gets lower, proving the tunability of acoustic metamaterials, and more importantly, IM is a viable process to manufacture such structures with repeatability and accuracy needed.

2.3. Design of injection moulds

In IM, the mould is the fundamental component for the process to be carried out. The mould involves a certain level of complexity in terms of its design and functionality. Moreover, its construction quality directly affects the final manufactured part, necessitating strict processes during its fabrication. Therefore, this section will provide a general description of moulds and their components, as well as essential guidelines for their design and for the parts to be produced using IM.

2.3.1. Types of moulds

Simple open/close mould are the simplest mould used with the purpose of producing plastic parts with an unsophisticated design, i.e., hollow and flat parts with no derived elements from the demoulding direction. The mould is divided in a fixed and a moving half. The fixed half is composed of the clamping plate, holding the cavity plate of the mould to the machine and providing stability during the injection phase. On the other hand, the movable half is composed by the mould plate and the lower cavity plate. Also placed in this half are the risers positioned between the clamping plate and the cavity plate, making room for the ejectors. All these components are fixed and aligned by long screws from the clamping plate [53].

Moulds with moving elements are more complex than the previously described, because they are used for parts with features that make it impossible to be moulded in a simple mould core/cavity. For that, the mould is provided with structures like slides, core pins or inserts. Therefore, with the integration of these structures and the complexity of the parts to be manufactured, the mould needs to have multiple demoulding directions(undercuts), as shown in Figure 9. When the final part requires orifices on the side (perpendicular direction of demoulding), slides are put in the mould to act like a core to make the orifice (Figure 9). In the step of demoulding, they slide in parallel to the surface of the core plate, enabling the demoulding action in the common demoulding direction. The mechanism that gives motion to the slide, could be hydraulic or by an inclined pin. The pin in question is installed in the movable half with an inclination relative to the surface, which enables the movement of the slide when the mould opens, since the pin travels in a hole on the slide (Figure 9) [53]. More recently, a new method was developed by Vieten et al. [54], where an automated soft slide that besides the slide function, it auto-aligns with the mould and haves a sealing function to prevent defects like warping in the final part. When tested, in general, this system has fulfilled all the functions presented. However, the automated slider suffered some damage after the machine was cooled and reheated again. The author proposes for future jobs, the integration of a cooling system on the automated slider to reduce the problems with temperature gradients. Besides this problem, this idea has significant improvements compared to the other two ways of moving the slider, especially for complex parts with undercuts.

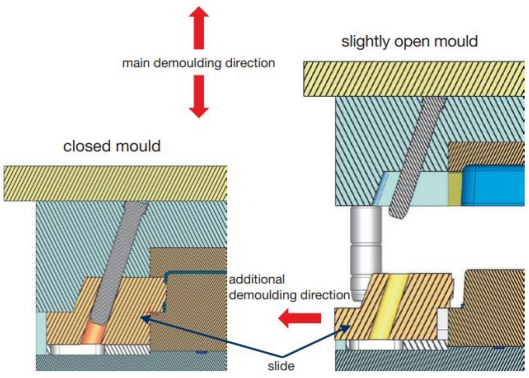

Figure 9- Mould with multiple demoulding directions and provided with a pin slide system [53]

Non-single injection moulds are increasingly being used due to increasing standards in the industry. In these cases, the mould is submitted to multiple injections of different polymers to provide the final part with different mechanical characteristics, or just different visual colours. An example is the manufacturing of rear lights with different colours for vehicles. The first difference of these moulds is the number of cavities. They are composed of more than just one cavity, and the process has the complexity of not producing the final part in one step. The part is processed by adding polymer in each cavity, and it´s handled by a shifting technology or by a rotary table. The most common mechanism is the rotary table, where the mould has the cavity side by side, and in the first step, one component is injected into the first cavity, and after the table rotates and positions the unfinished part facing the other core, the next injection occurs over the first material [53].

2.3.2. Overview of golden rules in the design of parts

To make the process of IM feasible, some considerations must be taken in the design of parts. Having attention to some details will facilitate the design of the moulds by diminishing their complexity, and in the process itself by an easy demoulding action.

Draft angle is the angle that a wall has in relation to a surface, directly impacting the demoulding operation of a part. Therefore, 90° angles (straight walls) must be avoided, since they need large amounts of force to be demoulded, leading to deformation of the final part. To avoid such defects, the minimum draft angle must be 0.5°, and the average angle should be between 1° and 3° [53]. Applying these draft angles will make the air flow escape more easily from the cavity while demoulding, otherwise, with straight angles, vacuum will be formed. In the case of existing undercuts and if the final part is in contact with the split line, a special need has to be taken, and 3° draft angle has to be designed [50]. To help with the process of identification of surfaces to be drafted and to accelerate the process, Jong et al. [55] has developed an algorithm that automatically designs drafts with the correct configurations in CAD parts. However, the program has certain limitations. When surfaces include design features such as fillets between walls and surfaces or undercuts, the program does not automatically generate drafts. Instead, it identifies these surfaces using a distinct colour, providing specifications for the engineer to manually design the drafts. Despite these limitations, the program saves approximately 80% of the workload involved in the design process.

Despite the application of a draft angle in deep hollow pieces like a cup, it is not enough to prevent the formation of vacuum. In these cases, air valves are installed on the movable half but also in the fixed half to let the air flow. The **Surface quality** also has a role, since it allows for an easier demoulding operation with less ejection force, resulting in smooth finished walls. In terms of milling operations to manufacture the mould, it is advised that the cutting tools work in the demoulding orientation, making the roughness even with the direction of demoulding. After the milling operations, polishing treatments are advised to ensure a better surface quality [53,56]. The **split-line face** is the surface of contact between the moving and fixed halves of the mould. Ideally, this split surface should be aligned with the level planes of the final part and, preferably, with surfaces in contact with edges. This ensures better sealing between the halves, preventing the formation of thin plastic sheets due to leaks (flashing). However, in some cases, the design of the part makes it impossible for the split line to lie on level surfaces. In such situations, the split face should follow the top edge of the wavy surface. Additionally, the mould surfaces creating these wavy features should be inclined to enhance sealing and alignment while preventing the mould surfaces from locking together [53,57].

Uniform wall thickness is also an important parameter to be considered, since it will affect the cooling efficiency and the flow behaviour during injection. To avoid defects in the final piece, it is recommended that the design of the part have a uniform wall thickness, and when this is not possible, a slow and gradual variation of thickness must be considered. Which means that rectangular corners must be avoided and rounded corners must be used. Also, the distance variation between surfaces must be gradual, the variation needs to be three times the difference between thicknesses. Along the length from the point of injection to the extremities of the part, the thickness needs to be evaluated to not affect the flow behaviour. When making the ratio flow length by thickness, it needs to be between 100 and 200, above 300, the part needs to be redesigned, and for thin parts above 200, it needs to[6]. In order to spare hours analysing the thickness of parts and to optimise their design, Studer and Ehrig [58] had developed an algorithm that solves this problem leading to the reduction of warpage by 80%. However, exist cases where the design can't be changed, leading to flow behaviour problems. To solve this problem, Minh and Le [59] made a study of fixing the flow behaviour by tuning the temperature of the process, with an inductive coil applied to the mould. Using this method in thin part walls, the flow length behaviour increased from 71.5mm to 168.1mm and filling by 99,8%, maintaining approximately the same cycle time. Having also operational and saving energy advantages, since it only heats up the surface of the mould that influences the part.

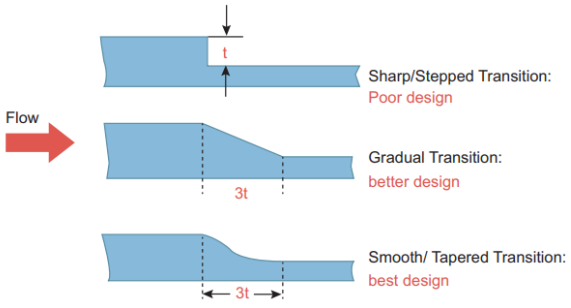

Figure 10- Part design [6]

2.3.3. Feed system design

Integrated in the feed system is the feed point. Which is the source of the plastic flow to fill the cavity, needing to be in a spot that fills the cavity evenly. To take the melted plastic to the feed point, the mould has a special system composed of the sprue, runner and gate (Figure 11). The sprue is responsible for conducting the melted plastic from the nozzle of the injection machine to a network of channels called runners that drive the flow to each cavity of the mould, and finally, the runner is connected to the cavity by the gate.

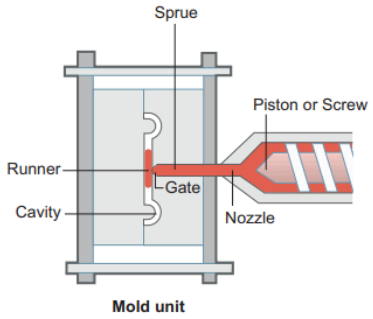

Figure 11- Feed system [6]

The **sprue** and its conical design are critical for directing molten material efficiently while preventing sticking to facilitate ejection after cooling. Sprue's taper (rate of reduction of the diameter along the sprue channel) must be sufficient to reduce frictional losses while ensuring smooth material flow. The diameter of the sprue is also important because an undersized sprue can induce back pressure and shear stress, whereas an oversized sprue results in material waste and prolonged cooling times. Length optimisation of the sprue is essential, particularly for large moulds, to maintain thermal consistency and prevent premature solidification that can disrupt material flow [6,53]. In a simple mould, the sprue can alone conduct the plastic flow to the cavity, however, this case has the disadvantage of the plastic within the sprue staying on the final part after cooling, taking extra work in reprocessing the part to cut the extra plastic of the sprue, wasting material and time[50]. To reduce the waste of material within the sprue, Dawale [60] has redesigned a conventional sprue by applying a taper angle of 45° and a sprue insert. Also, with this design, the sprue is connected directly to the gates, not requiring a runner layout. Leading to a reduction in plastic waste of 10%.

The **runner** carries the plastic to each cavity of the mould and is designed to maximise the solidification of the plastic to have short cycles. However, if only short cycles are considered, it will impact the quality of the final part because the design directly impacts the uniformity of cavity filling, especially in multi-cavity moulds. In terms of the cross-section of a runner, the perfect design is the one that possesses the biggest cross-section, but reduced wall area to diminish flow contact with the wall and avoid heat losses without impacting the flow behaviour [4,6,61]. Among all the designs of the cross-section of a runner, trapezoidal and rounded are the most appropriate. Although circular runners are the ideal shape for minimising shear stress and heat loss, they are not the most used due to economic reasons. Since each semi-circle is in each half of the mould, precise machining is needed to guarantee the perfect alignment of the

semi-circles when closing the mould. Therefore, trapezoidal runners are preferred because they are only machined in one part of the mould [4,6,53]. The layout of the runners must be symmetric to ensure the material reaches all cavities simultaneously. Additionally, the runners should be as short as possible to minimise material waste and pressure loss, otherwise, it can result in defects such as short shots or overpacking in individual cavities [4].

Runners can be classified as cold or hot runners. Cold runners are simple and are kept at the same temperature as the mould. The plastic within the channel solidifies with the part and is removed as waste or recycled. Although they are cost-effective initially and easy to maintain because the mould is less complex and requires low maintenance, they contribute to increased material waste and cycle time. In another way, hot runners maintain the material in a molten state by an independent heat system. The system can be within the mould that is indicated for controlling the flow of melted plastic, and outside of the mould to applications that involve sensitive heat polymers. With this configuration, hot runners reduce waste and increase production efficiency, have a good adaptation to changes in part dimensions, and parts have better end quality. However, they have a higher initial cost, complexity and are not feasible for some heat-sensitive materials [4,6,53,62]. To try to balance the handicap of hot runners in terms of mould complexity construction, Goud and Prasad [63] has developed a successful study combining finite elements and experimental designs to achieve a more pragmatic and less complex design of manufacturing a mould that integrates a hot runner. Some of the modifications made were the use of titanium-zirconium-Molybdenum, maintaining a constant thermal profile, guaranteeing a uniform cooling and maintaining an even pressure. With this modification, a less complex hot runner was made, maintaining good flow properties and a robust runner structure, achieving 40% control damage compared with the traditional runners.

The **gate** is the final structure for the molten material before entering the mould cavity and plays a critical role in the moulding process. Its design interferes with the flow rate, cavity filling behaviour, and cooling patterns, all of which directly affect the part's structural integrity and surface quality, like warpage [6,64]. Gates are designed for specific applications, with common types including sprue gates, restricted gates, side gates, tab gates, flash gates, fan gates and pin gates. The restricted gate is suited for multicavity moulds, and due to its small dimension, a post-process is not needed because the plastic gate snaps while demoulding. However, some precautions must be taken with dimensions, if the gate is too small, it can provoke splashing or burn marks due to the shear stress of the flow passing the narrow gate. The tab gate is an improvement of the side gate and is made for thin parts in a multi-print mould. It is considered an improvement because the distinctive design reduces jetting of the material and the probability of the final part having cracks. Fan gates are particularly effective in distributing material evenly across large flat parts, while pin gates are preferred for leaving minimal visible marks on finished components [4,6]. A well-sized gate facilitates optimal flow without introducing defects. Having this in mind, some considerations must be taken when designing and positioning the gate. The gate should not be positioned on surfaces of the part where a good visual aspect is required, also, the area around the gate typically suffers the highest concentration of stress, so it is important to avoid placing the gate in locations that are exposed

to external forces or prone to damage. To minimise pressure loss and ensure effective material packing, the gate should be positioned in a thick-walled area, Figure 12 [6].

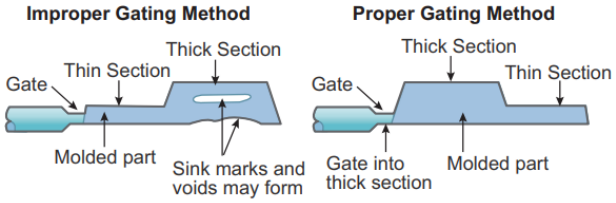

Figure 12- Ideal gate location [6]

2.3.4. State of the art of electronic inserts in injection moulding

With the spread of IM in the world of manufacturing, there is a need to apply objects within plastic parts. These objects can be from many types, like metal parts, ceramic parts, optical devices or electronic components. In the case of this thesis, the focus is on the application of electronic components, since it will be studying the application of piezoelectric elements in the process of manufacturing active metamaterials by IM. In Table 2 are presented studies that focus on the integration of electronics components in the process of IM.

Table 2- Integration of electronics components in the process of IM

Bibliographic references	**Description**
Bakr et al. [65]	To study the integration of photovoltaic cells in plastic products, the author developed a study where the over-moulded process was used to demonstrate the viability of the idea. The study consists of a photovoltaic cell glued to a polyurethane thermoplastic and inserted in a mould to be submitted to the injection of PP. The reason for the previous application of polyurethane to only one surface of the cell is to guarantee the adhesion of the injected plastic to the photovoltaic cell, since the PP will fuse with the thermoplastic polyurethane. After some tests, it was concluded that the idea works well with great electronic efficiency by the cell.
Goument et al [66]	The most used plastic in IM to process electronic inserts is Polycarbonate. To find new promising materials and more environmentally friendly ones, the author has tested the viability of Polylactic acid (PLA) in over-moulding. Using a profile temperature on the injection machine, beginning in zone one until the nozzle of 160-190-200-210 °C, respectively, and screw speed of 56 rpm, it was proved the viability of using PLA in IM for mass production. PLA prove to be an approachable plastic to work with due to its easy adhesion to the electronics and easy conformability.

Table 2- Integration of electronics components in the process of IM (continued)

Bakr et al. [67]	To improve the reliability and the quality process of over-moulding flexible electronic components, ohm resistors were connected in different positions by a copper circuit, embedded in PI or PET, and positioned in a mould with two designs, a flat surface and a corner surface. After testing, it was concluded that the conductive adhesive is not a satisfactory solution to assemble electric components that will be subjected to injection moulding, since the components must be soldered to withstand the process. In terms of process parameters to inject PC, it was set a temperature of 100°C in the mould, a nozzle temperature of 300°C and a packing pressure of 400 bar. Enabling good adhesion of the PC with the components and a low presence of residual stress in the parts. Moreover, the author recommends the use of a glob-top (epoxy sealing used to protect chips from damage) to protect the over-moulded electronics from damage.
Bakr et al. [68]	In this study, researchers tried to over-mould electronic components under two different injection cycles. The first cycle, the nozzle temperature is 250°C, the mould 50°C, the injection pressure 562 bar and the injection time is 0.22 seconds. In the second cycle, the melted plastic had a temperature of 270°C, the mould 80°C, and an injection pressure of 451 bar with a time of injection of 0.46 seconds. From the test, researchers concluded that cycle number 2 promotes higher adhesion due to a higher mould temperature and lower stress on the components, because of the lower pressure applied. Moreover, authors also advised applying an underfill material before the injection process to give extra protection to the electrical sheet.
Schirmer et al. [69]	To evaluate the effect of stress on parts during injection, the author conducted research using chip resistors of 0402 and 0603 size applied in PET, PC/PBT and PC polymer sheets, in an injection process using PC as material. The sheet was positioned near the injection gate with electric components located at varying distances from the gate to study the effects of direction and length of the plastic flow. The chip resistors were fixed in the sheets using high-temperature adhesive to ensure stability during moulding. Analysing the results, it was concluded that components near the injection gate experience less stress and higher survival rates, because of lower velocity and viscosity in those spots. Longer melt flow paths subject components to higher mechanical stress due to increased values of cooling and viscosity, leading to failures. In addition, faster injection speeds mitigated component damage by reducing melt viscosity and stress. Recommendations include using protective measures like glob tops and underfills on the electronics.

Table 2- Integration of electronics components in the process of IM (continued)

Ott and Drummer [70]	To address the challenge of IM sensitive electronics with minimal stress while maintaining material integrity, the authors utilised thermoplastic foam to encapsulate circuit boards printed in an epoxy sheet with polyamide to analyse if it can produce strong bonding between the foam and the electronics, and excellent sealing properties for protecting electronics from external elements, such as corrosive substances. Specimens with different foaming degrees (0%, 10%, 20%, 30%, and 40%) were tested. Results showed that specimens with a 10% and 20% foaming degree achieved optimal performance. These samples had leakage rates (ability to encapsulate an electronic component) as low as 0.025 ml/minute, well below the acceptable limit of 0.5 ml/minute, and values of shear stresses on the electronics of 6.5 MPa. For higher foaming degrees (30%-40%), the formation of large pores led to a drop in shear stress and increased leakage, attributed to insufficient shrinkage compensation and reduced bonding surface. Microscopic analysis revealed that pore formation at the interface was a critical factor. For lower foaming degrees, small, closed pores enhanced bonding and sealing, while higher foaming degrees resulted in larger, elongated pores, which degraded performance. The results indicate that thermoplastic foam IM is a viable method for encapsulation of non-power electronics, providing a balance between stress reduction and mechanical integrity.

In conclusion, the studies show that over-moulding electronic components is viable for mass production when material compatibility and optimised process parameters are ensured. Mould temperatures (80–100°C) and barrel temperatures (280–300°C) enhance adhesion and reduce mechanical stress, while low temperatures increase the risk of defects such as delamination and poor bonding [64], [65]. Thermoplastics like PI and PC demonstrate effective adhesion with injected plastics under suitable conditions, which all depends on the compatibility between the injected plastic and the plastic of the electronic printed sheets. Mechanical stress, caused by low injection speeds, long flow paths, and inadequate mould designs, increases failure rates, necessitating high injection speeds and protective measures like glob tops and underfills [69]. Conductive adhesives are unsuitable, requiring soldered connections for reliability. Thermoplastic foam moulding effectively reduces stress and enhances sealing, with optimal foaming degrees (10%-20%), achieving strong mechanical and sealing performance. Sustainable materials like PLA also show potential for mass production due to good adhesion and ease of processing [70].

3. Over moulding of piezoelectric elements

3.1. Methodology

The methodology adopted can be described as an iterative process based on empirical observations and the application of scientific knowledge acquired through the literature review. The COMSOL software was employed to perform piezoelectric simulations, supporting the selection of the dimensions that the piezo should present to meet the objectives. Subsequently, injection moulding tests were conducted using the Demag Ergotech IntElect 50/330-10 injection machine to assess the influence of injection parameters on the over-moulding process of the piezo and to validate the selected mould design that was selected through a selection matrix. To perform injection simulations and draw conclusions regarding cavity filling, shrinkage, and warpage of the hosting part, the MOLDEX3D software was used. The simulations carried out in MOLDEX3D were validated in terms of their fidelity in replicating the injection process, through a comparative analysis of the results from simulations and the machine for a sequence of short shots.

3.2. Challenges

The injection moulding process is characterised by its ability to produce parts on a large scale with high repeatability, at a relatively low cost per piece. However, due to its nature involving thermal and rheological cycles, certain challenges may arise in manufacturing parts with desirable properties and geometrical restrictions, especially when incorporating mould inserts such as bonding fasteners, metallic ribs, and electronics.

Since piezoelectric elements are, by their nature, considered electronic components, several considerations can be established that will impact the feasibility of integrating them into a plastic part through injection moulding, in order to produce a metamaterial with acoustic properties.

The first anticipated challenge is the high temperature encountered by the piezo during the injection process. This concern is not with its structure, but rather with the welding connection between the piezo and the electrical components, as the materials typically used to bond electrical components have low melting points. Therefore, the injection temperature must account for both the polymer's transition temperature and the solder's melting point to maintain the structural connection during the injection phase, thus avoiding circuit inoperability. Moreover, the selection of solder based on its melting point is also a critical factor

to enhance the likelihood of the connection enduring the injection process. Table 3 indicates the common solder types used in electrical joints.

Table 3- Types of solder used in electrical joints and their respective melting range [71,72]

Alloy designation	Composition [wt.%]	Melting range [℃]
Sn–Bi–In	Sn–20Bi–10In	143–193
Sn–Zn	Sn–9Zn (eutectic)	198.5
Sn–Ag	Sn–3.5Ag (eutectic)	221
Sn–Cu	Sn–0.7Cu (eutectic)	227
Pb-Sn	Sn-65Pb	248
Pb-Sn	Sn-80Pb	279
Pb-Sn	Sn-98Pb	316

According to Table 3, a wide spectrum of melting temperatures is observed among solders, with cases containing lead (Pb) in their composition exhibiting higher melting points. Thus, it is reasonable to select a solder that contains lead. However, despite this clear advantage of solder containing lead over others, its negative impact on the environment may raise market availability problems [73], which can constrain the selection of the solder that best fits the injection moulding process.

The second obstacle identified is the high pressure exerted on the piezoelectric elements and electrical components. An injection moulding process features high pressures during its cycle to force the polymer into the mould to provide the desired component shape without any flaws or voids. In this sense, the high amount of pressure could damage the piezoelectric element by inducing cracks on its surface and detaching all the electric connections from its position. Furthermore, the possible fissures formed have the potential of being amplified due to the dimensional variation of the piezo, attributable to high temperature changes in the injection cycle. Therefore, it is important to develop a mould design that can counterweight the impact of pressure on the piezo integrity and, at the same time, stabilise the piezo in a fixed position to prevent it from moving and causing additional damage to it.

This task of finding a good solution that combines the ability to stabilise the piezo and mitigate the risk of cracks can be difficult to perform since the piezo nature makes it a challenge, I.e, a piezoelectric element is made of ceramics and therefore is considered a brittle material that is not able to absorb or deform significantly before fracturing. Moreover, the piezo must have a reduced thickness, ranging from 0.1 mm to 0.5 mm, because of the mechanical coupling between the polymer part and the piezo (a concept further explained in section 3.4). Therefore, one important conclusion reached is that the piezo surface must be fully supported on the mould interface, allowing an even distributed pressure over a larger area, preventing stress concentration, and enhancing the piezo survival rate.

Along with the mould design, multiple injection parameters also need to be balanced, creating a third obstacle to integrate the piezoelectric element into injection moulding. Regarding packing and injection pressures, these parameters can be adjusted to lower values, thus reducing the risk of damaging the elements. Although a cautious approach must be taken when

altering these values, because reducing them can lead to poor part filling and low material compression which, in turn, cause higher shrinkage and warpage rates, increasing the likelihood of piezoelectric failure during post-processing. In this context, the injection and packing pressures should be sufficient to fill and compact the polymer with the correct geometry, but not exceed this point to prevent component damage. In combination with these two parameters, the melt temperature must also assume a value that would not compromise the piezo integrity and melt the solder. Moreover, it needs to consider the temperature influence on the polymer viscosity to avoid two failures: excessive warpage (high melt temperature) and component detachment due to high viscosity that exerts a higher force on the piezo.

3.3. Host structure for piezoelectric integration

With the production of the metamaterial by injection moulding through over-moulding of a piezo, the second objective is to construct a panel that prevents acoustic energy from spreading between two regions. Given this feature, to achieve a reliable solution, each part with its respective piezoelectric element must have the ability to be assembled with each part to ultimately form a panel. This results in a solution that combines excellent tunable vibration reduction capabilities, potential for mass production, and applicability in real-world contexts.

Therefore, the polymer part that houses the piezo must be capable of allowing the part to be assembled and disassembled multiple times without developing fatigue cracks. Additionally, the mechanical design of each housing part must enable bending movement without significant restrictions in the horizontal position, to ensure the structure possesses vibration modes at lower frequencies, where the traditional solutions using mass addition and isolation materials have difficulties in preventing acoustic transmission.

Although one solution with resembling characteristics is already in the literature [4], which follows the same principle of using a host structure with a metamaterial to form a panel that blocks acoustic transmission in lower frequencies, the innovative solution proposed in this study overcomes this solution in multiple ways. First, and most importantly, in the present study with the introduction of piezoelectric elements on a host material to function as a metamaterial allows the self-tunability to counterweight sound propagation in any frequency spectrum, standing out from [74] where the stop band effect is only verified at 155 – 160 Hz. Second, the production time to manufacture one panel will be reduced by using injection moulding, instead of thermoforming, which consumes more time to produce a panel of the same size. Third, by combining the benefits of using injection moulding with a new concept design, it enables the production of panels with variable sizes that can respond to any application, allowing for product customisation to any application without redesign.

To address the challenge of designing a host material with the described characteristics, as a starting point, a polymer part already developed in-house (Mecha(tro)nic System Dynamics (LMSD)) is used, which enable assembly into a panel [75]. In this way, the focus of this section is to describe and characterise the single parts that form this structure.

The part developed is illustrated in Figure 13 , and it is evident that the ring connection type is present on it. Normally, this type of connection is characterised by a spherical geometry that

enables part assembly. However, in this case, it was modified to a cylindrical shape to restrict rotation along the longitudinal axis. Moreover, four ribs (black arrow Figure 13) were also added at each corner of the part to prevent rotational movement along the cylindrical axis. Otherwise, the constraint between parts would not be fixed, compromising the stiffness required to ensure the structural integrity.

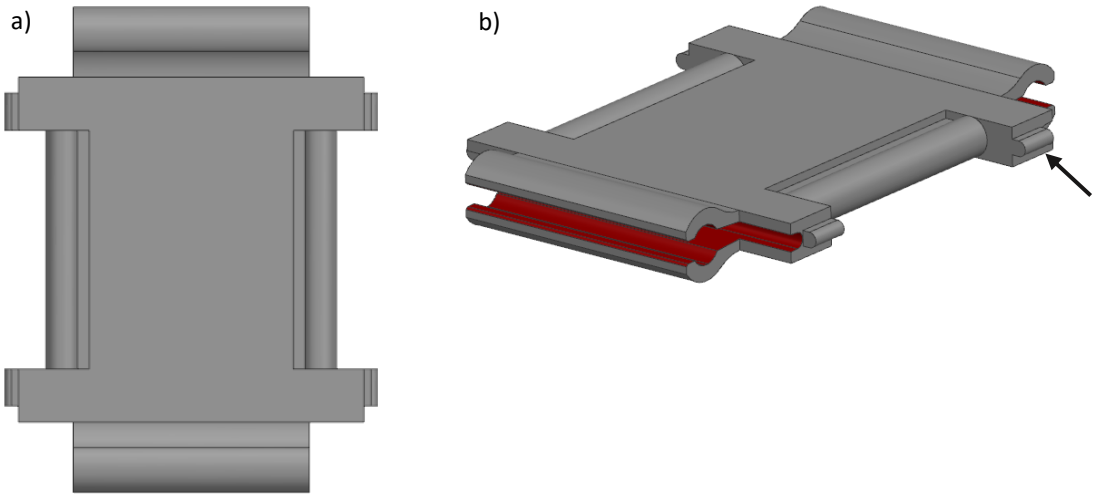

Figure 13- a) Polymer host part top view, b) Polymer host part perspective view

Another aspect taken into consideration was the force necessary to assemble and disassemble the multiple parts that constitute the panel. This parameter is important, since its value directly influences the part's life span during its utilisation, the user's convenience during assembly and disassembly cycles, and the panel integrity when subject to external forces in working conditions (the panel is for general applications, some safety margin must be considered). Excessive force can cause plastic deformation and cracks, while insufficient force may result in a poor fit and instability. Regarding the part lifespan, in this situation where polymers are used, what is more important is planning for a correct value. Unlike metals, polymers exhibit viscoelastic behaviour, meaning they can deform over time under stress and may not return to their original shape, causing poor fit in connections over time. Thus, a balance must be found between structural integrity and user convenience, in compliance with a force high enough to ensure that the panel remains secure under operational conditions.

To address the force condition, the connector design was based on Guo and Sun [76] findings. Since, as stated in their work, the dimensions of the female and male parts that constitute the connector have a direct influence on the disassembly force, when the cylindrical body radius is larger in comparison with its clamping connector, the force necessary to disassemble and assemble the part is higher because a continuous compression force is exerted on the cylindrical body, establishing a connection by interference rather than on geometric interlocking. Therefore, since the objective is to manufacture a panel where a balance between malfunction prevention and material fatigue is reached, the geometrical interlocking prevails over the interference connection. Leading to the clamping claws (Figure 14 a) having the same diameter as the cylindrical connector (Figure 14 b). With only the flat feature represented in red in Figure 14 b), it is fitted by interference to enhance the connection.

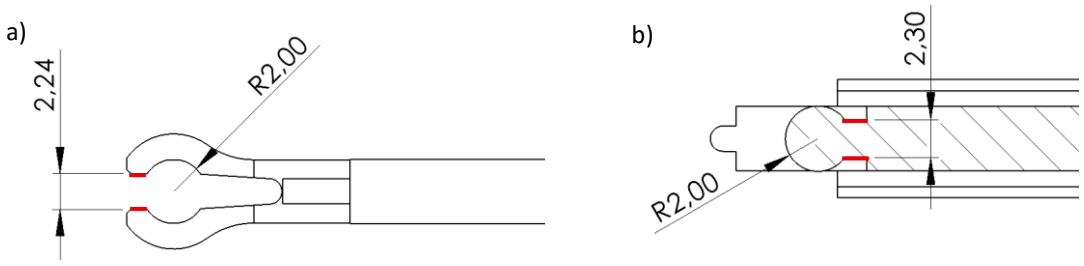

Figure 14- Connection section view, a) clamping claws, b) cylindrical connector

In the design, the opening angle described by the cylindrical feature during the assembly process, with larger angles being associated with higher coupling forces (Figure 15). Moreover, Figure 15 also confirms the appropriateness of selecting cylindrical snap fit connections over spherical ones, not only due to the previously discussed constraints on degrees of freedom, but also for the lower forces experienced by the connection during its assembly.

In Figure 15, Φ represents the opening angle on connection in rad, B the connector bending stiffness (equation 3), Rs the internal radius of the male part, and F the exerted force.

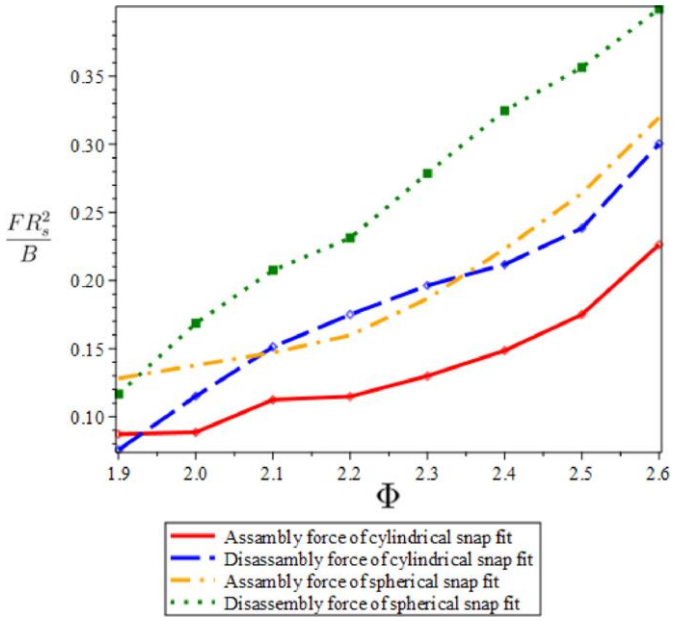

Figure 15- Opening angle influence on disassembly and assembly force, on a generic snap fit connection [76].

The part opening angle regards the engagement angle (Φ) represented on the connection in Figure 16. After measuring the angle (145.94°= 2.54 rad), it is possible to calculate the force following the next steps [76]:

$$B = \frac{Et^3 b}{12(1-v^2)} \qquad 3$$

Where B as stated represents the connector bending stiffness, t the clamping claw thickness and b its width.

Substituting equation 3 with the respective values (the material properties are from ABS, measured in house):

$$B = \frac{2240 \times 1^3 \times 26}{12(1 - 0.34^2)} = 0.0291\ N.mm^2 \qquad 4$$

From equation 4 result, using the equation 5 formula taken from Figure 15, and the respective Y-axis value that corresponds to the engagement angle (2.54 rad, Figure 16), the assembly force is calculated.

$$\frac{F \times R_s^2}{B} = 0.17 \cong F = \frac{0.17 \times 0.0291}{2^2} \cong F = 5.83\ N \qquad 5$$

Based on the assembly force results, F= 5.83 N is considered acceptable, particularly in the context of the panel application, in which simple and practical assembly improves the product.

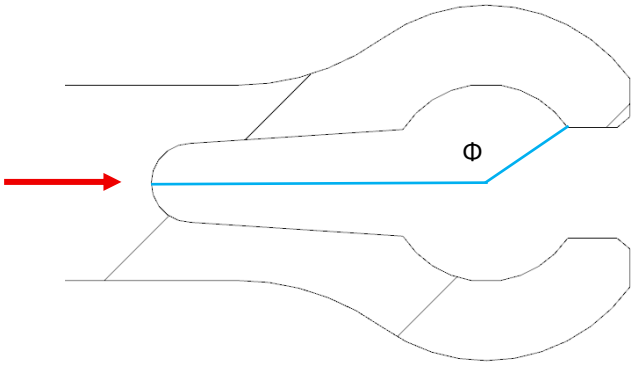

Figure 16- Opening angle of snap fit connection and the assembly force vector

3.3.1. Part manufacturing

As stated in the objective of the present study, this work aims to apply injection moulding to produce a panel incorporating piezoelectric elements. Throughout this subsection, focus will be placed exclusively on the manufacturing process of each component constituting the panel, excluding the integration of the piezoelectric element. The incorporation of the piezoelectric element into the injection process will be addressed in subsequent sections.

As previously discussed in the literature review, the mould represents a fundamental component of the process, and particular attention must be paid to its design to avoid defects during both the injection phase and demoulding. Traditionally, once a mould has been designed and machined, if it proves to be the source of defects in the injection-moulded parts, the potential for corrective modifications is significantly limited, given that the material is no longer in its raw form. In such cases, the mould may need to be entirely remanufactured. To mitigate this issue, reduce production costs, and make possible design modifications to the mould cavities as needed to facilitate experimentation with different geometries, thereby streamlining the production process, a versatile mould developed in-house at KU Leuven will be employed

in this project. The mould should be capable of accommodating two large inserts, which will serve as the cavity and sprue bushing. This construction allows for design modifications to be implemented with minimal resource expenditure, while also enabling the use of the same mould to manufacture a different range of parts. Therefore, the mould (Figure 17) is characterised cold cavities without any external heating, where the material is injected through a cold runner that allows the insert fitting on the fixed side (Figure 17 b) without occupying too much space, which is a more efficient setup to conduct low series experiments. Moreover, the mould is equipped with nine straight-drilled cooling channels on the moving half (Figure 17 a), and with eight on the fixed side (Figure 17 b) which, despite not allowing a perfect heavenly cooling across the part surface as unlike conformal cooling channels, the impact on the final product is minimal [77], as the maximum distance between any point on the part and the cooling system is only 5.9 mm. Concerning the demoulding action, the mould is provided with a pin injector matrix across the insert fitting surface, enabling the selection of which pins are activated during the injection phase, depending on the part geometry. The small diameters pins are responsible for pushing out the part, and the larger ones (red circles, Figure 17 a) for expelling the runner.

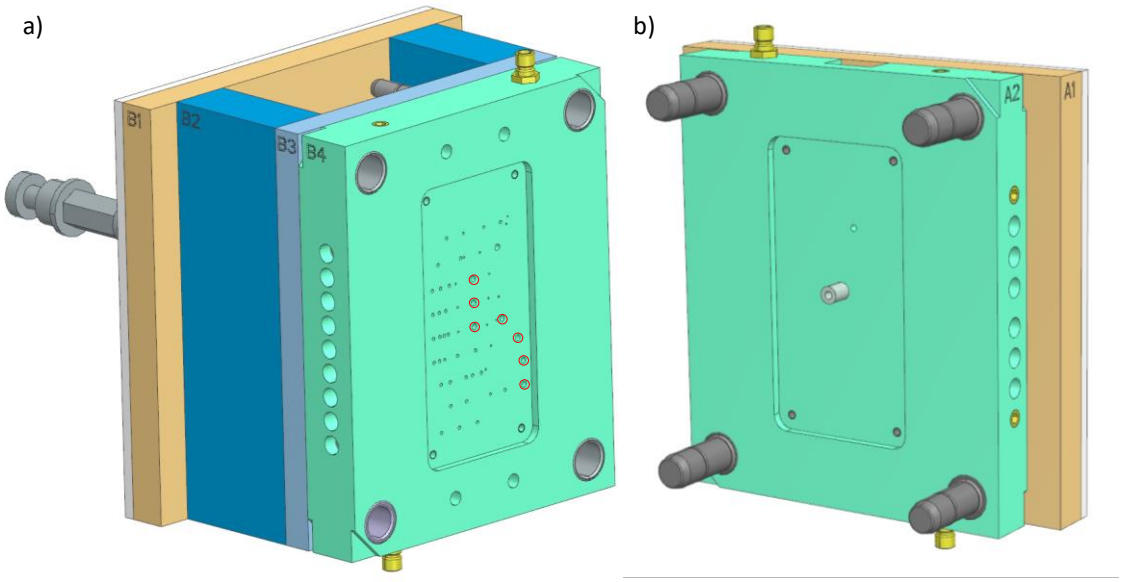

Figure 17- a) moving mould side, b) fixed mould side

The letter's identified in the preceding Figure 17 correspond to the mould components, as follows:

A1- Stationary clamping plate;

A2- Stationary side cavity retainer;

B1- Movable clamping plate;

B2- Support pillar;

B3- Ejector retainer plate;

B4- Movable side cavity retainer.

From that solid body, using Siemens NX software, it was possible to extract the two cavities that give shape to the part. However, although the cavity extraction process is carried out directly and in a single iteration, the presence of two clamping claws on the part results in the formation of an undercut. This geometric feature leads to the need to implement a mould system that enables both the moulding and a straightforward demoulding action of the clamping claws. As previously mentioned in section 2.3.1, the strategy traditionally adopted to allow the production of parts with undercuts involves the integration of rods, hydraulic systems, or electric actuators that drive a slide mechanism. Thus, enabling the desired part to be produced with the required quality, without the need for post-processing.

Nevertheless, this type of solution requires a three-plate mould configuration, which increases both the complexity and the cost of the tooling. In addition, due to polymer shrinkage and warpage during cooling, there is a risk of the material adhering to the sliding surfaces making the part prone to cracks during demoulding because of tear-off stresses. Since the mould used in this project does not support three-plate configurations due to its structural design, the current state is not mass production, and process complexity could increase due to material shrinkage-related problems. An alternative solution was adopted by involving the integration of inserts (Figure 18) within the mould insert itself, enabling the manufacture of the clamping claws without any actuation system. Since these inserts are ejected along with the part during demoulding, only a simple post-processing operation is required to detach them [75].

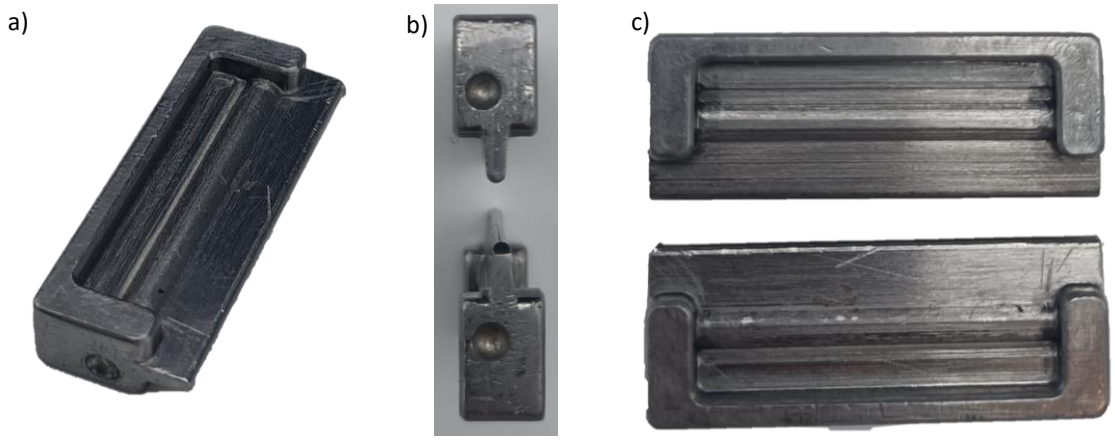

Figure 18- a) Demoulding insert perspective view, b) demoulding insert side view, c) demoulding insert top view

For the use of inserts to be effective in forming the geometry of the clamping claws without interfering with the normal operation of the mould, grooves must be machined into each half of the mould to accommodate the demoulding inserts. This configuration ensures a uniform filling of both cavities during the injection phase. As the moulded part must remain attached to the movable half of the mould upon opening, so that it can then be ejected automatically by the ejector pins, four spherical plungers (Figure 19) were incorporated into this half, two per demoulding insert. These plungers serve to prevent the inserts from causing the part to become trapped in the fixed half of the mould and also provide mechanical support during insert assembly. Since the plungers are internally threaded, their preload on the demoulding inserts can be adjusted using a dedicated tool.

Figure 19- Spherical plunger

With the objective of directing the polymer flow into the cavities, a trapezoidal runner was designed. Although this shape is not optimal when compared to a circular cross-section, as discussed in section 2.3.1, the trapezoidal profile allows the runner to be machined exclusively on the movable half of the mould. Consequently, the runner remains attached to this half upon mould opening, simplifying its removal during post-processing, as it remains fully connected to the part [75].

The gate it was positioned on the female surface where the clamping claws are fitted. This location was selected to ensure that any surface roughness resulting from gate and runner separation is concealed during panel assembly, as it will be covered by the inserted claw. A fan gate geometry was chosen to promote rapid and uniform filling of the entire part [75].

The mould with the designed inserts is represented in Figure 20.

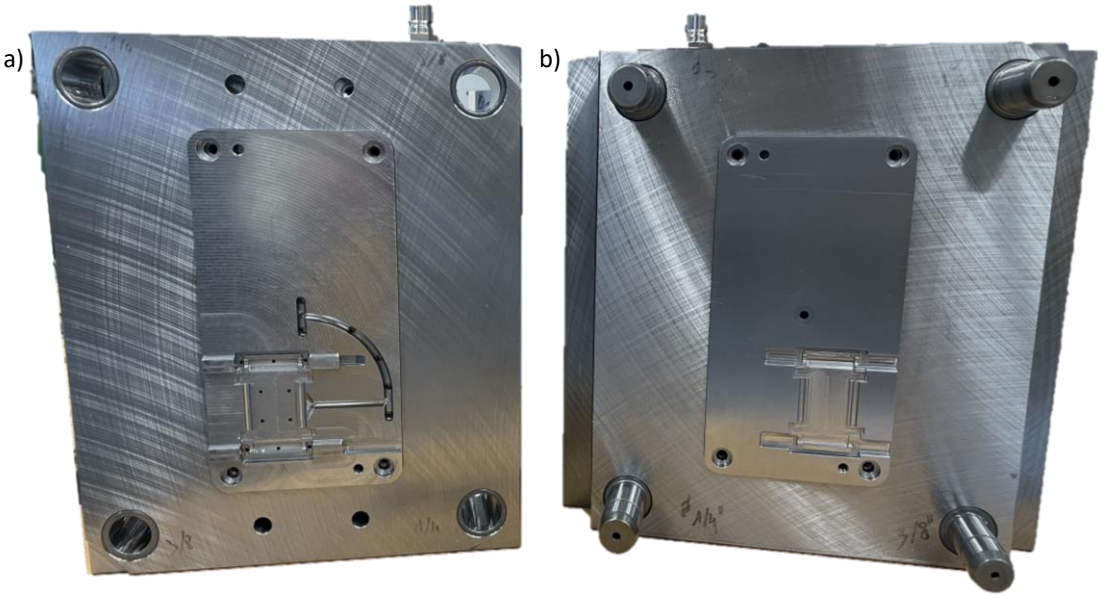

Figure 20- a) Moving and b) fixed mould halves with the respective inserts [75]

3.3.2. Material Selection

To select the most suitable material, a selection table was prepared to identify which option best fulfils the defined requirements, following the Ashby method [78]. As mentioned throughout this section 3.3, the chosen material must be easy to process by injection moulding, thereby avoiding production issues and defects in the manufactured parts. This requirement is crucial, as a high level of repeatability is needed to ensure that no vibration discretisation problems occur. Two other important characteristics that directly influence production repeatability are shrinkage and warpage, both of which should remain as low as possible.

Furthermore, the material should provide adequate mechanical strength, combined with the ability to undergo repeated elastic deformation during assembly, without risk of fracture.

To carry out the selection process, first an exposition of the polymers must be done, next the properties regarding each polymer haves are ranked based on their importance in the project. For that, to each property, a weight is established and then normalized on scale of 0 to 1 and with these normalized values, a final score is calculated and the material is chosen. Thus, by consulting the literature, in Table 4, it can be found polymers that are typically used in injection moulding and their respective properties.

Table 4- Polymer properties for selection purposes [79,80]

Material	Processability via injection moulding	Young's modulus [GPa]	Shrinkage [%]	Price [€/kg]	Flexural strain [%]
Polymethyl methacrylate (PMMA)	Acceptable	2.24- 3.24	0.4-0.74	3.59	2-5.5
Acrylonitrile butadiene-styrene (ABS)	Perfect	1.9- 2.7	0.5-0.8	2.01	15.3-20.9
Polycarbonate (PC)	Acceptable	2.1-2.4	0.5-0.7	2.99	110-150
polypropylene (PP)	Perfect	1.37-1.58	1.4-1.96	1.57	52.1-232

Next, according to Ashby [78], a weight from 0 to 1 is attributed to each property in compliance with its importance on the panel part (Table 5).

Table 5- Weight attribution for each attribute

Property	Processability via injection moulding	Young´s modulus	Shrinkage	Price	Flexural strain
Weight (w_i)	0.3	0.1	0.3	0.1	0.2

Both processability via injection moulding and shrinkage were assigned the highest weighting, due to their significant impact on the quality of the final part. If the manufacturing process is not straightforward, defects such as short shots, uneven shrinkage, sprue sticking to the mould, or flashing, may occur. These issues often require halting the machine to readjust processing parameters, which in turn reduces process efficiency. Moreover, such defects compromise the repeatability of the produced parts, potentially causing acoustic issues since the components may not behave dynamically in the same way.

Flexural strain was given the second-highest weighting, as it is crucial that each panel part can be assembled by interlocking, which requires the material to withstand repeated elastic deformation without failure. Regarding the Young's modulus, a relatively low weighting was assigned, since this property does not significantly vary among the polymers under consideration. Similarly, cost was also assigned a low weighting, given that polymers in general are relatively inexpensive materials. Continuing the process, the Ashby procedure dictates to normalise each attribute on a scale from 0 to 1. To do it, the next two equations are used:

$$u = \frac{x - x_{min}}{x_{max} - x_{min}} \qquad 6$$

Equation number 6 is used when the attributed subject to normalisation must have its property value as high as possible. On another hand, when the property value must be as low as possible, equation 7 must be used.

$$u = \frac{x_{max} - x}{x_{max} - x_{min}} \qquad 7$$

In both equation 6 and equation 7, x_{max} represents the highest property value along all the polymers, and x_{min} the lowest. x stands for the property value to be normalised.

Since in Table 4 some properties present a range of values, for each one the highest value is considered for normalisation purposes. And in the case of the attribute processability via injection, because it is a qualitative classification, 0.7 and 1 values are assigned to acceptable and perfect, respectively.

Finally, once all attributes are normalised, their respective scores are calculated using equation 8, and the attribute with the highest score is chosen

$$Score = \sum u_i \times w_i \qquad 8$$

Table 6- Material selection based on the obtained scoring results

Material	**Normalised attribute values**					**Score [%]**
	Processability via injection moulding	Young´s modulus	Shrinkage	Price	Flexural strain	
PMMA	0.7	1	0.968	0	0	60.40
ABS	1	0.675	0.921	0.782	0.080	73.80
PC	0.7	0.494	1	0.297	0.637	71.65
PP	1	0	0	1	1	60

Analysis of Table 6 reveals that ABS and PC present comparable final scores. Nevertheless, ABS attains the highest value, which justifies its selection. Therefore, ABS is the material used in the next steps of the process of over-moulding the piezo by injection moulding (Annex A).

3.4. Choice of piezoelectric elements for integration

Throughout this section, the characteristics of piezoelectric elements and the influence of the attachment method used to mount them onto structures will be examined, and their impact on the vibration reduction.

3.4.1. Piezoelectric metamaterial performance criteria

In the panel structure, the piezoelectric element is responsible for actively counteracting the sound vibrations induced into the panel. Thus, the coupling capability between the piezoelectric element and the panel must be as high as possible, so that the piezoelectric element can absorb the vibration with higher efficiency and, therefore, create a wider stop band effect. In this way,

scientists developed a factor known as electromechanical coupling to assess the energy transfer efficiency of a host structure to a piezoelectric element, determining the system's operational feasibility. This factor configures an important performance criterion that needs to be considered when selecting the piezo that's used in the panel.

Moreover, the calculation of this factor permits the exploration of multiple solutions involving different piezo configurations in each injected part, with a standard that can be compared. Configuring an important guideline for piezo applications, since its assembly nature in the part also influences its performance. This means that numerous configurations need to be tested to find which piezo best suits the panel function, leading to important restrictions that must be followed during the piezoelectric element selection and application in the injection process.

Since the nature of a piezoelectric element is the conversion of mechanical deformation applied to it into voltage, or vice versa, the method normally used to assess its coupling factor with a host structure involves energy measures using capacitance registrations to quantify the energy conversion involved. First, with one terminal grounded and the other connected to a high impedance circuit, configuring an open circuit layout, a force is applied to the piezo to deform it, building up an electrical energy potential that the piezo stores, much like a capacitor (path a to b in Figure 21). With the piezo deformed, making its terminals short-circuited, the energy will flow along the piezo body between its poles, lowering its stiffness since the piezo is being discharged, but maintaining its deformed position (path b to c in Figure 21), until eventually all the current flows and after released the piezo gets back to a non-deformed position (path c to a Figure 21) [81,82]. With this step sequence, it is possible to calculate the coupling factor using the following formula:

$$k_{ij}^2 = \frac{U_{conv}}{U_{OC}} = \frac{U_{OC} - U_{SC}}{U_{OC}} \qquad 9$$

With k_{ij}^2 representing the coupling factor, U_{conv} the portion of electrical energy that is converted to mechanical energy, U_{OC} the energy stored in the piezo in open circuit, and U_{SC} the mechanical energy in short circuit.

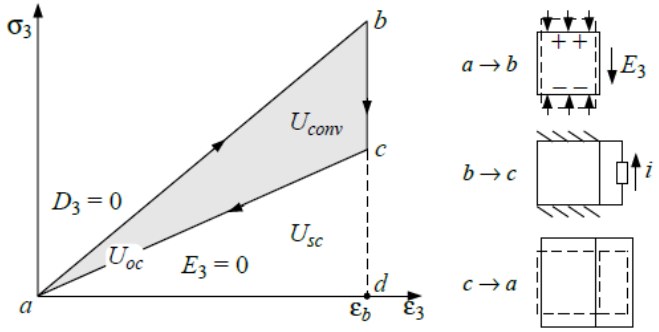

Figure 21- Energy cycle of a piezoelectric element when deformed [81]

Based on equation 9, the capacitance can be measured as a way of quantifying the energies present in the Figure 21 cycle. However, when it comes to cases where piezos are subjected to applications involving vibrations, such method can produce inaccurate results. Because

vibrations can produce uneven deformations along the piezo. Resulting in an equation where the piezo volume is taken into account [81]:

$$k_{ij}^2 = \frac{U_{OC}^{max} - U_{SC}^{max}}{U_{OC}^{max}} = \frac{w_{OC}^2 - w_{SC}^2}{w_{OC}^2} \qquad 10$$

Where k_{ij}^2 represents the coupling factor, U_{OC}^{max} the maximum value of energy stored in the piezo in open circuit, $U_{SC}^{max}$the maximum value of mechanical energy in short circuit, w_{OC}^2 the piezoelectric element resonance frequency in open circuit, and w_{SC}^2 the piezoelectric resonant frequency in short circuit.

3.4.2. Parametric study on the optimal piezoelectric element dimensions

Knowing the factors that influence the coupling factor of the piezo in the hosting structure, it becomes crucial to determine their impact on the coupling factor of a piezo assembled in the panel, and which piezo dimensions best suit the application proposed in this study. To access this information, it is necessary to simulate multiple conditions involving the polymer part's solid mechanics and the piezo solid mechanics, in compliance with electro-mechanical interactions between the polymer part and the piezoelectric element. Thus, to carry out the simulations by FEM, the software COMSOL Multiphysics was selected.

With the polymeric component designed and imported into COMSOL Multiphysics, the piezoelectric element was modelled on the parts body as an independent body (Figure 22). Care was taken to parameterise its dimensions using variables, enabling the integration of COMSOL with MATLAB to allow the execution of multiple simulation runs across different parameter sets. In the initial setup, the piezoelectric element was assigned a length of 36 mm, a width of 20 mm, and a thickness of 0.1 mm. These values were selected to maximise the available surface area on the host structure for piezoelectric integration. A larger piezoelectric area allows for more effective tracking of the structural deformation across multiple vibrational modes, thereby enhancing the electromechanical coupling efficiency. A low thickness was intentionally chosen to ensure the piezoelectric element conforms evenly to the deformation of the host polymeric substrate, minimising the introduction of additional stiffness and avoiding disruption of the natural dynamic behaviour of the structure.

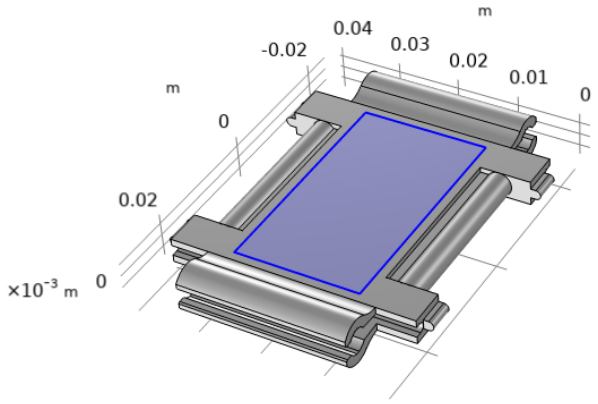

Figure 22- Piezoelectric element (blue body) integrated on the panel part

With the piezo modelled, there was a need to reconfigure the polarisation direction associated with its body. By definition, the program sets the polarisation direction in the Z direction. However, after importing the panel part and the piezo inclusion into COMSOL, its thickness now spaces along the Y direction, not matching the predefined polarisation direction. Therefore, given that piezos are characterised for the internal charges flowing along the thickness, in the sketching plane that gave rise to the piezo, the cartesian plane was rotated for the piezo thickness to match the predefined polarisation direction (Figure 23).

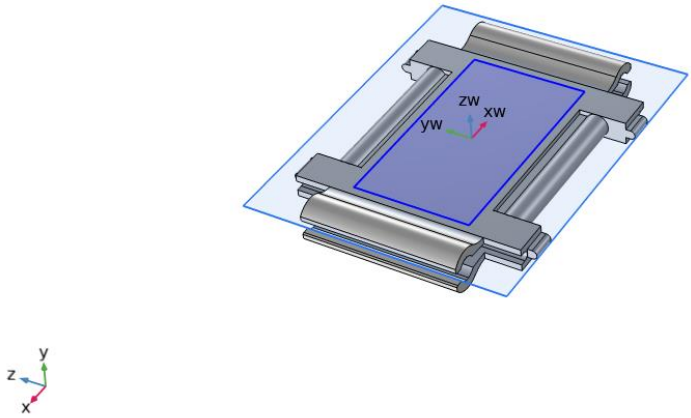

Figure 23- Cartesian plane system rotation in the direction of the polarisation orientation

By defining the geometries, material properties were assigned to the panel part (ABS) and to the piezoelectric element: PZT-5A. PZT-5A was selected as the piezoelectric material as it is one of the commonly used materials for this application. The material properties in Table 7 for both components were sourced from the COMSOL material library, apart from the Young's modulus and Poisson's ratio for ABS, which were modified according to the manufacturer's datasheet for the specific ABS used in the injection moulding process.

Table 7- ABS and PZT-5A material properties defined in COMSOL, from its library

Materials properties					
ABS			PZT-5A		
Property	Value	Units	Property	Value	Units
Density	1190	[kg/m³]	Density	7750	[kg/m³]
Young's modulus	2240	[MPa]	Young's modulus matrix (Voigt notation)	{1.20346e+4, 7.51791e+4, 1.20346e+5, 7.50901e+4, 7.50901e+4, 1.10867e+5, 0, 0, 0, 2.10526e+4, 0, 0, 0, 0, 2.10526e+4, 0, 0, 0, 0, 0, 2.25734e+4}	[MPa]
Relative permittivity	3		Relative permittivity matrix (Voigt notation)	{919.1, 919.1, 826.6}	
			Coupling matrix (Voigt notation)	{0, 0, -5.35116, 0, 0, -5.35116, 0, 0, 15.7835, 0, 12.2947, 0, 12.2947, 0, 0, 0, 0, 0}	[C/m²]

With the materials implemented, the next step was the attribution of the type of physics involved in each body. The panel part was defined as solid mechanics, and the piezo as solid mechanics and electrostatics. Subsequently, the boundary conditions for both Solid Mechanics and Electrostatics were defined.

For the Solid Mechanics interface, an identity boundary pair condition was applied between the piezoelectric element and the polymeric panel, ensuring that both domains behave as if they are bonded, thus simulating the embedding of the piezo element due to the injection moulding process. As each panel component will be mechanically connected to the others during assembly, a fixed constraint condition must be applied to the clamping claws. Logically, based on the assembly configuration, a fixed constraint should be imposed on all four clamping claws of each individual part. However, since the present study focuses on vibrations, it is only relevant to analyse acoustically significant bending waves. As a result, when an acoustic wave strikes the panel, which has a large surface area but is thin, the resulting deformation is predominantly bending, due to the differential pressure applied by the oscillating air particles. Moreover, the type of piezoelectric elements used in this study accumulates charge primarily under bending deformations. For these reasons, the analysis is restricted to cases of pure bending, which occurs when a structure is clamped at one end and subjected to a constant bending moment. Consequently, only a single fixed constraint must be applied to one of the clamping claws.

When choosing the surfaces of the clamping claw to which the fixed constraint condition should be applied, careful consideration must be given to the selection of the surfaces that are assumed to be clamped. This is because the designed joint relies on interlocking rather than mechanical interference. Consequently, not all surfaces of the claw, once clamped, actively contribute to preventing rotational movement (a critical condition in the case of pure bending). As shown in Figure 24 a), the circular surface (pointed by green arrows) only restricts longitudinal and transverse motion, therefore, the prevention of rotational movement is ensured exclusively by the other contact surfaces, pointed by orange arrows in Figure 24 b), when assembled with the other part (region where they are going to fit marked by yellow arrows). Accordingly, the surfaces to which the fixed constraint condition was assigned are those illustrated in blue in Figure 25.

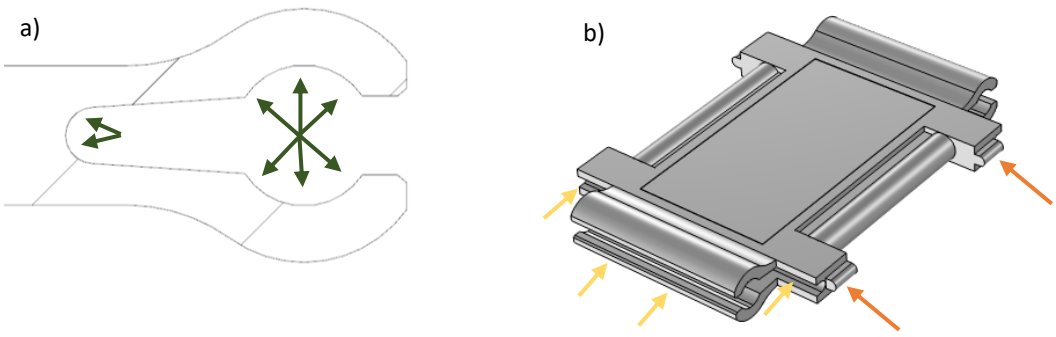

Figure 24- a) female claw side view, b) polymer part with its respective connector points marked

In contrast to other FEM software, in COMSOL, the selection of whether the study is dynamic or static is not made generically. To define it, it needs the specification of some initial

conditions, such as the initial velocity and displacement. Since a static analysis was performed, both conditions were defined as zero in the multiple Cartesian directions.

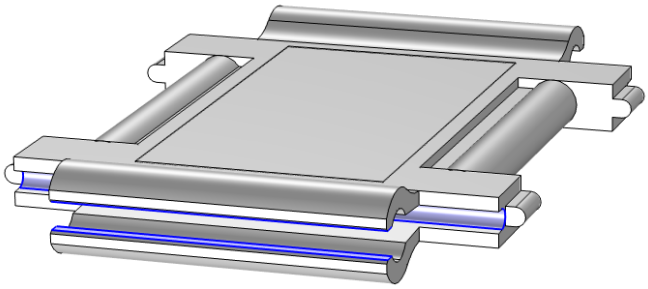

Figure 25- Representation of the fixed constraint on the polymer part with the piezo

Regarding the electrostatic conditions, as expected, only the piezoelectric element was assigned such physical properties. Specifically, all surfaces of the piezo were defined to have zero electric potential at the start of the simulation. In addition, the charge conservation condition was applied to the piezo body, enabling it to store electrical energy when subjected to deformation. Furthermore, since one of the objectives is to determine the modal coefficient, and its calculation requires the determination of the eigenfrequency through two FEM simulations, one under open-circuit conditions and another under short-circuit conditions, appropriate boundary conditions were applied. The floating potential condition was assigned to the upper surface of the piezo (one electrical pole), (Figure 26 a), while the ground condition was assigned to both the lower surface (second electrical pole) and the top surface, (Figure 26 b). Thus, for short-circuit simulation, the floating potential condition is suppressed. For open-circuit simulation, the software overrides the floating potential over the ground condition on the top surface, enabling the required simulation to be performed.

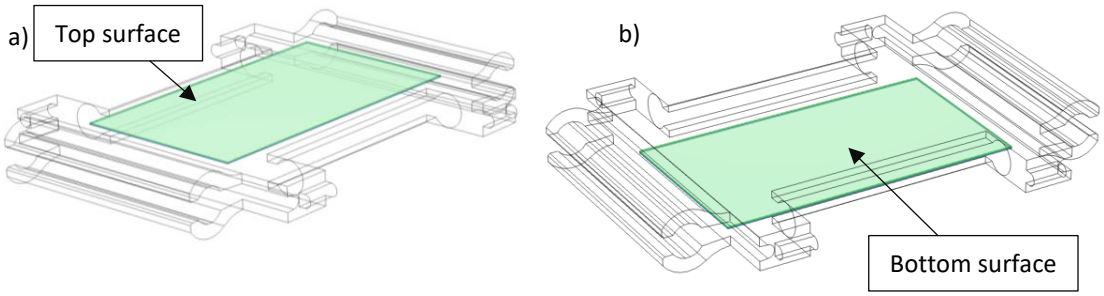

Figure 26- a) Floating potential and ground condition on the piezo top surface, b) ground condition on the piezo bottom surface

Due to the presence of the polymer part and the piezo, two separate meshing strategies were applied. For the piezoelectric element, which is extremely thin (0.1 mm), shell-type elements should be used, as these are specifically intended for thin structures. A free quad mesh generator was selected, producing a quadrilateral mesh (Figure 27). This approach allows the distribution and orientation of the mesh to be customised by selecting the upper and lower edges of the piezo. However, when generated, this type of mesh is applied only to the top and bottom surfaces of the piezo, and not through its thickness. Therefore, a geometry discretisation technique using a swept operation was applied to the quadrilateral elements, resulting in a mesh distributed along the thickness of the piezoelectric element.

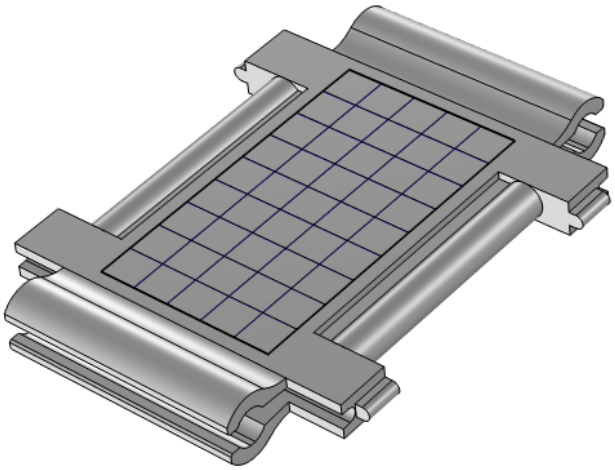

Figure 27- Piezo quadrilateral elements mesh

It should be noted that the distribution of quadrilateral elements followed a proportionality rule, defined as the ratio of the length to the width of the piezo, which in this case is 1.8. Consequently, for any given number of elements along the width, the length should be 1.8 times more. Maintaining this proportionality prevents element distortion, increases the accuracy of results, improves computational efficiency, and avoids mesh convergence issues [83]. Moreover, when it comes to the number of elements along the piezo thickness set with the sweep tool, three elements were defined because, when the piezo is bent, stresses range from the maximum value at the edges of the surfaces to zero at the neutral line at the centre. With the result being the piezo getting a mesh of stacked shell elements along its body (Figure 28).

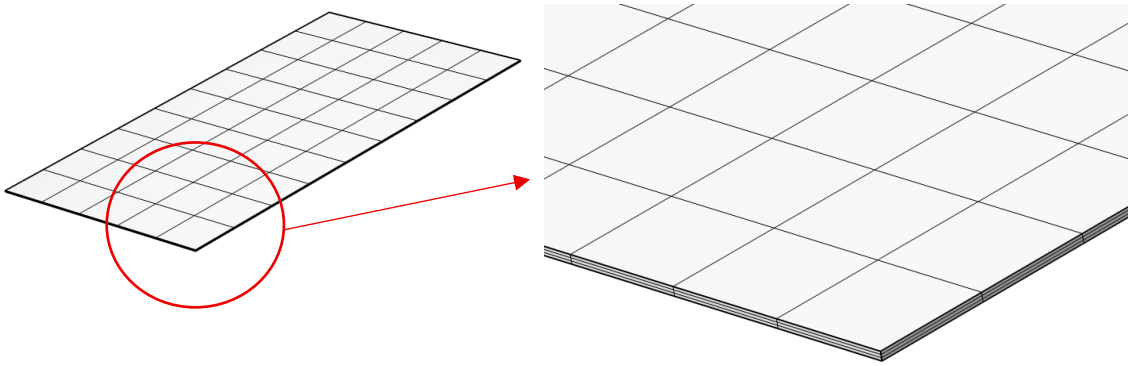

Figure 28- Three stacked shell elements along the piezo thickness with the sweep tool application

For the polymeric component, a tetrahedral element mesh was selected, as this type of element is well-suited for complex geometries. A basic optimisation level was applied during mesh generation to keep computational processing time low, with the additional constraint of avoiding inverted curved elements to prevent future issues in the simulation. Regarding mesh refinement and element size, an initial coarse element size was chosen to limit the total number of elements, to avoid high computational times.

As represented in Figure 29, despite the element size being defined as coarse, judging by its aspect, the element size seems proportional to the part dimensions.

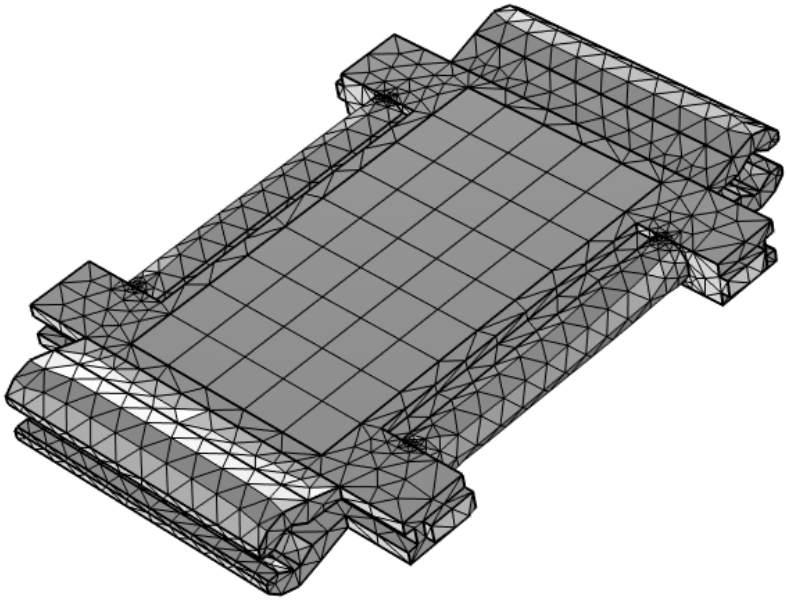

Figure 29- Panel part and piezo meshed

With the mesh and all the boundary conditions set, a first test was performed in open circuit and with an applied force (20 N), on the opposite edge of the fixed constraint, to evaluate if the simulation could run without any problems. In this particular simulation, the force was only applied in the part to provoke a higher electric potential. Otherwise, with only the piezo deformation caused by the eigenfrequency of the piezo plus the part, its electric potential would be reduced. The results shown in Figure 30 and Figure 31, and the displacement for the first vibration mode in Figure 32, without the 20N force load.

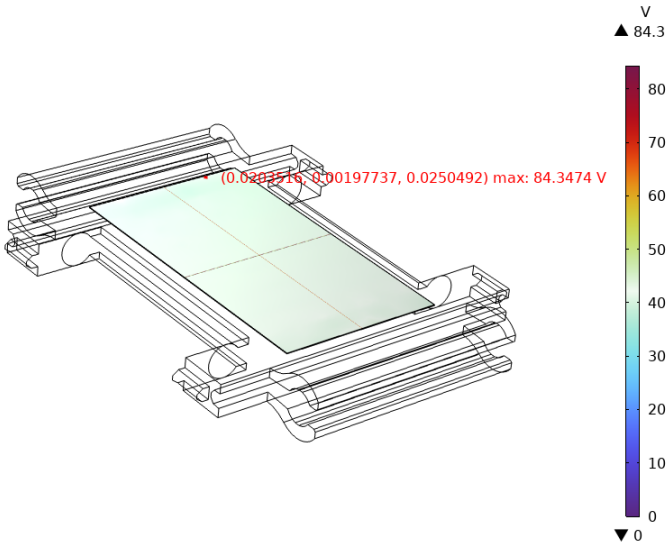

Figure 30- Electric potential accumulated in the piezo due to its deformation

From the analysis of the results, the maximum recorded electric potential was 84.34 V, with an average potential along the piezo of 43.02 V. As indicated by the coordinates of the maximum point, this location is at the upper edge of the piezo, close to the spot of maximum von Mises stress. This correlation is expected, as it is logical for the voltage peak to occur in this area.

Although a maximum electric potential value was identified, the value to be considered for the purposes of electrical potential is the average value across the surface (43.02 V). This consideration is valid because the maximum value represents the voltage of a single crystal within the piezoelectric element, and the disparity between maximum and average values can be significant.

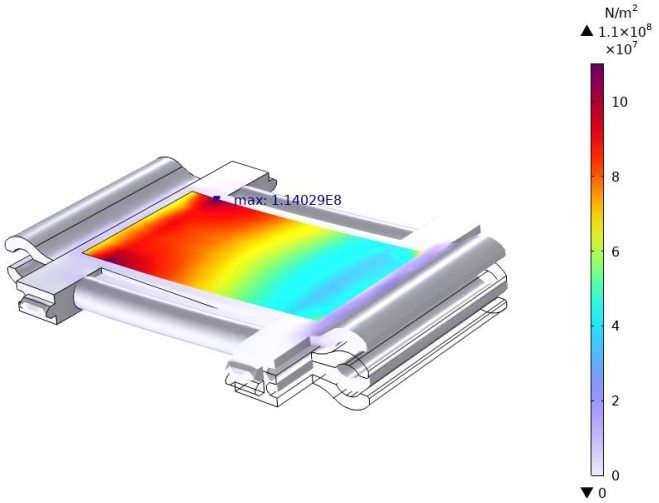

Figure 31- Von-Mises stress verified on the piezoelectric element

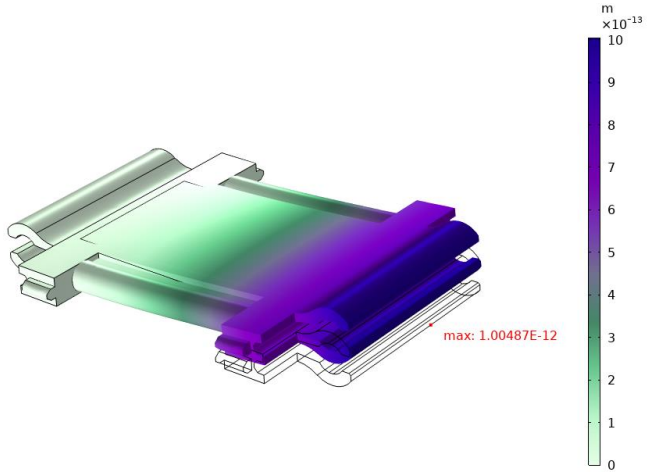

Figure 32- Part and piezo displacement due to its first vibration mode without force application

Regarding the maximum stress, it was expected that this would occur at the end of the piezo closest to the clamped boundary since, theoretically, this is the region where the bending moment is greatest. The fact that the maximum stress was instead located at the identified position is likely due to it being aligned with a sharp geometric transition (90° corner) in the panel part, creating a stress concentration zone that affects the piezo.

The displacement observed in the first vibration mode occurred at a frequency of 536.76 Hz. In this case, the study was conducted to determine the eigenfrequencies without applying the 20 N load used in the simulations for the electric potential and maximum von Mises stress. Preliminarily, it can be concluded that the design and characteristics of the selected

piezoelectric element are consistent with the defined objectives, as the pure bending vibration mode falls within the desired frequency range.

Following the preliminary results, a mesh convergence study was conducted to assess whether the chosen mesh configuration influences the accuracy of the results and to identify a mesh that offers an optimal balance between result reliability and computational efficiency.

Given that two types of meshes are involved, and that several parameters affect the refinement of each (part mesh size, piezo mesh size, and program default parameters), the process was divided into three stages. It should be noted that, for this convergence study, all simulations were performed under short-circuit conditions and without any applied load on the structure, considering only the computation of the structure's eigenfrequencies.

In the first convergence stage, the number of elements along the length, width, and thickness of the piezo, as well as the tetrahedral element size of the polymeric component, was kept the same as in the preliminary test. The only parameter varied was the mesh optimisation level, provided by the software's default settings (Table 8), to determine whether this parameter influences the results obtained across successive iterations in which the mesh optimisation level is progressively increased.

Table 8- Level of optimisation variation with focus on mesh convergence

Level of optimisation	First vibration mode [HZ]	Maximum stress [MPa]	Electrical potential [V]	Deviation first vibration mode [%]	Deviation maximum stress [%]	Deviation electrical potential [%]	Number of elements
Basic	536.26	39.8	4,42				19182
Medium	536.12	39.8	4,35	-0.26	0	-1.58	19784
High	535.96	39.8	4,5	-0.29	0	3.44	20112

From the analysis of the results in Table 8, it can be observed that the variation in mesh optimisation level automatically applied by the software does not have a significant influence on the results. The associated deviation between iterations, for both the frequency of the first vibration mode and the maximum recorded stress, remained below 1%. Only the electric potential showed an error greater than 1%, although still without any meaningful impact across iterations. Therefore, as the optimisation level does not affect the results, and considering that an increase in optimisation level also led to a higher number of mesh elements, likely due to the program's better mesh complex geometries, for the subsequent stages of the mesh convergence study, the basic optimisation setting was adopted, hence reducing computational time.

With the optimisation setting defined, the next step involves refining the size of the elements composing the mesh. Since the polymeric part is discretised with a tetrahedral mesh and the piezoelectric element with shell elements, the variation in element size must be carried out independently to separately assess the influence of each on the simulation results. The first step was to vary the size of the tetrahedral elements of the polymeric part with a constant growth rate of 1.4 (Table 9), successively refining them using the refinement levels available in

COMSOL: coarse, normal, finer, and extremely finer. If stabilisation of the results is not achieved, the element size will then be further reduced proportionally.

Table 9- Part mesh refinement to pursue mesh convergence

Refinement level	Max. size element [mm]	Min. size element [mm]	First vibration mode [HZ]	Max. stress [MPa]	Electrical potential [V]	Deviation first vibration mode [%]	Deviation max. stress [%]	Deviation electrical potential [%]	Number of elements
Coarse	5.49	0.988	536.26	39.8	4.42				19182
Normal	4.39	0.549	535.96	41.2	5.01	-0.55	3.51	13.34	42660
Finer	3.02	0.220	535.81	41.3	4.83	-0.27	-0.24	-3.59	100366
Extremely finer	1.98	0.088	535.04	41.6	4.84	-3.30	0.72	0.207	236342

From the analysis of Table 9, it can be concluded that the tetrahedral element size has already converged, based on the deviation values. The successive results show only negligible variations and, more importantly, the associated deviation remains consistently low. Consequently, it was not necessary to further reduce the element size. The next step is therefore the mesh convergence study for the piezoelectric element (Table 10), while keeping the tetrahedral element size fixed at the refinement level Finer. In this case, it is not possible to refine the piezo mesh by directly varying the minimum and maximum element sizes, since its construction was based on defining the number of elements along its length and width. Hence, mesh refinement is achieved by increasing the number of elements along these dimensions, which in turn reduces the element size. This increase follows the proportionality ratio of 1.8, as previously described.

Table 10- Piezoelectric element mesh refinement to pursuit mesh convergence

Number of elements along the length	Number of elements along the width	First vibration mode [HZ]	Maximum stress [MPa]	Electrical potential [V]	Deviation first vibration mode [%]	Deviation maximum stress [%]	Deviation electrical potential [%]	Number of elements
9	5	535.81	41.30	4.83				100366
18	10	533.48	4.12	8.84	0.20%	0.24%	0.11%	100411
27	15	533.24	4.16	13.00	0.06%	0.97%	47.06%	107645
36	20	533.19	52.0	16.80	0.01%	25.00%	29.23%	113901
45	25	533.11	56.5	20.30	0.02%	8.65%	20.83%	124009
54	30	533.09	62.7	22.08	0.00%	10.97%	8.77%	134804
63	35	533.00	65.8	24.08	0.02%	4.94%	9.06%	148956
72	40	533.00	75.4	26.50	0.00%	14.59%	10.05%	167200

In this final stage of the mesh convergence study, unlike the two previous steps, some variations in the results were observed across successive iterations (Table 10). With regard to the values of the first vibration mode, these remained stable. However, the other parameters varied with progressive refinement. This behaviour is expected, since refining the piezo mesh (responsible for the piezoelectric response) naturally affects both the electrical potential and the maximum stress, as the latter consistently occurs on the surface of the piezoelectric element. Although

the deviation in electrical potential and maximum stress did not stabilise below 5%, it can nevertheless be concluded that the mesh had already reached convergence prior to refining the piezoelectric element. This conclusion is supported by the significantly low errors observed between the results reported in Table 8 and Table 9. Furthermore, for the determination of the coupling coefficient, only the eigenfrequency values are required, values which showed no significant variation throughout the entire convergence study.

Therefore, it was decided that, for the subsequent simulations, the mesh configuration defined in Table 11 will be adopted.

Table 11- Converged mesh parameters

Polymer part refinement level	**Level of optimization**	**Number of elements along the length (piezo)**	**Number of elements along the width (Piezo)**	**Tetrahedral growth rate**	**Total number of elements**
Finer	Basic	18	10	1.4	100411

Using the converged mesh, next, the optimal piezo dimensions in the polymer part are defined to enhance the modal electromechanical coupling for the first bending mode. Moreover, as stated at the beginning of the present section, not only is it necessary to know what are the dimensions that the piezo must have, but also to understand what is the individual impact of each dimension (length, width, and thickness) on the coupling factor. Therefore, if it is found that each dimension does not impact with the same degree the coupling performance, some restrictions and priorities must be outlined when it comes to the mould design to over-mould the piezoelectric element.

Similar as done in Janssen et al. [84], to conduct the coupling factor analysis, four different studies were performed with the piezoelectric element placed at the centre of the part. For the first study, the thickness over the coupling effect was evaluated. Thus, the thickness is varied from 0.01 mm to 1.2 mm, respecting a resolution of 0.01 mm, and the length and width are kept at 36 mm and 20 mm, respectively, with COMSOL calculating the coupling factor for these piezo dimensions. The reason behind the choice of this thickness value range is completely arbitrary. However, the piezo thickness was intentionally kept small to minimise the introduction of additional stiffness, thus ensuring the piezoelectric element conforms evenly with the deformation of the host polymeric part, enhancing the coupling effect.

From the results in Figure 33, some considerations can be outlined. First, if the coupling factor is tracked while the piezo thickness is increasing, it becomes clear, that the coupling factor decreases, confirming that superior thickness values interfere with the stiffness of the polymer part, negatively impacting the coupling factor and the polymer part's natural dynamic behaviour. If an analogy between a thick piezo with a brick embedded on a polymer object is made, on an attempt to bend the polymer part, naturally, the result would be the polymer deflection and the brick keeping still due to structural stiff differences, which, in the piezo case, prevent energy storage impairing the coupling factor. For this reason, the piezo must have the lowest possible thickness. The second consideration that the study also demonstrates is a

higher coupling factor for a piezo thickness of 0.05 mm, classifying it as the optimal thickness. However, this value cannot be considered because after a search through suppliers, a piezo with this thickness is not commercially available. Moreover, during injection, integrity problems may arise. For this reason, for the next simulations, after evaluating the optimal length and width and for the course of the project, 0.1 mm was the chosen thickness.

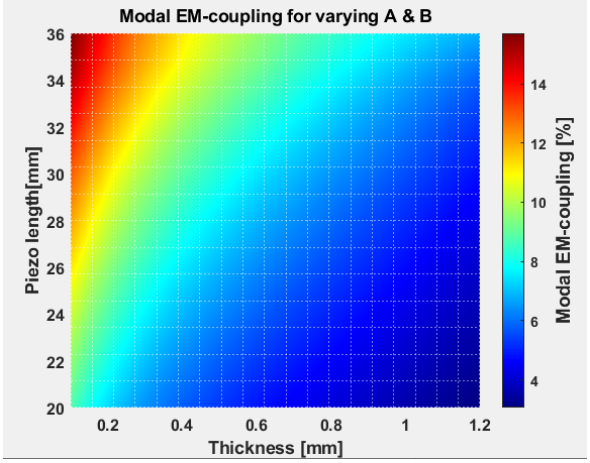

Figure 33- Impact evaluation of the piezo thickness on electro-mechanical coupling

With the optimal thickness found, to find the length and width that best suit the piezo, three more simulations were performed. On the first one, the length was varied between 10 mm and 36 mm, alongside the width from 10 mm to 20 mm. This spectrum of values was selected based on the dimension of the part surface where the piezo will rest (38 mm x 23 mm) leaving a material gap of 1 mm and 1.5 mm, respectively, not to interfere with the part's claw function. From the simulation and analysis (Figure 34), it becomes clear that the optimal length and width to produce a higher coupling effect should be 36 mm and 20 mm, respectively. With the coupling factor increasing with the increment of the dimensions, possibility due to the piezo being more sensitive to the part bending for the first vibration mode, converting more mechanical energy into electrical, thus enhancing the coupling factor.

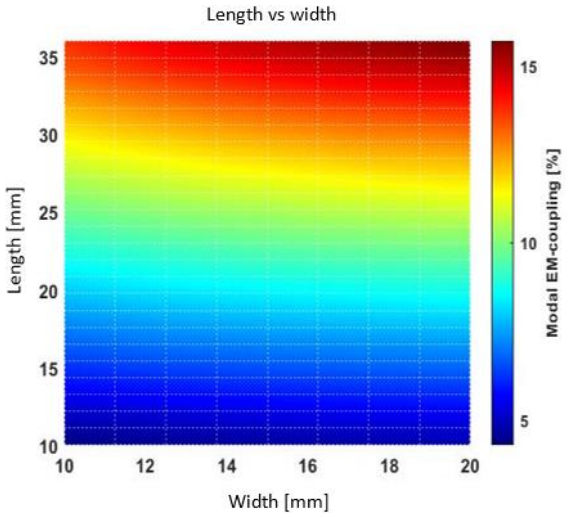

Figure 34- Impact evaluation of the width vs the length on the electro-mechanical performance

Although the preceding simulations determined the optimal piezoelectric dimensions, it is still necessary to understand if the length and the width have the same degree of impact on the coupling effect. Thus, two more sets of simulations were performed (Figure 35 and Figure 36), in which the width is varied along with the thickness and the length with the thickness. Permitting to conclude that, with the clamping position adopted, the length variation has more impact than the width on the coupling performance. The explanation beyond this effect is probably a consequence of the bending direction, since, for the first vibration mode, the pure bending occurs along the piezo length. Therefore, a higher piezo length makes the distance from the fixed point to the end of the opposite piezo edge bigger, increasing the bending moment on the piezo and thus, the piezo deflection. In turn, a higher piezo deflection makes a piezoelectric convert more mechanical energy into electrical energy.

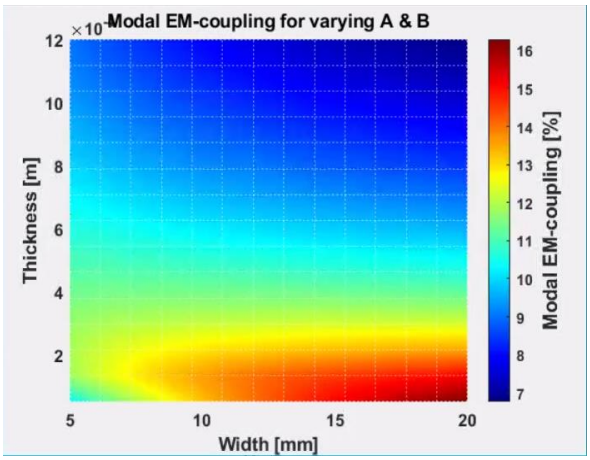

Figure 35- Impact evaluation of the width vs thickness on the electro-mechanical performance

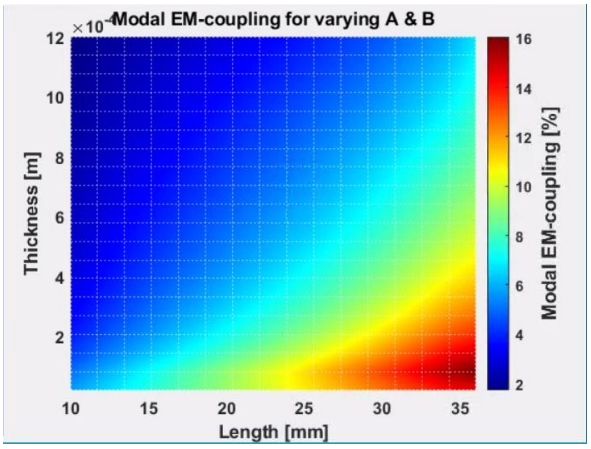

Figure 36- Impact evaluation of the length vs thickness on the electro-mechanical performance

In conclusion to the parametric study, as initially proposed, it was possible to determine the optimal dimensions of the piezoelectric element required to achieve a higher coupling effect. These dimensions are defined by a length of 36 mm, a width of 20 mm, and a thickness of 0.1 mm. The results demonstrate that the coupling factor increases with both length and width; however, priority should be given to the length of the piezo, as this parameter has a more significant impact on the coupling effect compared to the width. Therefore, in the following

section, which focuses on the design of various solutions for over-moulding the piezo, if it becomes necessary to adopt dimensions other than the optimal ones, the length should be changed as little as possible, while allowing greater flexibility in adjusting the width. With respect to thickness, the results indicate that it should be kept as low as possible, with the final value fixed at 0.1 mm. However, when consulting available piezo suppliers, it was not possible to find any option with a thickness of 0.1 mm for the optimal length and width dimensions. The smallest thickness available for these dimensions was 0.22 mm. Therefore, the selected piezoelectric element will adopt the following dimensions: length of 36 mm, width of 22 mm, and thickness of 0.22 mm.

3.5. Mould solutions development to over-mould the piezo

Along this section, the thesis focuses on achieving the best mould design to over-mould the piezo using injection moulding. To accomplish the objective, multiple solutions are designed and compared, exploring their strengths and weaknesses, culminating in one final solution. To support the development, mould flow simulations and in-situ tests are performed.

3.5.1. Design considerations

The process of over-moulding the piezo cannot be classified as a straightforward procedure of simply placing the piezo inside the mould and injecting the polymer. In addition to the inherent challenges of the process itself and the fragility of the piezo, as previously explained at the beginning of this section, the piezo must also be connected to an external synthetic inductance circuit after it has been integrated on the panel. Only in this way can the piezo be programmed to exhibit tunable resonant properties, and ensure that each panel component, and therefore the assembled panel, behaves as a locally resonant piezoelectric metamaterial.

For this reason, and since the piezo will be fully surrounded by polymer after injection, the injection process must also incorporate an embedded electrical connector that allows the electrical connection to the external inductance synthetic circuit, as well as two electrical cables to connect each pole of the connector to the corresponding pole of the piezo. In this way, once the part is demoulded, no additional post-processing will be required, and each unit will already be ready for commercial use. Hence, contributing to process efficiency and amplifying the concept of mass scale. Consequently, within the injection process, three elements must be placed inside the mould to be over-moulded: firstly, the piezo with the dimensions defined in the previous section, secondly, an electrical connector, and thirdly, two electrical cables to provide the connection between the connector and the piezo.

Knowing the components to be integrated into the mould to over-mould it, the initial mould insert geometry, and incorporating the lessons learned from the parametric study in determining the optimal piezo dimensions. In the following Table 12, some considerations and restrictions are presented that must be followed.

Table 12- Mould design constraints

Design constraint	Description
Only minimal modifications/changes can be made to the hosting polymer part	Since each polymer part that will host the piezo is designed and operates effectively all together in forming a panel, the design modifications executed to host the piezo must be minimal, not impacting the normal functioning of each part, i.e., the connecting claws can not be modified.
The piezo and all the electronics are placed on the fixed mould half	In the movable mould half, there are ejector pins that permit the demoulding operation. Thus, any component can't face that region. Otherwise, in the demoulding action the ejector pins would collide against them, cracking the piezo and potentially damaging the electronics.
The gate position can't change	Modifying the gate position would interfere with the panel part's functioning because of gate scars originate from the separation between the gate and the part. The current position where the gate is placed already compensates for it.
The over-moulded connector must face the large part area, and not the part sides. This means the connector is aligned with the part thickness.	Otherwise, in the moment of assembling the panel, room would not exist to connect it to the external inductance synthetic circuit, because the polymer part is laterally constrained by the neighbouring panel sections.
The two mould inserts' height is fixed	The electrical connections, especially the connector, aligned with the part thickness (explained in the last topic), must be compact because the insert height can not grow. Otherwise, it would compromise the normal mould functioning in terms of closing the mould and conducting the polymer to the cavities.
At least the piezo upper face must be connected by an electrical cable to the connector before the injection step	As explained, the two piezo poles (upper and bottom surfaces) must be connected to the connector. However, before injection, only the upper face needs to be connected by a cable to the connector, since, after injection, it is the only side fully over-moulded by polymer. Therefore, allows connecting the other pole after the injection process. Nevertheless, from a process efficiency and cable management perspective, the aim is to have the two poles already connected before injection to over-mould them.
The piezo surface resting on the mould surface must be fully supported	This constraint is critical to ensure the prevention of crack formation in the piezo element during the injection process. By doing it, the exerted high pressure from the polymer flows in the piezo is evenly distributed along the mould surface.
The mould requires a holding solution to secure all the components placed inside of it	This solution prevents the movement and the misalignment of the piezo and the electrical components, before and during injection.
The piezo edges should be fully impregnated with the piezo positioned as distant as possible from the neutral line of the part	Complying with this constraint enhances the coupling factor. With all the edges impregnated by polymer, the piezo can exert more of its influence on the hosting part. And by being positioned distant from the neutral line, stresses due to the part bending during its vibration are higher, further deforming the piezo.
The piezo dimensions defined must be respected	It is essential to ensure that the predefined dimensions remain unchanged. Otherwise, the acoustic performance will drop due to the decrease in the piezo dimensions.

3.5.2. Preliminary testing

Considering the designed constraints established, and some insights that the mould design must respect, before addressing the brainstorming stage, where multiple solutions are discussed and presented. A preliminary test involving the over-moulding of a piezo was carried out to collect some more knowledge of the process and identify any possible phenomena that may remain unidentified at this stage. In this test, since the objective is only to gather some preliminary information, only a piezo will be used. This simplifies the procedure, leaving aside the connector and electrical wires, as the current mould that shapes the panel part does not present any pocket or space for cable management. Thus, it is only necessary to place the piezo on the surface of the fixed part of the mould and proceed with the injection to over-mould it.

To place the piezo on the surface of the mould, it was necessary to implement a temporary system to stop the piezo from falling and keep it secured to the wall of the mould until the mould closes and injection occurs, while also ensuring some stability during the injection process. In this way, it was considered that some type of relatively weak adhesive could be used on the piezo, providing some adherence to the mould. For this reason, a Pritt glue stick, normally used for paper in manual work, was chosen. Otherwise, if a stronger adhesive was applied, the piezo could end up permanently bonded to the mould wall. In addition, by using a glue of stick type, the time window between placing the piezo in the mould and demoulding the part with the embedded piezo (≅ 40 s) is not sufficient for the glue to produce any significant permanent bonding effect.

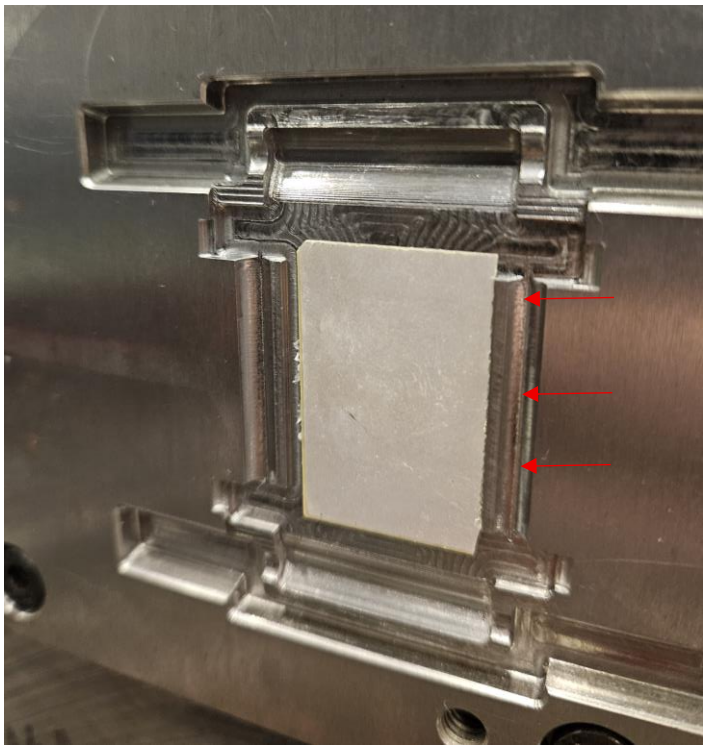

Figure 37- Piezo placing position in the mould

Preliminarily, as can be observed in Figure 37, the piezo remains secured in the mould in order to initiate the injection process. Beyond the piezo getting locked in place, it is also expected

that the piezo will remain relatively stable during the injection process, due to the combined action of the adhesive and the position that the piezo occupies in the mould (located at a level below the gate position). Therefore, when the polymer enters the cavity, although it describes a shearing movement relative to the piezo, it is also projected downward onto it, exerting a force with a vertical component that contributes to keeping the piezo in place. To compensate for the horizontal component of the force exerted by the polymer, the piezo, when positioned in the mould, should be placed against the geometry that forms the female claw (red arrows, Figure 37), so that it acts as a wall preventing the sliding movement of the piezo. In this way, the procedure adopted in the preliminary tests was as follows:

- Even glue application on the piezo surface;
- Place the piezo against the mould surface, and with the right edge contacting the mould wall that gives shape to the female connector;
- Start the injection procedure;
- Mould extraction;
- Result evaluation.

Concerning the injection parameters adopted, when it came to mould temperature and barrel temperature, the values indicated by the ABS supplier were adopted. On the other hand, the definition of the injecting pressure, packing pressure, injection velocity, and cooling time was based on practical knowledge. Thus, the parameters used are presented in Table 13.

Table 13- ABS injection parameters

Mould temperature	**65 °C**
Nozzle temperature	255 °C
Injection pressure	800 bar
Injection speed	50 mm/s
Packing pressure	300 bar
Cooling time	20 s

After the first two tests were carried out, it can be confirmed that the results were not as expected. As observed in Figure 38, the piezo was damaged during the process. This occurrence was not due to the injection phase in terms of cavity filling, but rather during the demoulding step, since part of the piezo remained over-moulded and another part adhered to the fixed half. Leading to the assumption that, despite the adhesive being of low adherence, under the pressure and temperature conditions it is subjected to, the degree of adhesion it provides between the piezo and the mould may be sufficiently high to damage the component during demoulding. However, when removing the broken piece of piezo from the fixed half of the mould, it was observed that the adhesion was not as strong as initially assumed, which further highlights the fragility of the piezo. In fact, the removal of the broken fragment was easier by applying a sliding movement rather than a pulling one. This once again explains the reason why the piezo broke during demoulding: the demoulding process takes place in the peel direction.

a)  b) 

Figure 38- a) broken piezo on the fixed half, b) broken over-moulded piezo

Based on these observations, in subsequent tests, the procedure was adjusted by applying adhesive only to the two opposite diagonal corners of the piezo. In this way, the piezo remains secured while the risk of damage during demoulding is reduced, since the adhesion force that must be overcome in the demoulding step is smaller. On top of that, because the adhesive is applied at two corners, any deformation that may occur should be minimal, thereby preventing fracture of the piezo.

a)  b) 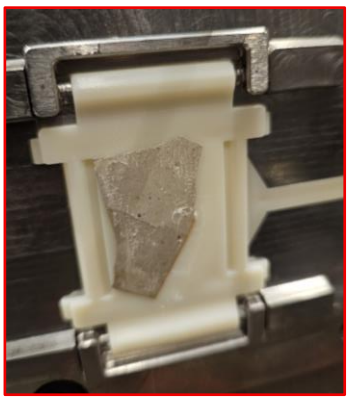

c) 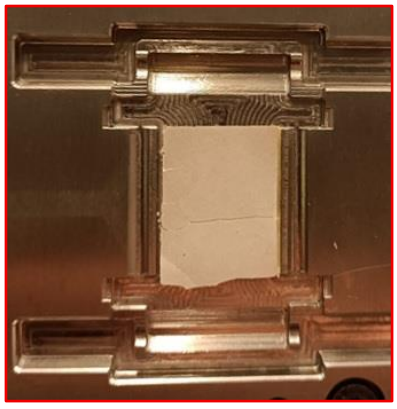 d) 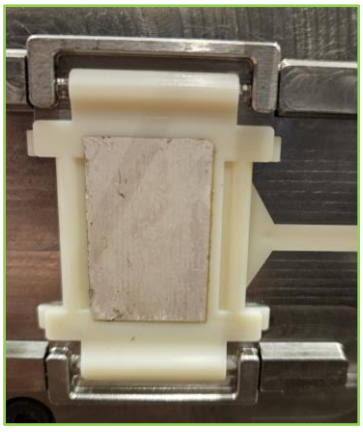

Figure 39- a) unsuccessful test due to piezo sliding movement, b) unsuccessful test due to piezo rotation, c) unsuccessful test due to the piezo staying glued don the moving half, d) successful over-moulding of the piezo

With the application of the new procedure, different results could be observed in successive injection cycles (Figure 39). In some attempts (Figure 39 a) and b)), due to the smaller amount of adhesive applied, the piezo moved during cavity filling as a result of the shear force component, while, in other attempts, it remained stable and intact throughout the entire injection cycle (Figure 39 d). This behaviour showed that a solution involving only an adhesive is not effective enough. Moreover, it is also evident that the force exerted by the melt front on the piezo is significant, since neither the adhesive nor the mould feature that acts as a wall was able to prevent its movement during injection. Making the piezo experience a sliding motion, overcoming the feature that functioned as a wall, and in some cases, even a rotational movement.

In the cases where the piezo survived (Figure 39 d) the injection and demoulding process, it was observed that, after an average of 50 seconds, it began to develop fractures. This degradation indicates that, during the cooling process outside the mould, shrinkage and warpage caused the piezo to deform and eventually fracture.

From this series of preliminary tests, it was possible to take some important conclusions, namely that the process is moving in the right direction despite the failed attempts, since in some trials the piezo was successfully over-moulded and survived the injection cycle without cracks. Only during the cooling stage outside the mould did it start to show the appearance and subsequent growth of cracks. This behaviour suggests that the issue does not lie in the mould design itself, but rather in the injection temperature, which needs to be adjusted to reduce the material shrinkage. It was also concluded that the mould design must incorporate a mechanism capable of effectively securing the piezo, since the forces exerted by the melt front are significant, as was possible to see due to the number of failed tests. Which also permits to conclude that, when electrical cables and connectors are integrated into the mould, they must be shielded or supported to prevent damage caused by the melt front forces. Furthermore, in the cases where the piezo was successfully over-moulded, it was observed that the embedding was not entirely perfect. Touching the over-moulded piezo in the host structure revealed a transition zone between the piezo and the host structure. Therefore, the future design must better guide the melt flow to achieve a more homogeneous and complete encapsulation.

3.5.3. Mould solutions presentation

Taking into account the constraints defined and the insights from the preliminary results, the next step under consideration is designing the mould inserts to successfully over-mould the piezo and the electronics. Therefore, first a set of solutions is presented and discussed, and after culminating all the information from each solution, a selection process is executed following the Ashby methods.

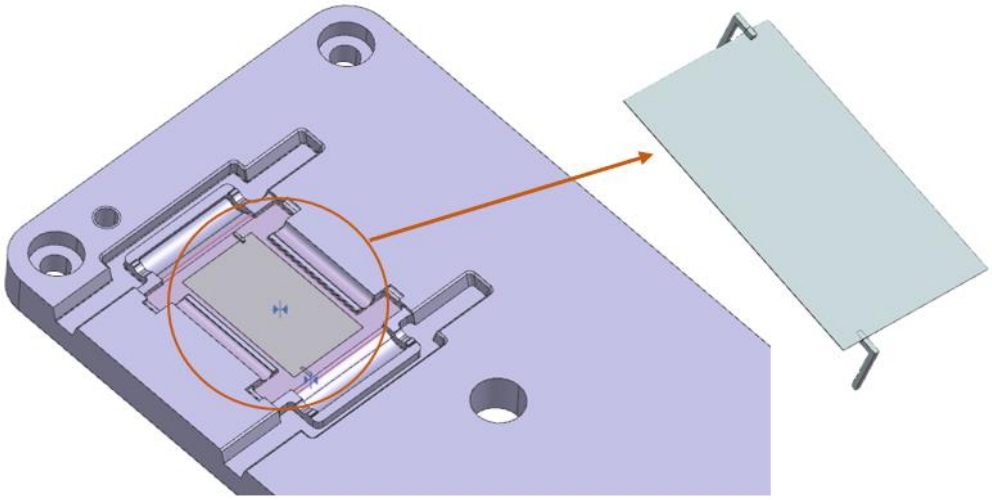

Figure 40- Mould design solution S1

Table 14- Mould S1 design specifications

Description:

In this solution, only a few modifications are made to the mould, prevailing design simplicity to avoid multiple components inside the mould. In this way, the idea of connecting the piezo to the connector via cables was abandoned. Instead, two 90° pin-header connectors are soldered directly to each piezo surface and accommodated in two pockets on the mould. This solution provides support to the piezo during the injection cycle, the electrical connection of the piezo to an external circuit when the panel is assembled, and a cleaner path to the melting flow when filling the cavity. Thus, the contact area between the polymer and the components is reduced, resulting in lower forces being applied to the components. This reduction enhances the piezo stabilisation and the likelihood of avoiding defects related to cable management.

The pin-headers position was also considered, so that they are at the opposite corner of the piezo, to provide greater stabilisation, and 5 mm apart from the piezo edge, to avoid stress concentration on the piezo corner due to the holding forces during cavity filling.

The process of positioning the piezo together with the respective pin-headers in the mould is also straightforward, since it only involves sliding the pins into place, whether executed by a robot or an operator.

Strengths:

- The pin-headers offer good support to the piezo during injection;
- Easy fitting and demoulding without concerns of damaging the piezo and the pin-headers;
- No need for cable management, making the mould cavity cleaner for the polymer to flow;
- The piezo is well supported along its surface;
- The two piezo poles have connectors.

Weakness:

- By soldering two connectors directly to the piezo, its performance can change. Since a higher amount of solder is needed compared to a cable, in combination with the connector, a higher number of anchoring points is created. This solution makes the piezo stiffness uneven along its surface;
- The connectors need to be soldered with extreme precision to the piezo. Otherwise, misalignments occur when fitting the connector into the mould;
- The connectors working as holders, and by being bonded in two tiny points, the melt front force can be high enough to peel off the solder.

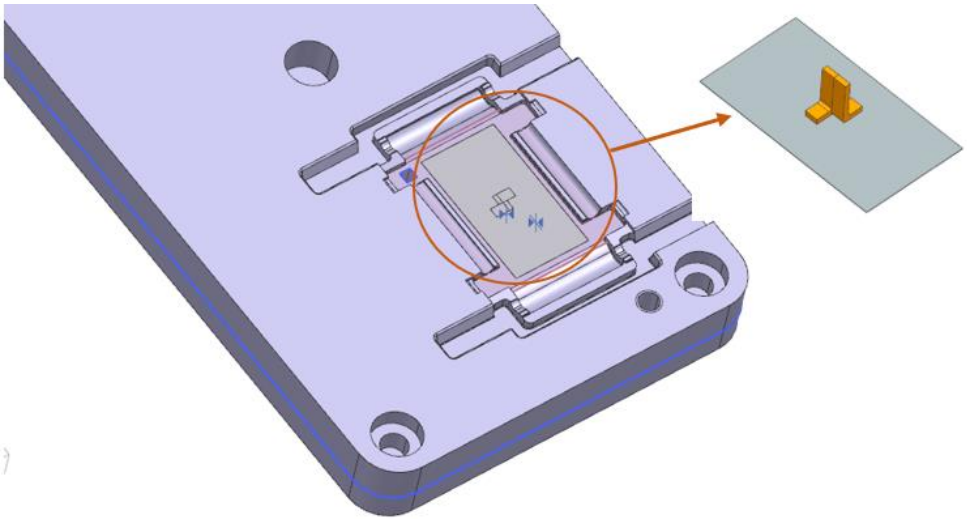

Figure 41- Moul design solution S2

Table 15- Mould solution S2 specifications

Description: In the present solution, a hybrid approach was adopted by using two types of electrical wires, serving the dual purpose of securing the piezo and establishing the electrical connection between the piezo and the external circuit. To achieve this purpose, a copper braid was soldered to the bottom face of the piezo, functioning both as an electrical link and as a support within the mould. By using this type of wire, which has a rectangular geometry and is manufactured by weaving thousands of small-diameter filaments, it presents a higher moment of inertia compared to single-core round wires. This suggests that it may provide sufficient structural stiffness to support the piezo. Moreover, to ensure that the copper braid fits properly into the mould, allowing the bottom face of the piezo to be in full contact with the mould surface, a pocket was created at the start of the groove accommodating the braid. This pocket houses the copper braid's legs and soldering points. As for the electrical connection of the top face of the piezo, a jumper connector was selected. This connector is inserted into a hole made in the mould and connected to the piezo through a 0.1 mm copper strap. By using such a strap, it is ensured that the connection lies perfectly flat against the mould surface, thereby minimising the contact area with the melt front during the injection process, compared to conventional round electrical wires.
Strengths: • Good support during injection. • All the electrical connections are fitted properly, not representing an obstacle to the polymer flow. • The two poles are electrically connected before injection takes place. • Easy soldering of the copper braid and the copper strap on the piezo. • Reduce impact on the piezo dynamics of soldering the copper strap • The piezo is fully supported along its surface
Weakness: • Since the copper strap has a flexible behaviour, and it is the one that provides the connection between the piezo and the jumper connector, fitting the jumper on the mould pocket can be a hard task for a robot, requiring human assistance, thus decreasing process efficiency. • Due to the copper braid being thin (0.54 mm) and long (10 mm), with the tools available in the workshop, the task of manufacturing the pocket to fit the braid is hard to execute • Despite the copper strap being flat with the surface, if the polymer twists it, there is the chance of the strap being ripped off.

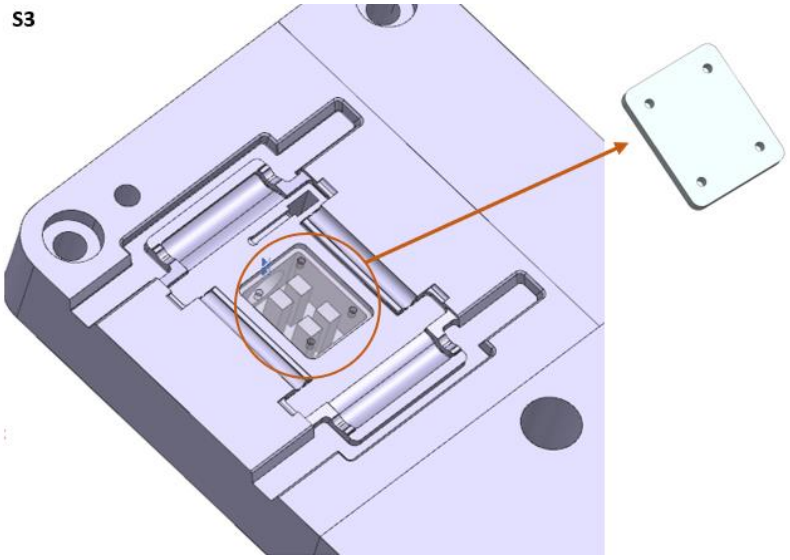

Figure 42- Mould design solution S3

Table 16- Mould solution S3 specifications

Description:

From the preliminary tests using glue as a supporting method, it became evident that the results varied between success and failure depending on the level of adhesion. This inconsistency tendency led to the development of a solution in which the glue is replaced by a vacuum system. Such a system allows for the adjustment of the suction force applied to the piezo, ensuring that it is held in position until the mould is closed and during injection. At the moment of demoulding, the suction can be stopped, allowing the over-moulded piezo to be released without damage. This solution consists of a chamber integrated into the mould insert, as shown in the figure, in which four supports hold a cover that seals the chamber. This cover contains four holes through which suction is applied to the piezo, which is placed directly on top of it. The configuration of a chamber with a removable cover offers two advantages: it simplifies the machining of the vacuum channels, since more space is available to use different tools, and it allows the cover to be replaced with different hole diameters. This option of choosing the hole diameter enables optimisation of the balance between the suction area and the surface area fully supporting the piezo.

Regarding the electrical connections, the piezo is linked through two electrical wires to two jumper connectors accommodated within a pocket. Similarly, the wires are placed within a groove to ensure that these do not obstruct the melt front. In addition, the wire that connects to the bottom surface of the piezo is positioned so that it does not lie between the piezo and the mould surface, thus enabling full support of the piezo.

Strengths:

- Ability to adjust the strength that holds the piezo.
- Easy piezo fitting into the mould, especially when considering a robot performing this task.
- Easy to manufacture the mould design.
- The cover allows for small adjustments without modifying all the mould.
- Both piezo surfaces are electrically connected.

Weakness:

- Air tightness challenges involving the installation of a vacuum system into the mould
- In the case of failure, where the piezo during the injection process moves from its place, allowing the polymer to be sucked into the vacuum system, it can require high stoppage times to clean it.
- The existence of vacuum holes to support the piezo results in the piezo not being fully supported, promoting cracking initiation.

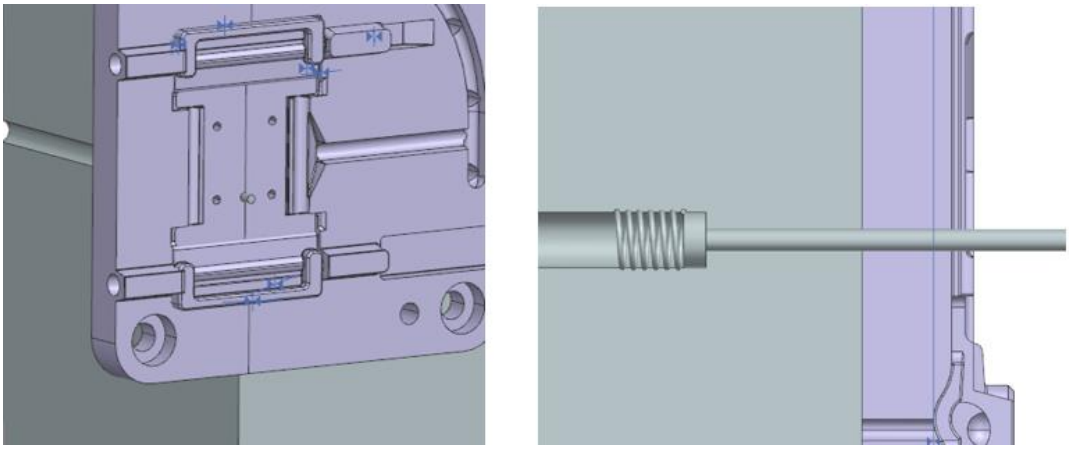

Figure 43- Mould design solution S4

Table 17- Mould solution S4 specifications

Description: In this solution S4, the adopted approach was rather unconventional compared to the previous ones, since the part of the mould undergoing modifications is the moving half instead of the fixed half. However, in order to prevent the piezo from being damaged during demoulding due to the action of the ejector pins, it is fixed on the moving half. As a result, the piezo is supported in two surfaces. In the first stage, a point of glue is applied to the piezo, as in the successful preliminary tests, and it is placed on the surface of the fixed half of the mould. Then, as the mould closes, a pin with a spring system gradually approaches the piezo until, at the final stage of closure, it contacts it. This contact is dampened by the spring, which is mechanically connected to the pin. In this way, the pin provides the necessary support during the filling of the cavity by the polymer. Once the injection is completed, the pin is automatically retracted by the injection machine to ensure that the piezo is not subjected to constant pressure, and the part is demoulded successfully. The electrical connection to the piezo, is carried out after the over-moulding process. A jumper wire with a connector is soldered to the exposed surface of the piezo and, by making use of the hole left in the part by the supporting pin, another jumper wire with a connector is soldered to the lower surface of the piezo. It should be noted that, since the installation of the pin extends beyond the insert that shapes the polymeric part, affecting the mould base that supports the insert, its position had to be carefully planned. This process was necessary to ensure that the pin passed between the cooling channels, while also accommodating the spring system responsible for damping the contact with the piezo, without interfering with the other components of the mould.	
Strengths: • The piezo stability is guaranteed. • Reduced number of components inside the mould, reducing the likelihood of failures.	Weakness: • Need for post-processing to establish an electrical connection between a piezo and a connector. • The electrical connections will be on the two sides of the panel. • Since the piezo is only supported at one point by the pin, it can originate crack initiation on the piezo. • The positioning of the piezo into the mould requires glue application in the initial step, not contributing to process efficiency

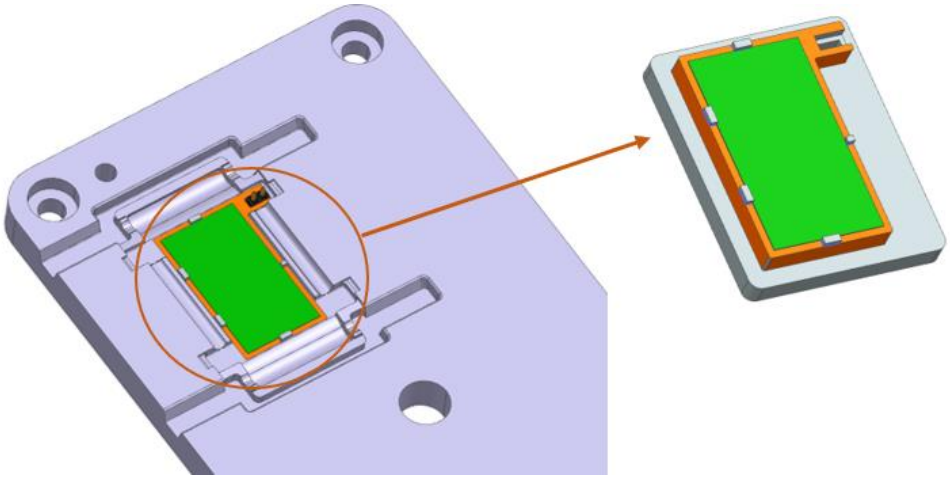

Figure 44- Mould design solution S5

Table 18- Mould solution S5 specifications

Description: In contrast to the first two solutions presented, this one restricts the use of connectors to establish only an electrical connection, rather than for holding purposes. To secure the piezo during the injection phase, 5 holders were designed to retain the piezo within the region where it stands (green area), preventing it from rotating or lifting. Moreover, to enhance the piezo's connection to the hosting part and improve its embedding, the region where the piezo rests (green region) is offset 0.2 mm relative to the mould surface. This separation creates a 0.2 mm polymer wall when the piezo is over-moulded, which restrains the piezo more effectively. The position of the holders was defined considering the direction of the polymer flow, and to ensure that they would not damage the piezo while supporting it. As a result, the holders were positioned along the edges of the piezo rather than at the corners so that, when the piezo was pressed against them due to the force of the melt front, the contact force between the piezo and the holders would be distributed and would not trigger crack initiation. This is also the reason why two holders were placed along the direction of the polymer flow instead of just one. When it comes to establishing an electrical connection with an external circuit, a pin-header connector with two pins was selected and placed in a pocket in the mould (see image), which, in turn, is connected to the piezo via two 0.2 mm annealed copper wires. This description provides low resistance to the melting flow, due to their low thickness. When it comes to manufacturing, as observed in the image, the structure with the holders where the piezo rests, and with the pocket to fit the connector, is removable to allow quick design improvements without necessitating modifications on the mould, saving manufacturing time.
Strengths: • Easy fitting of the piezo in the mould. • With the application of 5 block holders, the chance of stabilising the piezo during injection is high. • Both sides of the piezo are electrically connected. • The possibility of removing the insert where the piezo rests allows for small adjustments without modifying the mould. • The use of thin annealed copper wires has a lower impact on the polymer flow.
Weakness: • Despite the distribution of the holders, they can induce stress concentration on the piezo due to the contact force exerted by the polymer filling the cavity. • The piezo needs to be with the perfect dimension to fit within the holders, requiring a precise cut before being placed.

3.5.4. Selection of the best mould design

With the presentation of the different concepts, it was possible to calculate that, in general, they all share the same work principle when it comes to securing the piezo and accommodating the connector and the electrical wires. The main differences lie only in the method or in the additional components used to achieve this. For instance, in cases S1 and S2, the electrical connectors themselves were used to support the piezo, whereas in solutions S3, S4, and S5, extra elements were integrated into the mould, such as vacuum systems, pins, and holders, respectively, to stabilise the piezo during the injection process. Consequently, the cable management in each solution followed its own specific path, but with the common requirement of being placed within a pocket or slot, to minimise contact with the melt front and avoid potential damage. This set of alternatives means that each solution carries its own advantages and disadvantages over the others, making the direct choice of the best mould design far from straightforward. Therefore, a selection process will be carried out following the Ashby method, leading to the definition of a final solution to be implemented.

As the first step in the procedure to select the best mould design, each solution is evaluated against a set of defined parameters that characterise the attributes that the mould design must meet to successfully over-mould the piezo. Normally, in the case of material selection using the Ashby method, this step is ignored. However, since the present case does not deal with materials with quantitative properties, but rather with designs that present qualitative properties, this evaluation becomes necessary. Therefore, to carry out the assessment of each attribute, the scale shown in Table 19 will be used.

Table 19- Scale classification to evaluate each attribute

Classification	
1	Poor
2	Fair
3	Meet the expectations
4	Good
5	Very good

With the classification established, the attributes by which each solution will be evaluated according to the scale Table 19 in are:

- Level of support to the piezo expected during the injection (Table 20);
- Components mould fitting feasibility by an autonomous means (Table 21);
- Mould manufacturing feasibility and opportunities to make improvements (Table 22);
- Pre and post-process efficiency in mass-scale (Table 23);
- Level of protection offered against damage to the piezo due to crack initiation (Table 24).

Having presented the attributes according to the expected mould performance in over-moulding the piezo, the next step is to evaluate each solution for a specific attribute. To next with the classifications, proceed to the selection of the best solution using a selection matrix.

Table 20- Evaluation of the level of support expected for the piezo during injection

Solution	Evaluation	Justification
S1	3	Although the pin-head connectors could, in theory, serve as a good supporting base and withstand the pressures experienced during cavity filling with polymer, since they are attached to the piezo by tin soldering, the high temperature of the melt front (255 °C) may cause the solder joint to melt, resulting in a loss of support for the piezo.
S2	2	Since the piezo is only supported by the copper braid, the integrity level of its support is not high, because although the copper braid is manufactured through weaving, it still exhibits flexible behaviour.
S3	4	This solution demonstrates good reliability regarding the fixation of the piezo, since the vacuum method, in a way, replicates the use of adhesive but with greater adhesion, along with the possibility of adjusting both its intensity and the timing of its activation. This feature addresses the shortcomings observed with the adhesive in the failed tests, while reproducing the successful outcomes achieved in the preliminary trials.
S4	5	This solution is the most reliable of all, as the pin securing the piezo continuously applies a vertical force, preventing any vertical or horizontal displacement. Furthermore, the magnitude of this force can be adjusted, according to the necessities, by modifying the tension of the spring associated with the pin.
S5	4	By employing holders around the piezo, this method also demonstrates a good level of reliability, as it does not rely on components susceptible to high temperatures and provides support to the piezo along all four of its edges. This type of support prevents any lateral displacement and, consequently, avoids the possibility of the piezo sliding onto another surface of the mould in an upward lateral motion, eliminating the risk of polymer penetrating beneath it.

Table 21- Evaluation of the components fitting feasibility into the mould by autonomous means

Solution	Evaluation	Justification
S1	5	Since it is only necessary to insert the two pin-head connectors into their respective holes in the mould cavity, this operation is relatively straightforward for a robot integrated with the injection machine, as it can perform the task with high precision, and the connectors offer no resistance to hole insertion.
S2	3	Since the robot needs to insert the copper braid soldered to the piezo into its pocket while simultaneously placing the jumper connector into its respective pocket, this action is considered relatively feasible for the robot. However, due to the flexible nature of the electrical wires, these may offer some resistance when inserting the connector, requiring the movements to be executed precisely and slowly.

Table 21- Evaluation of the components fitting feasibility into the mould by autonomous means (continued)

Solution	Evaluation	Justification
S3	3	Similar to solution S2, the robot will need to handle the challenge of inserting jumper connectors attached to electrical wires, requiring slow and precise movements. If the connector encounters resistance from the pocket walls during insertion, the electrical wire may lack sufficient stiffness to assist in pushing the connector fully into the pocket.
S4	4	Although the robot does not need to handle the fitting of connectors and electrical wires, as these are only attached to the piezo after it has been over-moulded, it must perform the placement of the piezo in the mould in two steps. First, it needs to apply a drop of contact glue or spray glue, and only then can it position the piezo on the mould surface, to be supported by the glue. This requirement makes the process more time-consuming and may present challenges for the robot in accurately applying the adhesive.
S5	3	Similar to solutions S1, S2, and S3, the robot needs to overcome the challenge of fitting connectors linked to flexible wires.

Table 22- Evaluation of mould manufacturing feasibility and opportunities to make improvements

Solution	Evaluation	Justification
S1	2	From a manufacturing perspective, the process is quite straightforward, requiring only the drilling of two holes to accommodate the pinheads, which both support the piezo and establish an electrical connection. However, significant modifications to the mould insert design are not permitted without having to machine the insert from scratch, which limits the options for design improvements.
S2	2	To machine the design of this solution, a pocket must be milled to accommodate the jumper connector, and a slot must be opened to place the copper braid strap soldered to the piezo. Some difficulties may arise when machining the slot, as it requires a depth of 10 mm and a width of 0.35 mm, making it challenging to find a milling tool with a diameter of 0.35 mm and sufficient length to reach the full depth. In addition to this manufacturing challenge, the mould cannot undergo significant modifications without having to be entirely remade.
S3	4	The machining process for the vacuum system in this solution can be considered of low complexity. It requires milling a pocket that serves as the vacuum chamber on the surface where the piezo is positioned, and a hole in the top part of the mould that connects to the vacuum chamber to provide air evacuation. Additionally, a cover with four holes must be manufactured to create suction, sealing the vacuum chamber and holding the piezo in place. In terms of modifications, only the holes in the cover can be altered.

Table 22- Evaluation of mould manufacturing feasibility and opportunities to make improvements (continued)

Solution	Evaluation	Justification
S4	1	For potential modifications, this solution is quite limited, as it requires alterations to the mould that accommodates the insert mould forming the hosting part. This alteration to the main mould are highly undesirable, since the mould needs to remain universal to support different insert moulds with varying cavity geometries. Additionally, machining challenges arise because the cavity to install the pin must be done without damaging the cooling channels, which is hard given the limited space between them.
S5	5	In this solution, both the manufacturing process and the ability to perform modifications are completely feasible. Because the surface where the piezo rests and where the pocket to fit the connector, is manufactured on a separate body that fits on the insert-mould. So, to carry out modifications, these are only required on this separated body, leaving aside the insert mould. Moreover, the holder's geometry to secure the piezo is easy to mill.

Table 23- Evaluation of pre and post-processability on a mass scale way

Solution	Evaluation	Justification
S1	4	Regarding pre-processing before the injection process, it is only necessary to solder the two pin-head connectors to the piezo. However, the soldering and positioning of the pin-heads must be carried out with high precision, as any misalignment will prevent them from fitting correctly into the mould holes.
S2	2	Before placing the piezo in the mould, the jumper wire and the copper braid strap must be soldered to it. Characterising itself for being an easy process, but since two types of cables need to be soldered, it takes longer as two separate soldering stations must be used.
S3	4	The pre-processing required involves only soldering two electrical wires with a jumper connector to the piezo. Although the process is relatively simple, the need to solder two different types of cables increases its duration, as it necessitates the use of two independent soldering stations.
S4	1	In this solution, the only pre-processing required is the application of a spot of adhesive, since the connectors and electrical wires connecting them to the piezo are only soldered after the piezo has been over-moulded. This procedure represents a significant process inefficiency due to the need for post-processing.
S5	4	The pre-processing only involves soldering two electrical wires with a jumper connector to the piezo. This makes the process very efficient, as it only requires two solder points between the wires and the piezo.

Table 24- Evaluation of the level of protection against crack initiation

Solution	Evaluation	Justification
S1	2	Since the piezo is supported by the pin-head connectors, which are soldered to it at two small points, the piezo becomes susceptible to fracture at those very locations. Thus the mould design offers limited protection against crack initiation in the piezo.
S2	3	This solution does not offer any active protection against crack initiation. However, the holding system or the electronics associated with the piezo are not prone to provoking cracks in the piezo.
S3	2	In this mould design, the piezo rests on a cover with 4 holes responsible for vacuuming the piezo against the surface to hold it. Due to the existence of these 4 holes, the piezo will not be fully supported along the cover surface, which can lead to crack initiation.
S4	1	Due to the exclusive use of a pin pushed against the piezo to hold it, there is the likelihood of cracks developing around the point where the pin touches the piezo during injection, or even in the moment of contact between the piezo and the pin.
S5	3	Since the piezo is fully supported and held on its four edges, stress's resulting from the injection process are well distributed along the features supporting the piezo. However, there is no active protection to mitigate crack initiation.

With the evaluation performed on all solutions, the next step is to rank all the attributes based on their importance in over-moulding the piezo and the electronics. For that, to each attribute, a weight is established as in the selection process made on the section 3.3.2. Beginning with the expected level of support provided by each solution, a weight of 0.3% was assigned. This represents the highest value among all the weights, as it constitutes a vital condition. If this requirement is not met, the mould cannot fulfil its purpose, regardless of whether the other attributes are achieved. As observed in the preliminary tests, if the piezo and the electronic components are not stabilised during the injection stage, successful over-moulding cannot be achieved. Regarding the feasibility of a robot placing the piezo and the electronic components in the mould before injection, a lower weight of 0.1% was assigned. This lower value is given because it is neither fundamental to achieving the proposed objective nor the attribute with the greatest impact on process efficiency in mass production. In practice, dedicated accessories can be developed to enable the robot to carry out this task with the required precision. By contrast, the attribute describing the efficiency of the pre- or post-processing necessary to solder the wires and connectors to the piezo was assigned a higher weight of 0.2%. This value reflects its greater significance, as such operations may require different equipment and thereby affect production time and overall efficiency. Considering all attributes collectively, process efficiency during the manufacture of each part remains essential, as the final assembly must be classified as suitable for mass production. For mould manufacturing, a weight of 0.15% was assigned. This weight was not determined primarily by the potential challenges of machining the mould cavities, but rather by the capacity to modify them without the need to remake the entire mould. Such flexibility is essential to improving the effectiveness of the design optimisation process when developing an ideal mould for over-moulding the piezo. Finally, the attribute concerning the level of protection provided by each mould design against

crack initiation in the piezo during injection was assigned a weight of 0.25%. This attribute is regarded as fundamental, as preventing structural damage to the piezo is critical to meeting the objectives of this study.

Table 25- Weight assigned to each attribute

Attribute	**Weight (w_i)**
Level of support expected for the piezo during injection.	0.3
Components fitting feasibility into the mould by autonomous means.	0.1
Mould manufacturing feasibility and opportunities to make improvements on it.	0.15
Efficiency of the piezo pre- or post-processability on a mass scale way.	0.2
Level of protection offered against crack initiation.	0.25

From this point, to select the best mould solution, the conditions are reunited to choose the best solution based on the final score calculated using equation 5. Normally, before the score for each solution is calculated, a normalisation procedure is done. However, since all the solutions were scored following the same scale, the normalisation procedure is not required.

Table 26- Selection table for the best mould design

Normalised attribute values	**Solutions**				
	S1	S2	S3	S4	S5
Level of support expected for the piezo during injection.	3	2	4	5	4
Components fitting feasibility into the mould by autonomous means.	5	3	3	4	3
Mould manufacturing feasibility and opportunities to make improvements on it.	2	2	4	1	5
Efficiency of the piezo pre- or post-processability on a mass scale way.	4	2	4	1	4
Level of protection offered against crack initiation.	2	3	2	1	3
Final score	3.00	2.35	3.40	2.50	3.80

By analysing the results in Table 26, it is possible to observe that solution S5 stands out from the others, making it the solution selected. The key factor behind achieving the highest overall rating lies in its balanced design, which fulfils the expected requirements in all defined attributes, without showing inconsistencies such as being very good in certain attributes while underperforming in others, except for manufacturing feasibility and the ability to introduce modifications that were rated as very good. This score arises from the fact that the surface where the piezo and electronic components are secured is implemented as an insert that fits within the mould-insert itself. Such a configuration allows the insert to be easily removed and modified without the need to re-machine the entire mould, enhancing the iterative process of optimising the design for over-moulding the piezo. Furthermore, solution S5 incorporates a well-conceived stabilisation design, with five holders distributed along the edges of the piezo. These holders provide passive stabilisation during cavity filling, ensuring that the piezo remains fixed under the high pressures of the polymer flow.

In second place is solution S3 which, despite also demonstrating several strong characteristics, presents certain limitations. Specifically, the lower surface of the piezo is not fully supported, as the mould-insert relies on vacuum orifices to secure it, which increases the risk of crack initiation in the regions surrounding these orifices. In addition, unlike solution S5, this prototype offers reduced flexibility for subsequent design modifications that negatively impact the iterative process of optimising the insert-mould design.

The selected solution S5, after being manufactured, is presented in Figure 45.

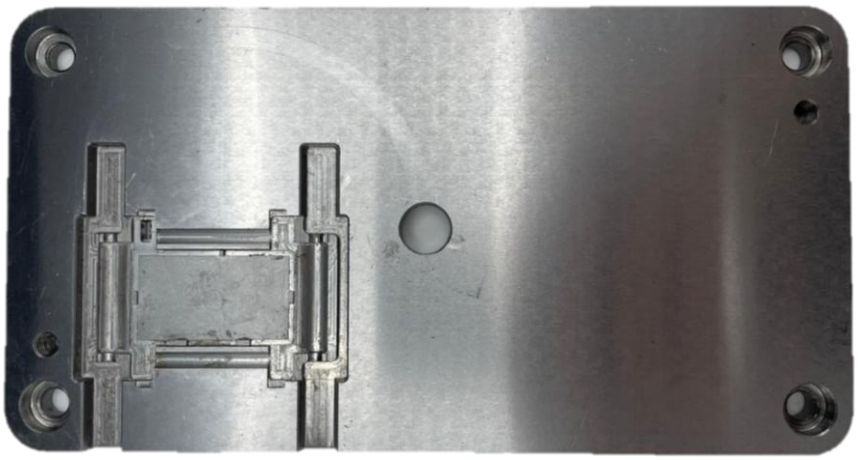

Figure 45- Selected S5 solution

3.6. Piezoelectric element over-moulding by injection moulding

This section focuses on the evolution of multiple approaches to over-mould the piezo and its electronics, using the S5 selected mould design as a starting point. The evolution process congregates injection tests involving process parameter tunability, new materials testing and mould flow simulations.

3.6.1. Pre-processing

In the previous parametric study section, based on the results obtained and considering the available options in the market for purchasing piezoelectric elements, the dimensions that the piezo should have to achieve optimal vibration performance were analysed and defined as 36 × 20 × 0.22 mm^3. In collaboration with the supplier PIEZO.COM, it was informed that, due to the order volume being below 100,000 units, it would be necessary to purchase a standard size of 45.7 × 38.1 × 0.22 mm^3. However, this difference does not classify as a problem, since the ideal dimensions can still be achieved by cutting the piezo to the required size. Moreover, in a mass-production context, this step can be avoided, as it is possible to directly negotiate the piezo dimension with the supplier.

To perform the cutting of the piezo, an experimental trial-and-error approach was followed according to the in-house LSMD knowledge in this topic, to determine the most suitable method. Initially, water-jet cutting was attempted based on the procedure found in the

literature [85]. However, this process proved to be time-consuming, as each piezo had to be positioned individually on the cutting table, and the machine's clamping system had to be adapted to the reduced size of the piezo. In addition, the cut produced by the water jet was not clean, since the cut edge exhibited pronounced irregularities. This was likely due to the fragility of the piezo, which caused the water jet not to perform a continuous cut but instead to chip away micro-fragments along the cutting line. Such a result was undesirable, as handling the piezo subsequently revealed crack propagation originating from these irregularities. Given these difficulties, an alternative method involving laser cutting was tested, with the expectation of achieving a cleaner cut. While this indeed produced sharper edges, multiple trials showed the presence of visible burn marks resulting from the elevated laser temperature, which led to damage of the piezo. As a last resort, a more rudimentary approach was employed, involving the use of a razor blade and a guide ruler to cut the piezo. This method proved successful, delivering an acceptable cut quality while being significantly faster. The process merely required positioning the ruler at the correct measurement and performing successive passes with the razor along the guide until the piezo was completely cut.

After the cutting process, the electrical wires were soldered to the piezo using a common soldering station. As a first step, the piezo was cleaned using an alcohol solution to remove any grease and oxides that might be on its surface. After, with the respective cable touching each piezo side (poles), a drop of solder was applied. Following this step, the connector was soldered to the wires and together with the piezo positioned on the mould. However, in the future, with the purpose of mass-scale production, a point soldering machine integrated on an automated production line is required to avoid human labour in soldering, to enhance production efficiency.

a) b) c)

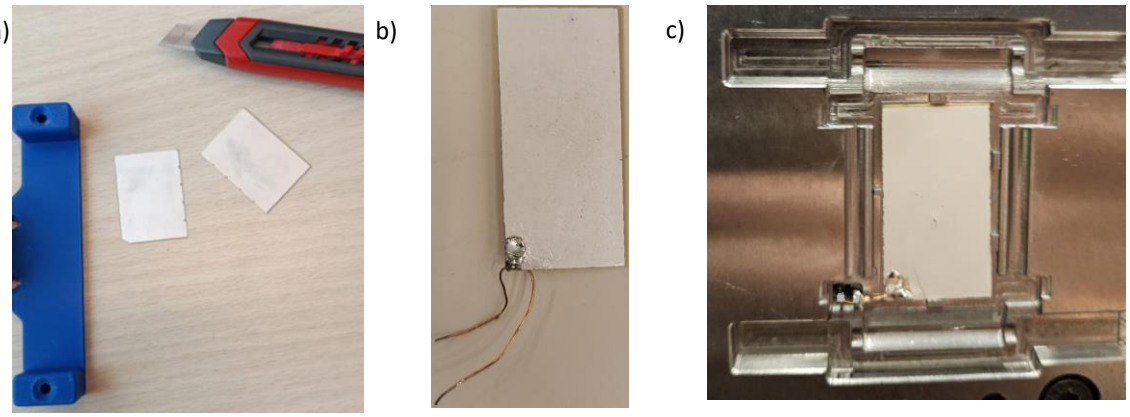

Figure 46- a) cutting process with a razor, b) piezo with the wires soldered, c) piezo positioned on the mould with the wires and connector soldered to it

3.6.2. First phase of testing

With the pre-processing of each piezo completed, the necessary conditions were established to proceed to the next stage, which consisted of testing the selected mould in order to determine whether it was capable of successfully over-moulding the piezo and the associated electronic components. Since multiple components are to be over-moulded within the mould, the testing

procedure was divided into two stages. In the first stage, only the pin-header connector and the piezo with the specified dimensions were placed in the mould. If both the piezo and the connector withstood the injection process, the second stage followed, in which two wires were soldered between the piezo and the pin-header, as carried out during pre-processing. By adopting this two-step approach, it became possible to observe and analyse in greater detail the ability of each component to be over-moulded, as well as any potential influences each might exert on the process. As previously analysed in the preceding section, the wires, when exposed to the high-pressure melting front, could be pulled out, potentially causing damage to the piezo at the soldering points. Additionally, since the piezo would be fully encapsulated by the polymer except for the face in contact with the mould, such effects or other defects could be difficult to detect, making it challenging to determine the roots of the problems.

Putting the first stage into practice, the piezo and the connector were positioned inside the mould and the injection process was carried out under the parameters defined in Table 13. Representative results are found in Figure 47.

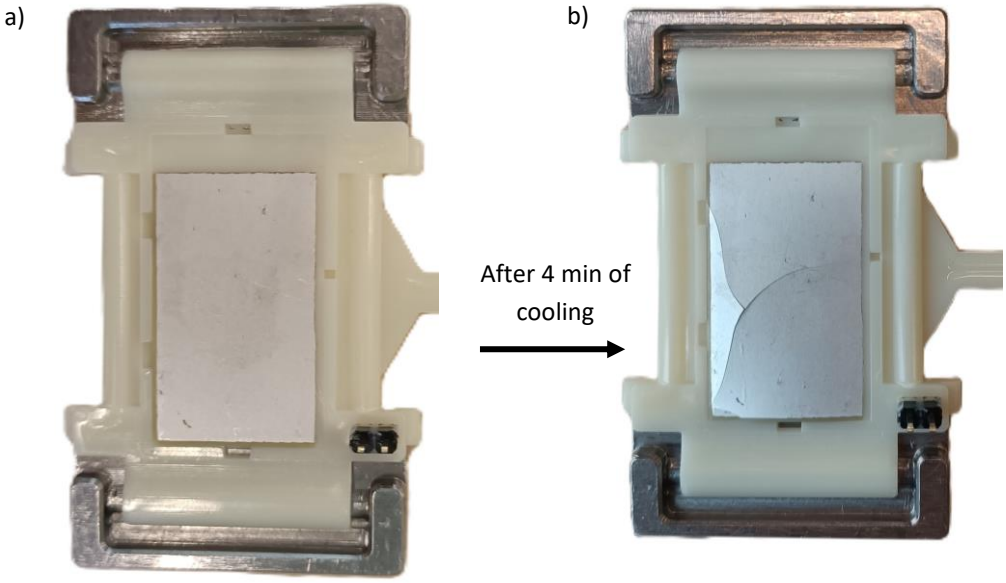

Figure 47- a) Piezo and pin-holder over-moulded right after demoulding, b) result after 4 min of cooling time outside the mould

From the results obtained, it can be stated that an improvement was achieved when compared to the preliminary tests. However, a successful over-moulding of the piezo was not accomplished. Actually, across the eight tests carried out, the piezo (Figure 47 a) survived the injection process, remaining perfectly stabilised by the holders and being demoulded without any damage. But in contrast, during the cooling phase outside the mould, the piezo bent and subsequently cracked. Despite this failure in the cooling stage, the outcome still represents a significant improvement, since in the preliminary trials, achieving a balance between holding the piezo during injection and ensuring its release during demoulding proved to be highly challenging, with only 2 out of 11 tests succeeding. On the other hand, the pin-header connector component was successfully over-moulded without any damage. It remained intact, and no penetration of the melt front into the material encapsulating its two pins was observed.

Such penetration, if it had occurred, would have caused the connector to get locked with the mould, thus damaging the hosting part during demoulding.

Focusing on the results observed during the cooling of the over-moulded piezo, several key findings were identified. Firstly, changes in the piezo were not immediately visible, appearing only approximately two minutes after the part was demoulded. Secondly, when changes began to manifest, the piezo progressively bent with its concavity facing downwards and along its length, until stabilising at a certain curvature for a period of around 1.5 minutes. After this period, the piezo suddenly increased its deformation curvature and fractured. Thirdly, it was consistently observed that fractures occurred in one of two patterns: either in a cross shape or in a star shape. This behaviour suggests that contraction forces acted uniformly in all four directions. Otherwise, the fractures would have been aligned perpendicular to the dominant force. It is therefore evident that a pulling force is exerted from the extremities towards the centre of the part, resulting from material shrinkage.

Furthermore, the ease with which bending occurred indicated that no significant surface energy adhesion existed between the ABS and the surface of the piezo, most likely due to the chemically inactive nature of the piezo surface. Taking all these findings, it is important to consider the need for a deeper evaluation of the shrinkage and warpage phenomena within the part, to identify a viable solution to the problem.

3.6.3. Injection moulding simulation

To conduct a more detailed assessment of shrinkage and warpage, it was decided to perform flow simulations to analyse how the polymer fills the cavity and to quantify process-related phenomena such as the evolution of melt front temperature, cavity filling times, as well as the resulting warpage and shrinkage. In addition, these simulations allow for visualisation of the described phenomena and their impact on specific regions of the hosting part, thereby providing a more comprehensive understanding of the process. To carry out the simulations, Moldex3D software was employed.

For the simulations to be reliable and representative of reality, it is first necessary to define a set of parameters as applied in the injection moulding machine. Typically, the first step would involve importing the real mould geometry into the software so that the program can recognise the cavity model to be simulated. However, this approach would require the additional complexity of requiring to define all boundary conditions and associated mould systems, such as cooling channels, thereby increasing the likelihood of introducing errors. To avoid this limitation, instead of importing the full mould geometry, only the hosting part was imported together with the corresponding gate, runner, and sprue. Then, using an automated tool, a standardised mould is generated around the hosting part.

Once the hosting part was imported, the procedure required assigning a function to each object in the model. Accordingly, the hosting part geometry was defined as the part, while the runner and gate were assigned their respective functions. It is important to note that the piezo element was not imported together with the hosting part, because the software would not recognise any interaction between the piezo and the part, and it would only interpret the piezo as a solid

body without functional relevance, offering no advantage for the simulation. Subsequently, the melt entrance point was specified by selecting the top surface of the sprue. After completing this step, the mould was generated around the imported geometry by creating a block corresponding to the dimensions of the actual mould, 246 mm x 296 mm, and eight cooling channels were configured on each mould half as straight-line channels, with 6 mm of diameter, spaced by 14 mm, and a distance of 20.9 mm from the mould surface (Figure 48).

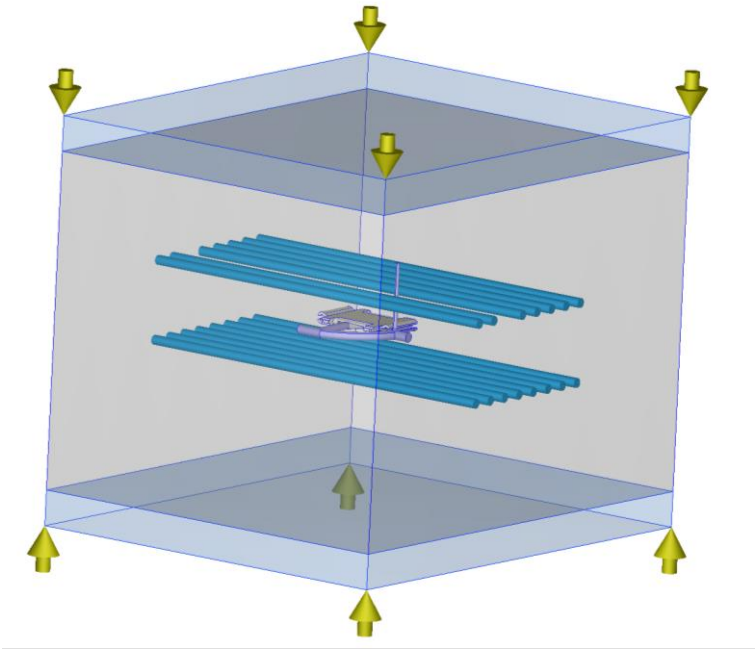

Figure 48- Imported part surrounded by the generated mould

With all the objects created and imported, the conditions were set for mesh generation. To ensure precise control over the type of mesh implemented, the mesh seeding parameters were individually adjusted for each object. For the hosting part, runner, gate, and sprue, different configurations were applied in terms of element size and type to achieve a balance between computational efficiency and result accuracy. Thus, since the hosting part was the main region of interest for the analysis, a more refined mesh was applied to this component, while a coarser mesh was assigned to the runner, gate, and sprue to optimise computational time. Specifically, the hosting part was meshed using a hybrid approach with a boundary layer mesh consisting of five layers of prismatic elements along the part walls, allowing a better capture of physical gradients in the regions where flow–wall interactions most significantly affect the results, in connection with tetrahedral elements distributed through the part thickness, with a node spacing of 1.1 mm applied to both element types. For the gate, which was defined as a fan gate, tetrahedral elements were used with a node spacing of 2.8 mm. Similarly, the runner and sprue were discretised with tetrahedral elements using a curvature-based meshing approach, also with a 2.8 mm node spacing (Figure 49). It is important to note that the mould base, generated around the hosting part, did not require detailed meshing since it was not the focus of the simulations. Therefore, only the default mesh was applied, consisting of beam elements assigned to the cooling channels.

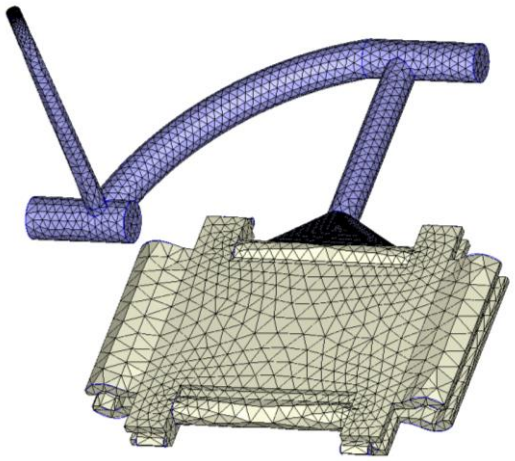

Figure 49- Hosting part and runner mesh

To complete the setup phase and carry out the simulations, the material ABS was attributed by importing the material data from the supplier, the injection machine technical information and the process parameters, to enhance the simulations' precision in representing real conditions. Therefore, when it comes to importing the process parameters, besides the parameters already stated in Table 13, more settings were defined in the program, like the injection profiles regarding injection speed and packing pressure, and the barrel temperature profile, see Figure 50.

a)

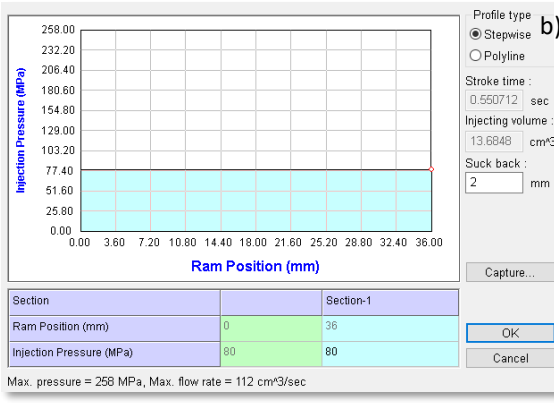

b)

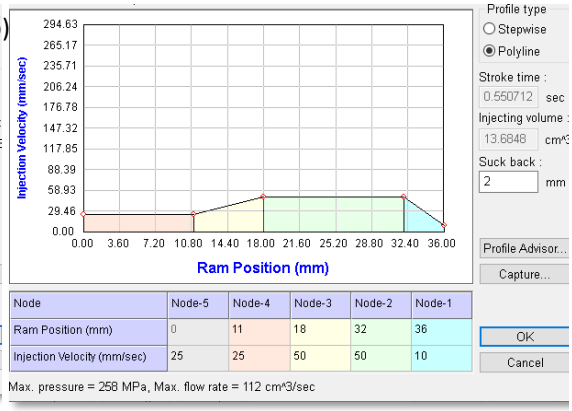

c)

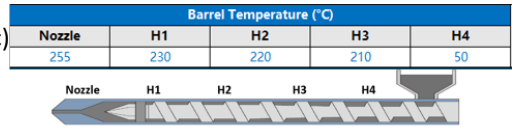

d)

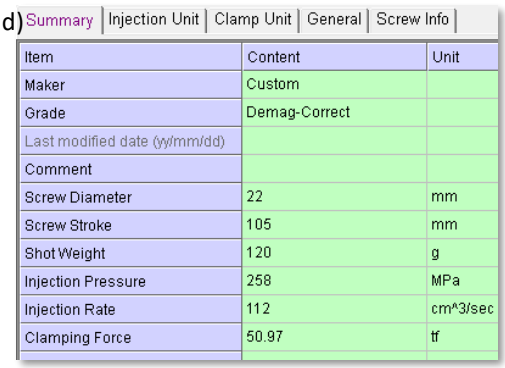

Figure 50- a) Injection pressure profile, b) injection profile, c) barrel temperatures, d) machine settings

By carrying out the simulations, it was possible to obtain a more detailed understanding of how the polymer behaves during cavity filling as well as the deformations that the part undergoes during cooling. Regarding the filling simulation (Figure 51), the Moldex3D animation provided clear insights into the progression of the melt front throughout the filling phase. The front propagated as a circular expansion wave, with the cavity being filled in 0.810 s. The first region to be filled was the area surrounding the piezo, followed by the two recesses near the gate, then the two recesses on the opposite side, and finally the lateral fixation clamps. This sequence contradicted the initially expected filling logic, in which the geometries directly in front of the gate and the lateral clamps would be filled first, followed only afterwards by the side features aligned with the gate, as the cavity progressively filled with polymer. Additionally, the filling simulation provided insight into the evolution of the melt front temperature. This analysis enabled validation of the chosen position for the pin-header connector. Among the four possible corner locations, the melt front arrived at each with identical temperature values. Thus, no corner exhibited a temperature drop that would provide thermal protection for the connector and its soldered wires. This is a critical result, since it was expected that the melt front would progressively lose thermal energy while filling the cavity, resulting in the last-filled regions being exposed to a lower-temperature polymer. However, such behaviour was not observed, confirming that none of the possible connector placements is thermally advantaged.

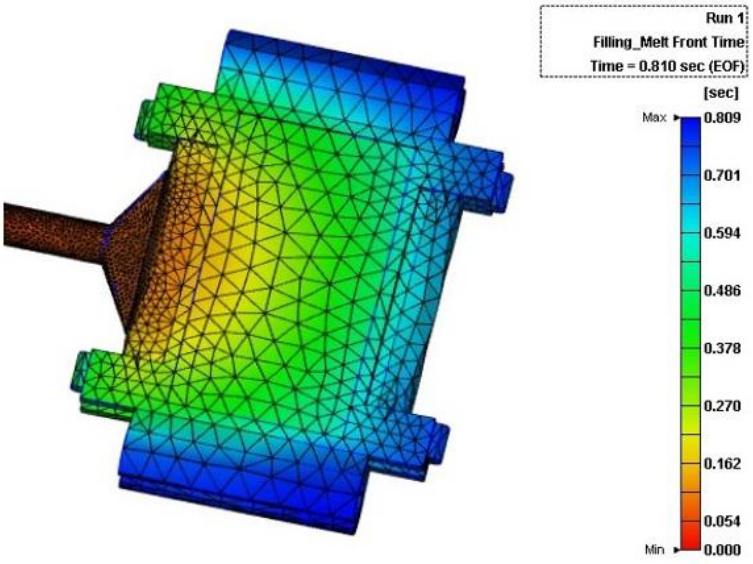

Figure 51- Filling simulation result

With respect to shrinkage (Figure 52) and warpage (Figure 53), the simulations revealed that the region where the piezo is over-moulded is subjected to significant contraction effects, confirming the earlier experimental findings that fracture occurred due to shrinkage-induced contraction forces. Specifically, shrinkage levels between 6% and 8% were observed at this region. Regarding warpage, the displacement values were found to be approximately 0.125 mm around the embedded piezo area. Interestingly, however, within the central zone of this region, a circular area with near-zero warpage was identified. This phenomenon can be explained by the interaction between shrinkage and warpage: as the material contracts, it is progressively

pulled toward the centre. Once it reaches the central region, no further displacement is possible, causing the polymer to become immobilised in a circular pattern.

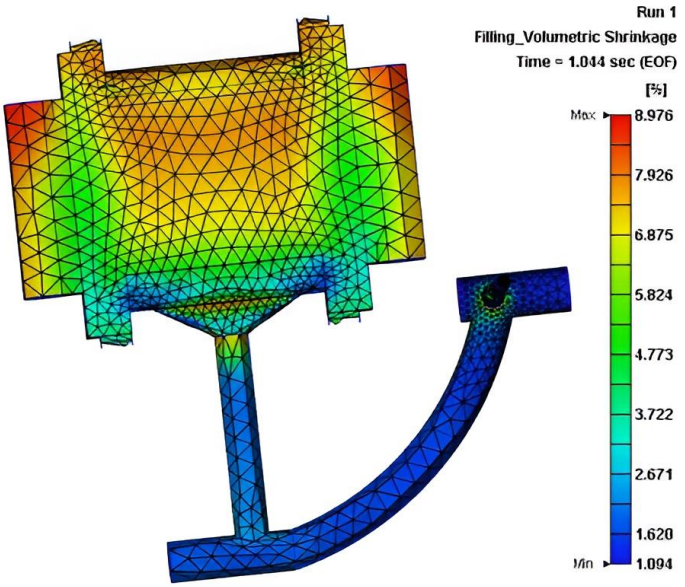

Figure 52- Shrinkage simulation result

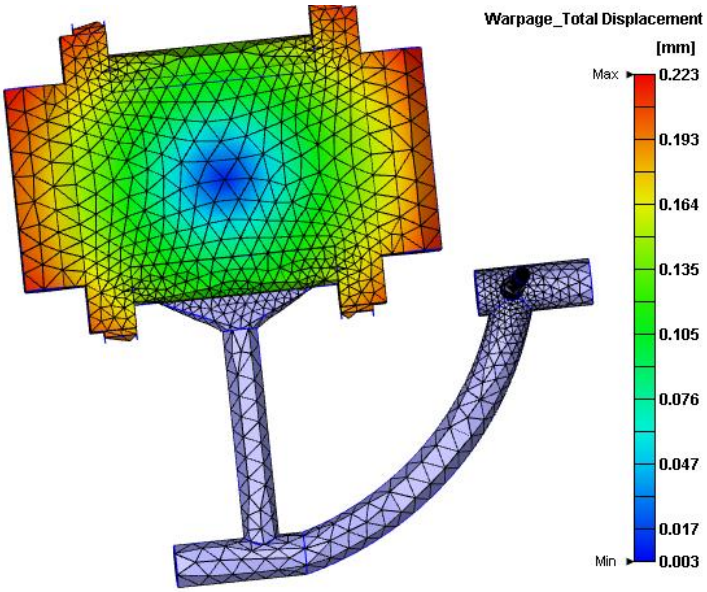

Figure 53- Warpage simulation result

To validate the accuracy of the obtained results and establish a solid knowledge base for the next stages of testing, a comparative study was carried out between Moldex3D results and experimental results. This validation was based on the execution of short-shot experiments, performed by removing the packing pressure and gradually reducing the screw stroke to decrease the injection volume. The final step involved comparing the successive outcomes in terms of both the geometric shape and the volume of the hosting part.

Figure 54 below presents the results of the short-shots produced by the injection moulding machine. The screw stroke reduction was not always performed with the same step size, in order to obtain a more meaningful analysis of the results. For instance, a 1 mm reduction in certain cases did not produce a significant difference between successive values of screw stroke, as observed when comparing 31 mm with 32 mm and 33 mm. Therefore, the reduction was carried out from 32 mm directly to 26 mm, to obtain a clearer distinction in the results. Furthermore, for some specific screw stroke values, more than one injection was performed, since process repeatability decreased as the stroke was progressively reduced. Conducting multiple injections at the same condition, therefore, provided a broader basis for comparison.

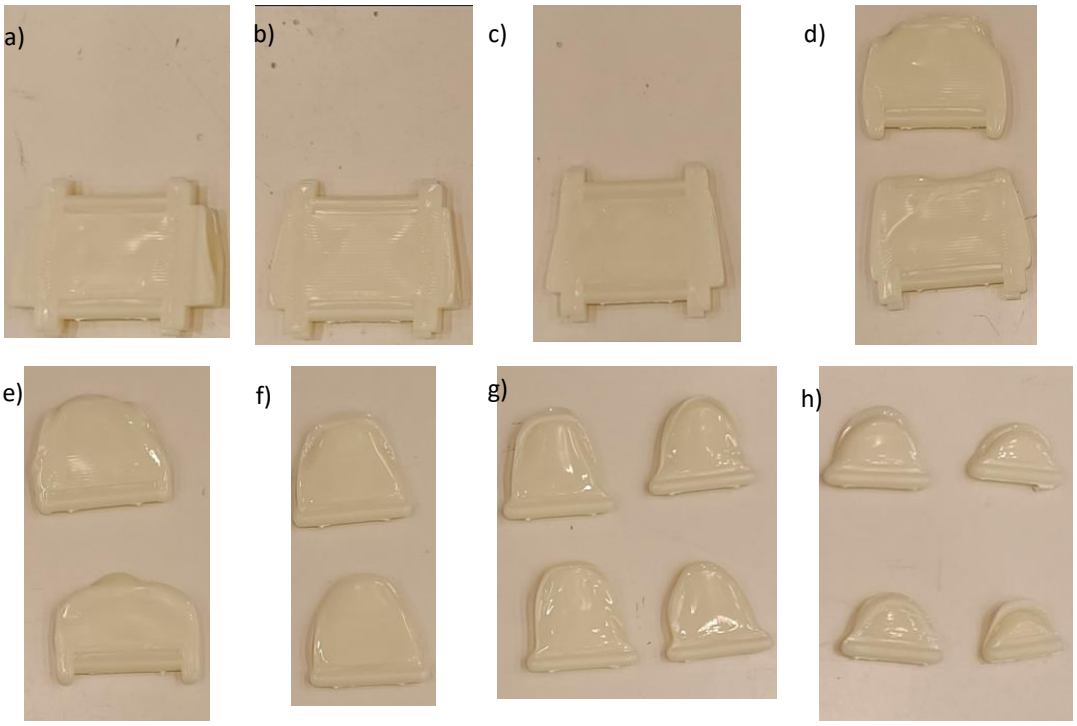

Figure 54- a) only without packing pressure, b) 35 mm, c) 34 mm, d) 32 mm, e) 26 mm, f) 25 mm, g) 24 mm, h) 22 mm

From Figure 54, the short-shot results appear to be positive when compared to the filling simulation of the hosting part. By analysing the sequence of images corresponding to the progressive reduction of the screw stroke, it is possible to understand approximately how the flow front evolves during the cavity filling process. Nevertheless, in Table 27 the comparison between the short-shots produced by the injection machine with those from Moldex3D is described. Then, the samples from the injection machines were weighed to calculate their volume, using the density of ABS as a reference. These experimental volumes were subsequently compared with the volumes obtained from the simulation results.

Table 27- Comparison between the short shots produced in the injection machine the Moldex3D ones.

Stroke	Injection machine samples	Moldex3D samples
34 mm		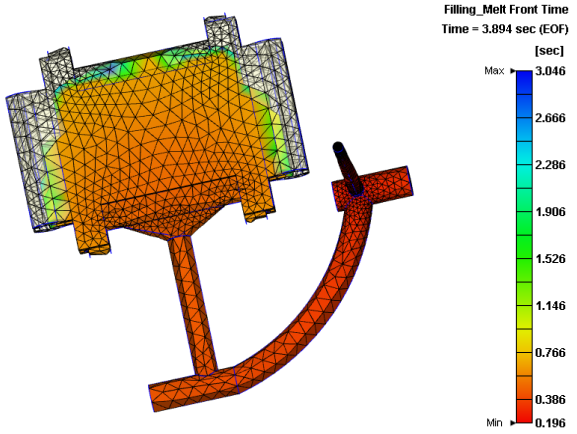
32 mm		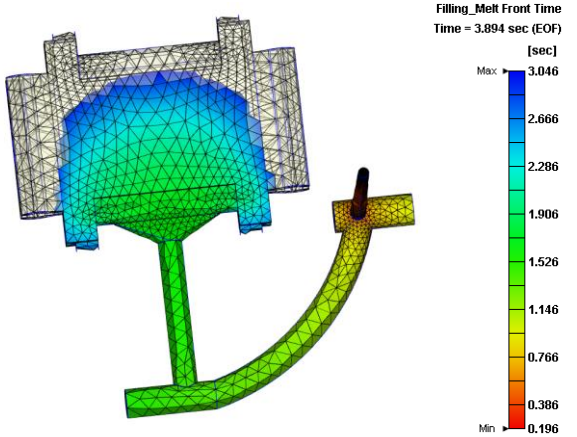
26 mm		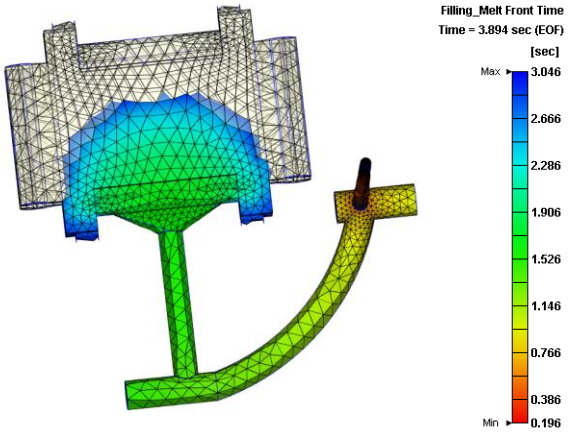

Table 27- Comparison between the short shots produced in the injection machine the Moldex3D ones (continued)

Stroke	Injection machine samples	Moldex3D samples
24 mm		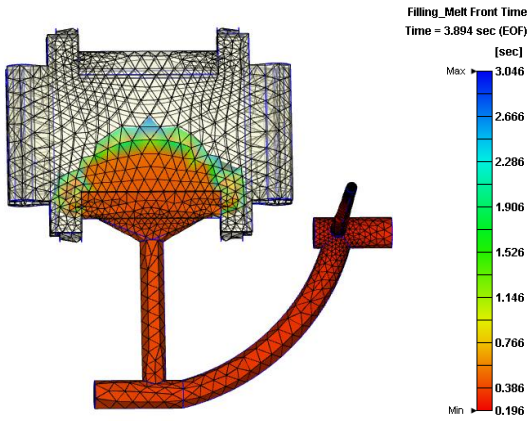
22 mm		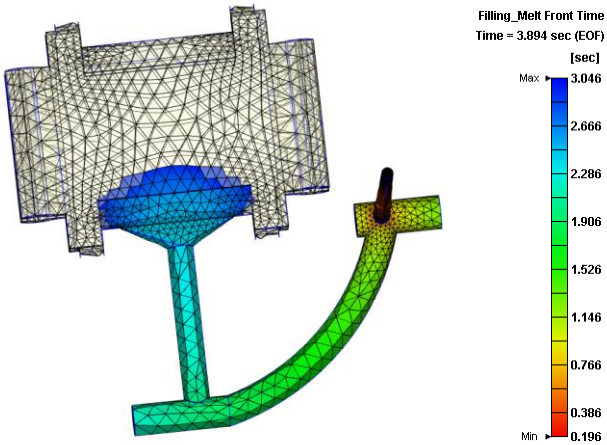

Table 28- Comparison of volumes between the injection-moulded samples and the Moldex3D results

	Real injection machine values		**Moldex3D values**	**Error between volume results [%]**
Stroke	Weight [g]	Volume [cm³]	Volume [cm³]	
36	6.516	6.206	6.20	0.09
32	4.413	4.200	4.08	2.85
26	3.013	2.870	2.81	2.09
24	2.003	1.907	1.81	5.30
23	1.253	1.194	1.07	10.38
22	0.933	0.889	0.81	9.750

From the comparative analysis of Table 27, it can be observed that, for the respective stroke values, Moldex3D is able to closely replicate the parts produced by the injection moulding machine. The simulation results reproduce not only the same flow-front propagation pattern but also the geometric details filled by the polymer at each short-shot stage. These findings, when considered alongside the volume data presented in Table 28, reinforce the conclusion

that the software accurately mimics the behaviour of the injection machine. Although the recorded volumes are not perfectly identical, the error between simulated and experimental values never exceeds 10%, apart from the 23 mm stroke case, where the deviation reached 10.38%. This slight disparity may be attributed to either the intrinsic limitations of the software or the element size used in the mesh. Since the observed discrepancies are in the order of tenths of a cubic centimetre, the corresponding volume variations are relatively small, suggesting that the mesh may not be sufficiently refined to capture such minor differences. Nevertheless, for the intended objectives and given the results obtained, it can be concluded that the mesh is adequately refined and, most importantly, that the simulation results are reliable, providing a precise representation of the injection moulding process.

3.6.4. Second phase of testing

Before initiating the next phase of testing, some considerations must be made to better understand the modifications to introduce to the process, with the objective of reducing the shrinkage and warpage that the hosting part is subjected to during cooling on the outside of the mould. Based on the literature review [86-88], it can be observed that there are several injection moulding parameters which, when adjusted, can lead to a reduction in shrinkage. One of the most influential parameters is the packing pressure: progressively higher values help distribute residual stresses more evenly within the part, thereby reducing both warpage and shrinkage [88]. Closely related to packing pressure is the cooling time, since longer cooling periods allow the part to solidify more uniformly, lowering stress concentrations and ultimately minimising shrinkage [87]. In contrast, lower melt temperatures tend to result in reduced shrinkage rates. These parameters, together with the pressure and temperature variations occurring throughout the injection process, can be summarised by the pressure-specific volume-temperature (PvT) curve (Figure 55), which illustrates their overall impact on shrinkage behaviour.

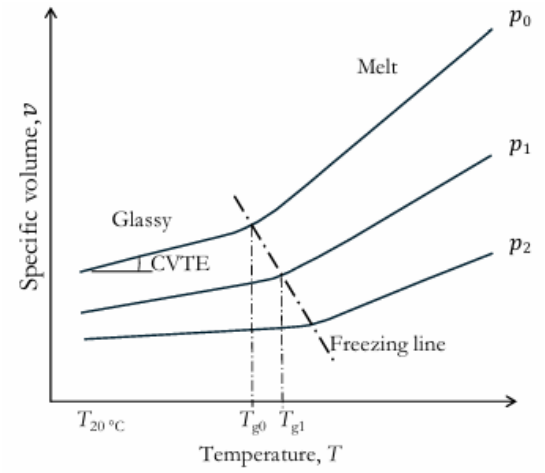

Figure 55- Representative Pvt curve for amorphous polymers [89]

With the knowledge of which parameters influence shrinkage, and how they should be adjusted to minimise it to prevent damage to the piezo during cooling, a series of tests were conducted

to evaluate their effectiveness. However, altering certain parameters can introduce negative side effects. One such example is packing pressure. While an increase in packing pressure is expected to reduce shrinkage, excessive values may result in defects at the connector region due to polymer penetration between the connector and the mould. This occurrence could cause the connector to become stuck during demoulding, as the polymer interlocks with the mould surfaces. Additionally, higher packing pressure may compromise the electrical connections between the piezo, the connector, and the soldered wires, as the polymer exerts significant force on these junctions during the packing stage. The situation can be further exacerbated if the injection temperature is reduced, since a lower melt temperature increases the viscosity of the polymer. As a result, the polymer flows less easily upon contact with surfaces, intensifying its mechanical interaction with both the piezo and the connector. Despite these potential issues, it was deemed necessary to systematically investigate the effect of parameter variations.

By considering the number of parameters involved and the possible combinations between them, the total number of tests required would be extensive. To avoid excessive costs associated with failed trials, an alternative to the piezo had to be introduced. A microscope glass cover slip was therefore selected to act as a dummy during injection moulding. The choice of the cover slip was based on its very low cost (approximately €12 for 1000 units), and more importantly, on the fact that it has the same thickness as the piezo and is also made of a ceramic material, thus providing a reasonably similar mechanical behaviour. The only difference lies in its dimensions, as the cover slip measures 22 mm × 22 mm, unlike the piezo. For this reason, in the tests, a glass cover slip was inserted into the mould to be over-moulded (Figure 56).

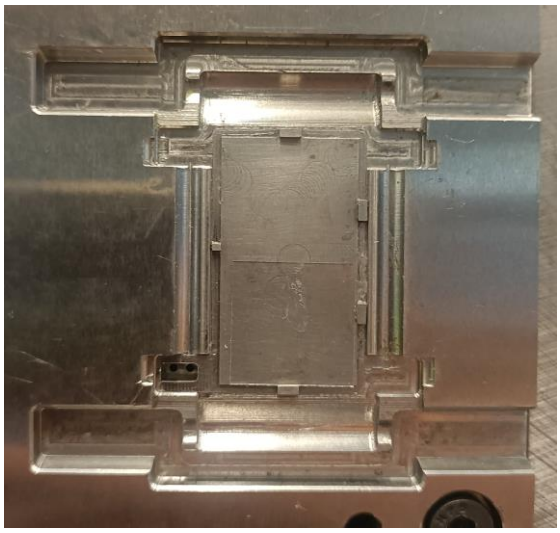

Figure 56- Glass cover slip inserted on the mould

Table 29- Packing pressure variation

Packing pressure [MPa]	**Injection temperature [℃]**	**Cooling time [s]**	**Mould temperature [℃]**	**Withstanding time**
400	255	20	65	3 min 24 s
700	255	20	65	2 min 40 s
900	255	20	65	2 min 55 s
1200	255	20	65	3 min 7 s

Table 30- Injection temperature variation

Injection temperature [℃]	Packing pressure [MPa]	Cooling time [s]	Mould temperature [℃]	Withstanding time
230	700	20	65	2 min 47 s
235	700	20	65	4 min 1 s
240	700	20	65	3 min 12 s
245	700	20	65	3 min 24 s

Table 31- Cooling time variation

Cooling time [℃]	Packing pressure [MPa]	Injection temperature [℃]	Mould temperature [℃]	Withstanding time
40	700	235	65	3 min 29 s
80	700	235	65	3 min 14 s
120	700	235	65	2 min 1 s
240	700	235	65	-

Table 32- Mould temperature variation

Mould temperature [℃]	Packing pressure [MPa]	Injection temperature [℃]	Cooling time [℃]	Withstanding time
60	700	235	20	3 min 01 s
70	700	235	20	2 min 57 s
75	700	235	20	3 min 41 s
85	700	235	20	3 min 17 s

The results presented between Table 29 and Table 32 are only a sample of the tests conducted, as it would not be meaningful to report the entirety of the experimental data due to its immense volume and the lack of any relevant outcomes. During testing, the injection parameters were adjusted as previously indicated, to reduce the shrinkage of the hosting part and ensure that the glass cover (used as a dummy for the piezo) could withstand the cooling stage. However, despite multiple attempts at parameter optimisation, none of the tests were successful in achieving this goal (Figure 57).

Therefore, an alternative evaluation method was implemented. This method consisted of recording the time taken for the glass cover to fracture after the hosting part was demoulded, to further analyse and compare the times between trials. Nonetheless, no significant increase in fracture time was observed, nor was there any progressive improvement with parameter variation. Another observation was that reducing the injection temperature (Table 30), which consequently increases polymer viscosity, led to displacement or rotation of the glass cover during moulding. In several cases, this temperature variation resulted in damage to the glass cover. Such behaviour, however, would not be expected with the actual piezo, as its dimensions fit perfectly into the holders. Nevertheless, this finding is relevant for future testing, as it highlights the influence of polymer viscosity on the stability of components being over-moulded. Furthermore, at packing pressure levels exceeding 1000 bar, flashing phenomena were observed. Given the poor results obtained, a secondary strategy was attempted,

consisting of keeping the part inside the mould for four minutes (longer than the average time recorded for the glass cover to fracture due to shrinkage), under the assumption that fully constraining the glass cover during cooling would prevent bending and subsequent fracture. However, this approach was also unsuccessful, as the glass cover was already broken upon mould opening (Table 31). Similarly, preheating the glass cover to 200 °C before injection was tested, with the intention of inducing thermal expansion before moulding, so that subsequent contraction during cooling would occur in synchrony with the hosting part. Yet again, no successful results were obtained.

In summary, it can be concluded that reducing shrinkage, or at least mitigating its impact on the piezo, cannot be achieved by adjusting processing parameters alone when using ABS. The material appears to present an intrinsic limitation for this application. Alternative solutions must therefore be considered, either by selecting polymers with lower shrinkage rates or by introducing different injection moulding techniques

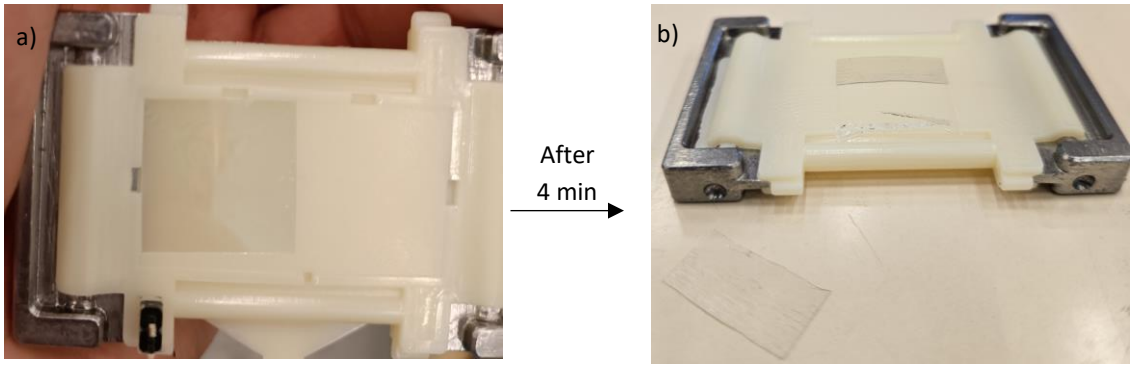

Figure 57- a) hosting part with glass cover slip right after demoulding, b) glass cover slip cracked in the cooling process due to shrinkage

Before attempting any alternative injection moulding techniques to mitigate the effects of shrinkage, experiments were conducted with polymers other than ABS, since implementing new moulding methods would probably require modifications to the mould design. In the search for alternative materials, the selection criterion was that the polymer should incorporate fibres in its composition. The basis for this choice is that the presence of such fillers constrains the material during cooling, hence reducing shrinkage along the fibre orientation. In addition, fibre reinforcement enhances the mechanical strength of the polymer, which is advantageous for the panel. Based on these considerations, two candidate materials were selected for testing. Their shrinkage values are compared with ABS in Table 33.

Table 33- Shrinkage data regarding the materials tested (Annex.A, Annex.B, Annex.C)

ABS	**Liner mould shrinkage [%]**	**0.4-0.7**
(PBT+PET)- Ultradur B4040 G10	Shrinkage along the fibres [%]	0.2
	Shrinkage transversal to the fibres [%]	0.8
LCP(Liquid crystal polymer)- Vectra A115	Shrinkage along the fibres [%]	0.1
	Shrinkage transversal to the fibres [%]	0.4

The injection parameters utilized to carry out tests using Ultradur B4040 G10 and Vectra A115, can be found in Annex B and C, respectively.

During the execution of the tests, several additional difficulties were encountered. Owing to the fibre content in the polymers, their processability proved to be a considerable challenge. In the case of Ultradur B4040 G10, after each injection, the material consistently solidified either in the nozzle or caused the sprue to stick inside the mould. This solidification required frequent interruptions of the machine to unclog the nozzle or remove the sprue, preventing the injection cycle from being carried out continuously. To mitigate this issue, the injection temperature was increased to the maximum limit recommended by the manufacturer (280 °C), so that the material would remain more fluid and carry a higher thermal load, thus delaying solidification. With respect to Vectra A115, similar problems were observed, and also material frequently became stuck in the feeding hopper due to agglomeration. This made it necessary to feed only small quantities into the hopper before each injection. Nevertheless, despite these difficulties, it was possible to produce parts, as shown in Figure 58.

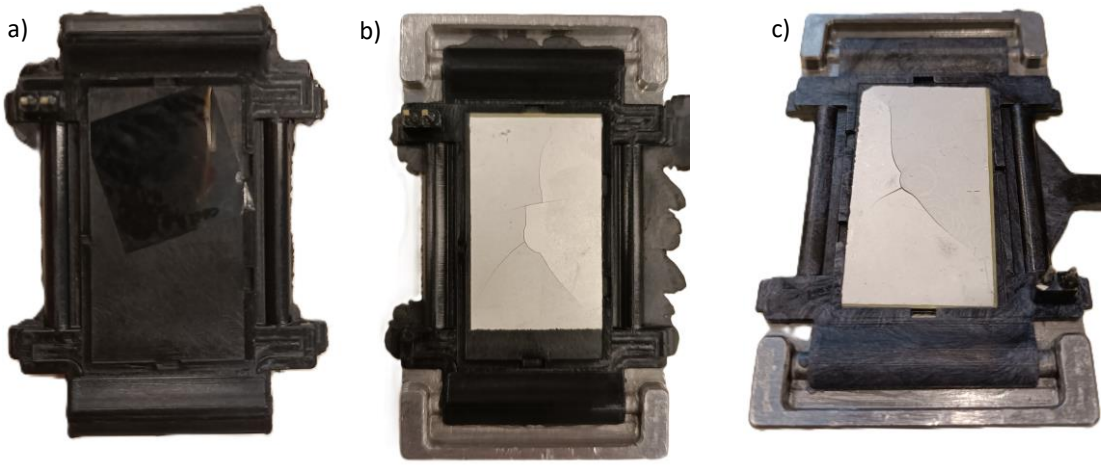

Figure 58- a) Ultradur sample with glass cover slip, b) Ultradur sample with piezo integration, c) Vectra A115 sample with piezo integration

When carrying out the tests, different outcomes were observed. Initially, PBT+PET was tested by positioning the glass cover inside the mould instead of the piezo, so that, as in the procedure with ABS, multiple tests could be conducted to adjust the injection parameters without risking piezo damage. Unlike with ABS, however, the glass cover slip was successfully over-moulded within the hosting part and survived the cooling process outside the mould, as shown in Figure 58 a). Defects only appeared after an average of eight hours, suggesting that the fracture occurred due to the constant stress exerted by the polymer as a consequence of shrinkage. This behaviour indicates that the use of a fibre-reinforced material yielded a positive result in mitigating shrinkage, since none of the numerous tests with ABS produced comparable success. Consequently, it was decided to proceed with testing the over-moulding of the piezo itself, given the high likelihood of success. However, once tested, the piezo again exhibited bending curvature induced by material shrinkage after 6 min, eventually leading to cracking, as illustrated in Figure 58 b). As no success was achieved with PBT+PET, a second attempt was made using the special polymer in the hope that its lower shrinkage would lead to improved

performance. Nevertheless, the piezo was again unable to survive the cooling stage of the hosting part Figure 58 c).

In an attempt to exploit the reduced shrinkage along the fibre direction, it was hypothesised that repositioning the gate could potentially mitigate the issue. Specifically, orienting the melt front along the length of the piezo might better constrain bending, since in the current mould design, the fibres follow the melt-front orientation, creating a semi-circular distribution across the part. However, implementing such a gate modification within the existing insert-mould design would be highly challenging and would introduce flashing in the clamping claw of the hosting part (design constraint, Table 12). Given that the glass cover slip survived shrinkage, it was also hypothesised that elements with smaller dimensions might be less susceptible to the effects of polymer contraction or exhibit a reduced tendency to bend. Tests were therefore conducted in this direction (Figure 59).

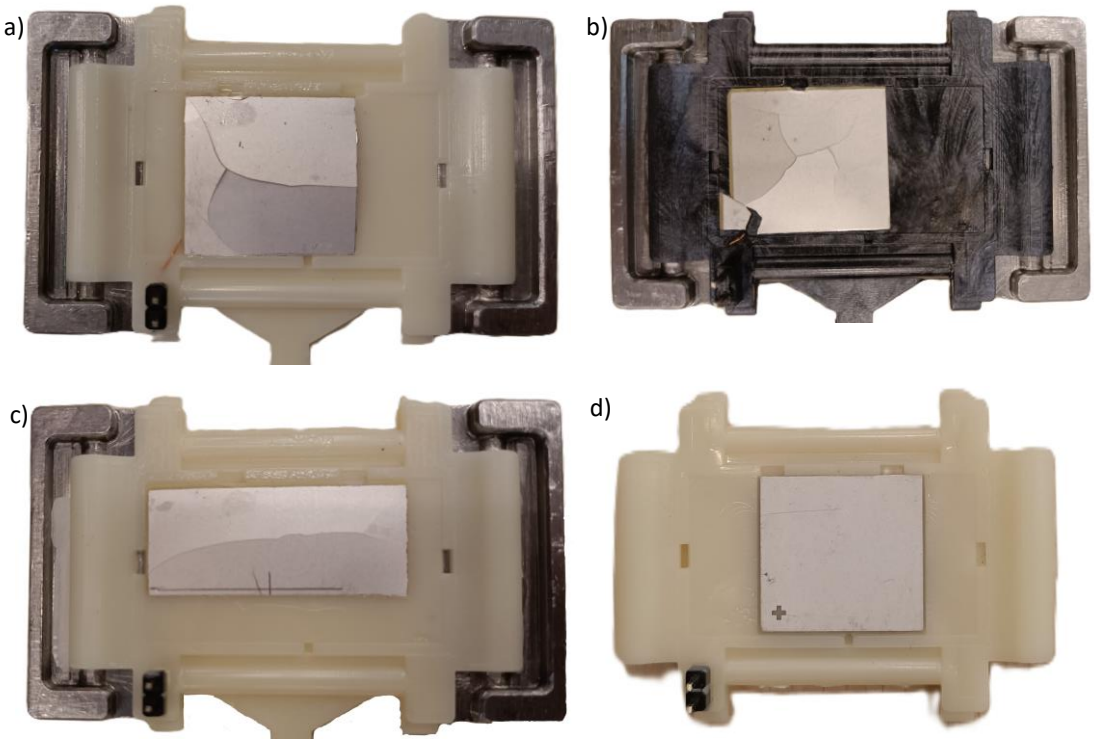

Figure 59- a) test using ABS with 22 x 22 mm piezo, b) test using (PBT+PET) with 22 x 22 mm piezo, c) test using ABS with 32 x 10 mm piezo, d) test using ABS with 20 x 21 x 0.5 mm piezo

Despite attempts to use piezo elements with smaller dimensions, in the expectation that they would be less affected by shrinkage-induced contraction forces, no improvements were observed, as shown in Figure 59 a), b), c). Moreover, an electrical wire was soldered between the connector and the piezo (Figure 59 a), b) to obtain preliminary insights, since in previous tests this step was disregarded because the focus was on the piezo getting over-moulded with success. It was confirmed that the solder joints withstood the injection process, as validated by current continuity checks performed with a multimeter. On another hand, since the failure of the piezo consistently followed the same pattern, accompanied by progressive bending along its length due to shrinkage, followed by fracture, it was decided to test a thicker piezo to increase its resistance to bending and possibly enable it to survive the cooling stage of the

hosting part. The results showed that this thicker piezo was successfully over-moulded and withstood the cooling process without undergoing deformation or subsequent fracture. However, this outcome comes with a cost, as noted in section 3.4.2, of reducing the modal electromechanical coupling and consequently the vibration performance, when reducing the in-plane dimensions of the piezo while increasing its thickness. In this specific case, for the thicker piezo tested, the performance dropped from 15.28 % to 5.4 %. Therefore, efforts should focus on ensuring the applicability of the originally selected piezo to survive the cooling stage of the hosting part, not to compromise its acoustic efficiency.

3.6.5. Third phase of testing

Ensuring that the optimally dimensioned piezo is over-moulded without being compromised by polymer shrinkage in the cooling process, it was decided to change strategy and follow an approach in which either the process or the mould design would have to be rethought, since no success had been achieved with different materials or injection parameters. In this context, and considering once again the behaviour observed before piezo fracture caused by shrinkage, it was defined as a vital objective that the piezo should not bend under the action of shrinkage forces. To achieve this objective, the only solution would be for a body to prevent or resist the bending movement of the piezo. Therefore, it was assumed that, if a polymer layer was placed on top of the piezo, the component would be fully encapsulated and would hardly bend by the action of shrinkage forces, due to the induced constraints.

To implement this objective using injection moulding, the only alternative identified was the use of a two-shot moulding machine. In this process, the piezo is first over-moulded in the same manner as performed during the preceding tests, the mould is opened, and the rotary table supporting the fixed half of the mould rotates with the hosting part and the over-moulded piezo is inserted. The mould is then closed again with a different moving half, where the second shot is carried out to cover the piezo with a polymer layer. After demoulding, the cooling of the part occurs outside the mould, but this time the polymer layer is theoretically expected to prevent the bending of the piezo caused by shrinkage.

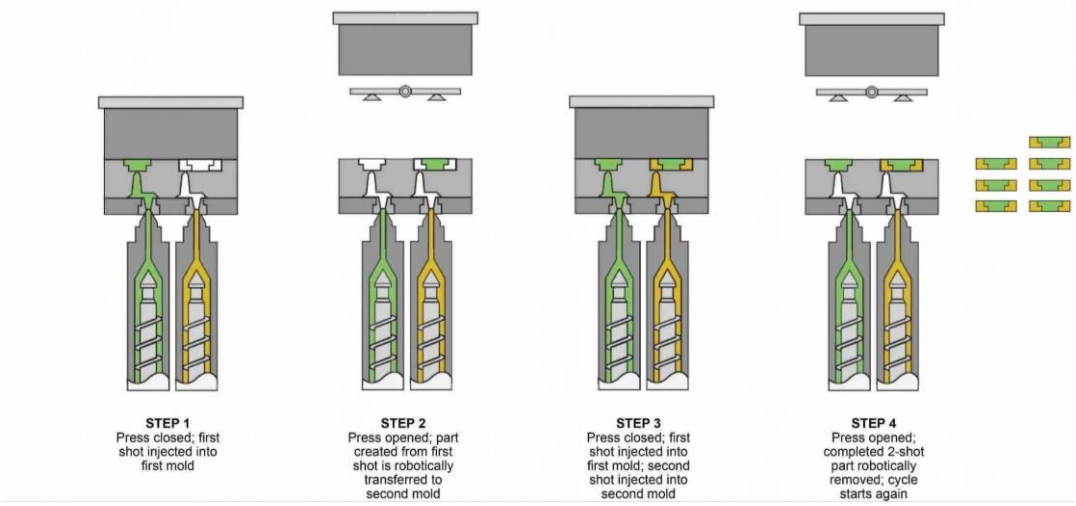

Figure 60- Diagram representative of two-shot injection moulding [90]

To implement the two-shot process, it would have been necessary to develop a completely new mould, which would have significantly increased the project cost. Furthermore, it would have required contracting an external company, as the laboratory is not equipped with such machinery. To overcome these constraints, an alternative solution was thought to simulate the two-shot injection moulding process. This solution involves the fabrication of a component via additive manufacturing (Figure 61 a) that serves as the protective layer for the piezo (second shot). The piezo, already connected to the connector via electrical wires, is positioned within this component (Figure 61 b) and subsequently inserted into the mould for over-moulding. In this approach, the second shot of the polymer protective layer, which would normally be applied after the piezo has been over-moulded, is effectively pre-applied and introduced into the mould alongside the piezo and other electronic components (Figure 61 c), thereby approximating the intended two-shot concept.

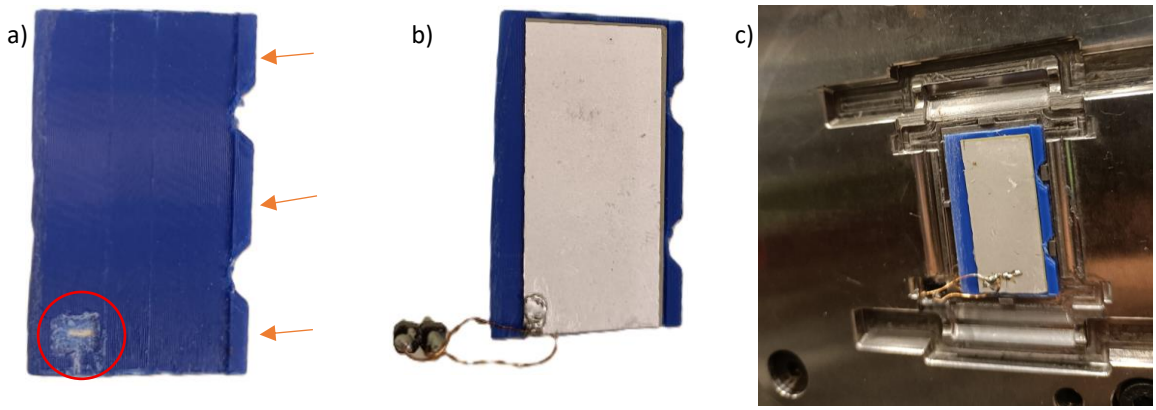

Figure 61- a) 3D printed part, b) piezo with its electrical connections together with the 3D printed part, c) set inserted on the mould

The component manufactured by additive processes was designed to integrate seamlessly into the current mould design. To achieve this goal, a 0.7 mm thick base was created to support the piezo. A higher thickness was avoided, as it would have excessively offset the piezo relative to the mould surface, resulting in the melt front hitting the piezo longitudinally rather than descending onto it, which could cause the displacement of the piezo. Connected to this base, a wall (orange arrows in Figure 61 a) was added against which the piezo is positioned, incorporating two grooves that fit into the existing holders of the mould, to provide stability during cavity filling. After the part was manufactured via additive manufacturing, a pocket (red circle in Figure 61 a) was machined using a drill to accommodate the solder joint of the electrical wire on the lower surface of the piezo, ensuring full support (Figure 61 b). Before placing the piezo into the part, a thin layer of adhesive was applied to secure it. In contrast to the preliminary tests, the use of adhesive in this configuration does not cause any negative effects, as the piezo is no longer in direct contact with the mould and will not suffer damage during demoulding.

Before testing this new concept, it was necessary to establish a method to verify the integrity of both the piezo and its electrical connections after the injection process, since they would be fully encapsulated in plastic, preventing visual inspection. Electrical continuity testing of the piezo and cables was also not feasible, as no direct access to the piezo terminals would be

available. For these reasons, it was decided to compare the capacitance of the piezo and the cables before and after the injection process. This approach only requires connecting the multimeter to the over-moulded connector, which is wired to the piezo. It should be noted that a reduction in capacitance relative to the initial measurement is expected after injection, due to the piezo being over-moulded and mechanically constrained by the polymer.

The injection tests were carried out using ABS due to its easy processability and its mechanical properties, which were previously detailed in section 3.5.2 The injection parameters used can be checked in Table 13.

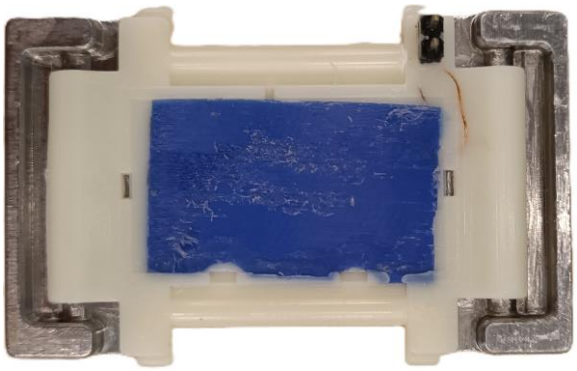

Figure 62- Over-moulded piezo and its electronics using an alternative two-shot injection process

Several injection tests were carried out, and visual inspection initially suggested that the piezo had been successfully over-moulded (Figure 62). After allowing the hosting part to cool, when held against a light source, the outline of the piezo body was visible, and no apparent damage was observed, indicating that it had seemingly withstood the cooling stage outside the mould. However, capacitance measurements after injection consistently showed progressively lower values, reaching 1.2 nF after a few hours, a substantial decrease when compared with the pre-test measurement of 54.5 nF.

To resolve any uncertainty regarding the condition of the piezo and its electrical connections, given that direct visual confirmation was not possible, it was decided to conduct further trials using PMMA as the polymer, due to its transparency. This change would allow clear visual inspection of both the piezo and the soldered connections after over-moulding (Figure 63), thus providing direct evidence of whether structural or electrical failures were occurring during the process.

Through the use of PMMA (Annex D), it was possible to visually confirm that both the piezo and the electrical connections had been successfully over-moulded and had withstood the shrinkage because of the cooling process outside the mould. In addition, capacitance measurements further supported this outcome, as the value decreased from 54 nF to 37.1 nF and remained stable at 37.1 nF over time. This reduction also indicates that the piezo is constrained by the polymer, demonstrating strong impregnation into the plastic, which enhances the coupling factor and consequently the acoustic performance. Given these results, it was necessary to investigate what was the root of the problem for the faulty capacitance measurements in ABS samples.

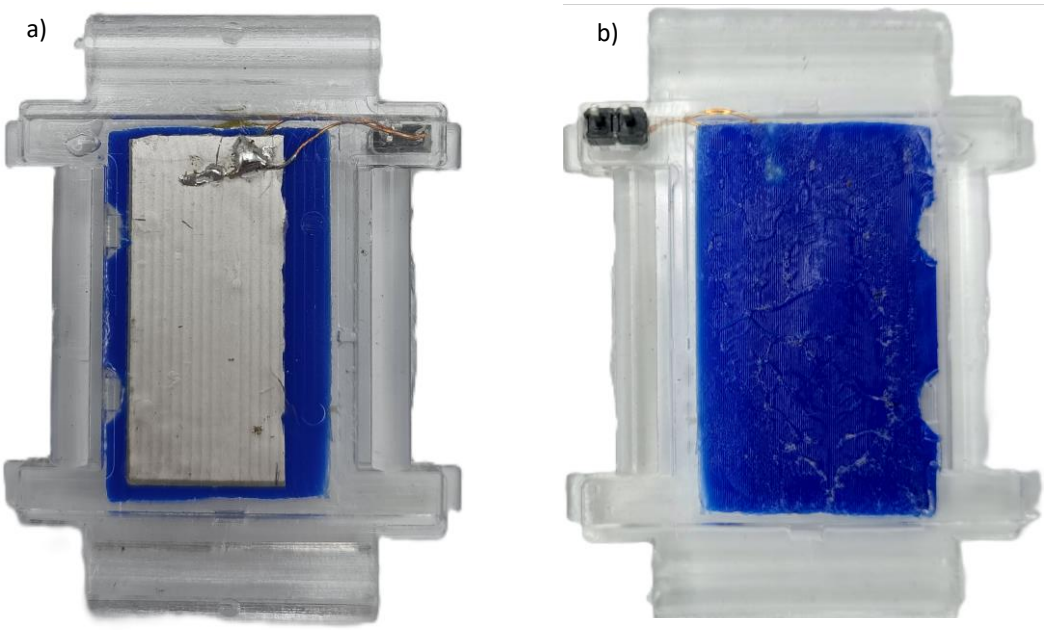

Figure 63- a) Hosting part front view injected using PMMA, b) Hosting part back view injected using PMMA

To this end, a destructive test was conducted on a sample equivalent to that shown in Figure 14, where the polymer was carefully removed from the hosting part to gain direct access to the piezo. Then, electrical continuity was verified using a multimeter, confirming that the piezo itself had survived. However, the cable connecting the lower surface of the piezo to the connector had been damaged. The most plausible explanation for this phenomenon lies in the cable management adopted for the ABS tests, since the cables were cut to a longer (Figure 64 a) length than those used for PMMA (Figure 64 b), under the assumption that the additional length would allow slight repositioning when impacted by the melt front. In practice, the opposite effect occurred: the polymer flow exerted a pulling force, ultimately detaching one of the cables.

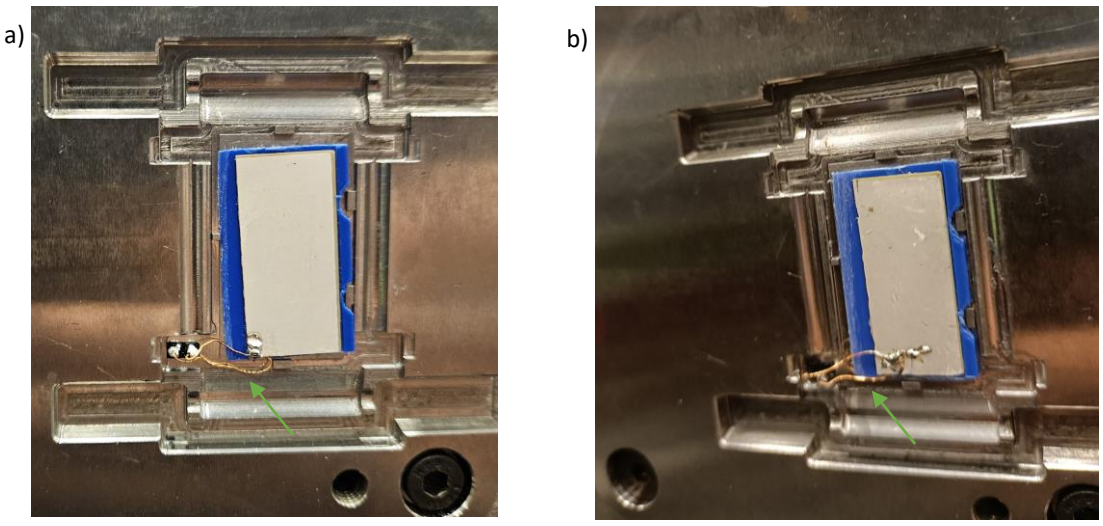

Figure 64- a) cable management for ABS tests, b) cable management for PMMA tests

Through the series of tests conducted, it was possible to validate the two-shot injection moulding concept for over-moulding the piezo and its electronic components without fracture during the cooling of the hosting part. The protective 0.7 mm layer, corresponding to the second shot, proved sufficient to prevent the piezo from bending under the contraction forces generated by material shrinkage. Consequently, a process suitable for mass production was achieved, enabling the manufacture of the panel with the piezo successfully over-moulded (Figure 65), while preserving the optimal piezo dimensions required to maximise the coupling factor.

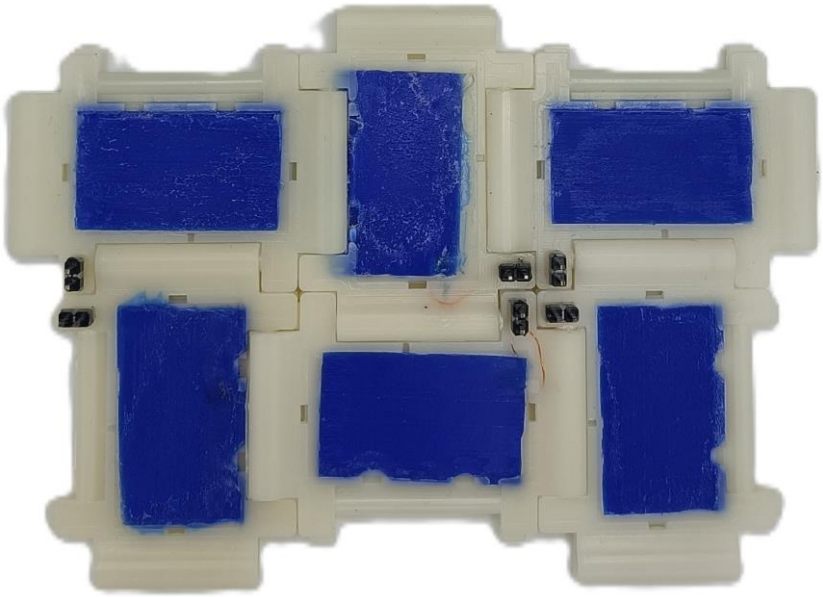

Figure 65- Modular panel representation with over-moulded piezos

4. Conclusion

4.1. Final Conclusions

Following an iterative and scientifically grounded approach, it was possible to achieve the main objective of the present study: over-mould a piezoelectric element by injection moulding to produce a mass-scale metamaterial panel. This goal was accomplished through the combined the use of computational tools, which enabled the understanding of the physical phenomena inherent to the injection process and the interaction between the piezo and the hosting part, with the practical development of the project. In this context, it was possible to establish several conclusions that summarise the work carried out and provide insights into the over-moulding of piezoelectric elements.

The established conclusions are:

- Through the use of COMSOL software, it was concluded that the dimensions of the piezo to be over-moulded into the hosting part have a direct impact on the modal coupling factor for the first vibration mode, as well as the position it occupies within the hosting part;
- The piezo dimensions analysis carried out on the COMSOL simulations, showed that, for the selected fixing position, variations in length have a greater influence on the modal coupling factor of the first vibration mode than variations in width. Furthermore, the thickness of the piezo should be kept as low as possible to maximise the coupling factor, thereby enhancing the vibration performance;
- The optimal dimensions of the piezo, while also considering the availability of piezoelectric elements on the market, were determined to be $36 \times 20 \times 0.22$ mm^3;
- A piezoelectric element in the form of a sheet, such as the one employed in this work, is inherently difficult to integrate into an injection moulding process due to its intrinsic brittleness. The main challenge lies in achieving a balance between establishing a solution capable of stabilising the element during the injection process, while simultaneously ensuring that it can be demoulded without cracks;
- The most effective mould design to stabilise the piezo and its electrical components during cavity filling, while allowing the piezo to be demoulded without damage, is the implementation of holders that secure the piezo by its edges, with the element supported against the mould surface and its electrical components accommodated within a pocket;

- Considering all physical phenomena occurring in the hosting part after it is injected with the over-moulded piezo, shrinkage is the only factor responsible for damaging the piezo once it has already been over-moulded. This damage arises from the compressive forces generated by the shrinkage of the part during cooling inducing a bending curvature in the piezo, ultimately leading to its fracture. This behaviour is supported by empirical tests and Moldex3D shrinkage simulations;
- The redefinition of parameters aimed at inducing lower shrinkage, or the use of polymers with fillers that enable reduced shrinkage rates, do not result in a sufficiently significant reduction for the piezo to withstand the compressive forces generated during the cooling of the hosting part;
- To minimise the impact of shrinkage on the piezo, it was concluded that the most viable approach is to prevent the piezo from undergoing any bending curvature, requiring it to be fully encapsulated. Consequently, a method simulating a two-shot injection moulding process was employed, which allowed the piezo to be successfully over-moulded without cracking during cooling, using ABS as the polymer.

4.2. Limitations and Future Work

The use of a protective layer part, as demonstrated throughout this study, allowed the concept of two-shot injection moulding to be validated, ensuring that the piezo could be successfully over-moulded without cracking from shrinkage. However, machines capable of performing two-shot injection moulding are uncommon in industrial production units and require the existence of two separate moulds, which imposes limitations on part production and increases costs. Consequently, future work should explore the application of a resin coating on the piezo, which provides additional resistance to bending, and therefore being capable of preventing the piezo from cracking due to the shrinkage forces in the cooling process outside the mould. This resin could be applied during a pre-processing stage, by immersing the piezo with its electrical components in a resin bath and curing it prior to injection, allowing for some extra protection to the electrical components.

In combination with this approach and the work developed in the present study, future research could also focus on the development of a robotic system capable of autonomously placing the piezo and its electrical components into the mould, thereby contributing to production efficiency.

References

[1] Christos, K., et al., 'Chronic Noise Exposure with Normal Hearing is Related to Adverse Quality of Life and Burnout', ESJ, vol 21, no. 37, pp 1, 2025. doi: 10.19044/esj.2025.v21n37p1

[2] Elkins, C.L. and J.L. Banks, 'Shaping a 21st century federal noise control program', J. Expo. Sci. Environ. Epidimiol, vol 35, no. 1, pp 3-5, 2025, doi: 10.1038/s41370-024-00657-y

[3] Su, R., et al., '3D-Printed Micro/Nano-Scaled Mechanical Metamaterials: Fundamentals, Technologies, Progress, Applications, and Challenges', Small, vol 19, no 29, 2206391, 2023, doi: 10.1002/smll.202206391

[4] V. Goodship, ARBURG practical guide to injection moulding, 2nd ed. Shrewsburyp: Smithers Rapra, 2017.

[5] H. Fu et al., 'Overview of Injection Molding Technology for Processing Polymers and Their Composites', ES Mater. Manuf., vol. 8, pp. 3–23, 2020, doi: 10.30919/esmm5f713.

[6] M.-L. Wang, R.-Y. Chang, and C.-H. (David) Hsu, Molding Simulation: Theory and Practice, vol. 11. München: Carl Hanser Verlag GmbH & Co. KG, 2018. doi: 10.3139/9781569906200.

[7] N. Y. Zhao, Z. Bin Xu, Y. Shan, H. P. Zhou, and X. Huang, 'The constant/variable kinematics adjustment of the crosshead and the mold's stability management in injection molding', Int. J. Adv. Manuf. Technol., vol. 133, no. 1–2, pp. 901–912, 2024, doi: 10.1007/s00170-023-11044-6.

[8] M. S. Huang, S. C. Nian, J. Y. Chen, and C. Y. Lin, 'Influence of clamping force on tie-bar elongation, mold separation, and part dimensions in injection molding', Precis. Eng., vol. 51, 2017, pp. 647–658, 2018, doi: 10.1016/j.precisioneng.2017.11.007.

[9] S. Koltzenburg, M. Maskos, and O. Nuyken, Polymer Chemistry. Berlin, Heidelberg: Springer Berlin Heidelberg, 2017. doi: 10.1007/978-3-662-49279-6.

[10] M. Kutz, Mechanical engineers' handbook, volume 1: Materials and engineering mechanics, 4a. New Jersey, 2015.

[11] Douglas M. Bryce, Plastic injection molding: material selection and product design fundamentals, Michigan: Society of Manufacturing Engineers, 1997.

[12] A. I. Isayev and D. L. Crouthamel, 'Residual Stress Development in the Injection Molding of Polymers', Polym. Plast. Technol. Eng., vol. 22, no. 2, pp. 177–232, 1984, doi: 10.1080/03602558408070038.

[13] W. Zhang and J. Chen, Polymer processing and rheology, Elsevier, pp. 149-178. 2020. doi: 10.1016/B978-0-12-816806-6.00008-X.

[14] Y. Lin, L. Zheng, and G. Chen, ‘Unsteady flow and heat transfer of pseudo-plastic nanoliquid in a finite thin film on a stretching surface with variable thermal conductivity and viscous dissipation’, Powder Technol., vol. 274, pp. 324–332, 2015, doi: 10.1016/j.powtec.2015.01.039.

[15] O. Bird, R B and Armstrong, R C and Hassager, Dynamics of polymeric liquids. Vol. 1, 2nd Ed. : Fluid mechanics, 2a. United Stades, 1987. [Online]. Available: https://www.osti.gov/biblio/6164599

[16] B. R. Gupta, Rheology Applied in Polymer Processing, 1st Editon. London: CRC Press, 2022. doi: 10.1201/9781003344971.

[17] M. Majder-Łopatka et al., ‘Thermal Analysis of Plastics Used in the Food Industry’, Materials, vol. 15, no. 1, pp. 1-19, 2021, doi: 10.3390/ma15010248.

[18] K. Wilczyński, K. J. Wilczyński, and K. Buziak, ‘Modeling and Experimental Studies on Polymer Melting and Flow in Injection Molding’, Polymers, vol. 14, no. 10, pp. 1-19, 2022, doi: 10.3390/polym14102106.

[19] S. A. Cummer, J. Christensen, and A. Alù, ‘Controlling sound with acoustic metamaterials’, Nat. Rev. Mater., vol. 1, no. 3, pp. 1-13, 2016, doi: 10.1038/natrevmats.2016.1.

[20] N. G. Rocha de Melo Filho, ‘Vibro-acoustic resonant metamaterials: from concept to engineering solution’, Ph.D dissertation, KU LEUVEN, 2020.

[21] Leon Brillouin, Wave PropagationinPeriodic Structures. Paris: McGEAW-HILL BOOK COMPANY, INC., 1946.

[22] M. R. Haberman and M. D. Guild, ‘Acoustic metamaterials’, Phys. Today, vol. 69, no. 6, pp. 42–48, 2016, doi: 10.1063/PT.3.3198.

[23] G. W. Milton and J. R. Willis, ‘On modifications of Newton’s second law and linear continuum elastodynamics’, Proc. R. Soc. A Math. Phys. Eng. Sci., vol. 463, pp. 855–880, 2007, doi: 10.1098/rspa.2006.1795.

[24] X.-L. G. Shaofan Li, Handbook of Micromechanics and Nanomechanics. Singapore: Jenny Stanford Publishing, 2013.

[25] M. I. Hussein, M. J. Leamy, and M. Ruzzene, ‘Dynamics of phononic materials and structures: Historical origins, recent progress, and future outlook’, Appl. Mech. Rev., vol. 66, no. 4, pp. 1–38, 2014, doi: 10.1115/1.4026911.

[26] L. D’Alessandro, V. Zega, R. Ardito, and A. Corigliano, ‘3D auxetic single material periodic structure with ultra-wide tunable bandgap’, Sci. Rep., vol. 8, no. 1, pp. 1–9, 2018, doi: 10.1038/s41598-018-19963-1.

[27] C. Goffaux et al., ‘Evidence of Fano-like interference phenomena in locally resonant materials’, Phys. Rev. Lett., vol. 88, no. 22, pp. 1-4, 2002, doi: 10.1103/PhysRevLett.88.225502.

[28] J. Liu, H. Guo, and T. Wang, ‘A Review of Acoustic Metamaterials and Phononic Crystals’, Crystals, vol. 10, no. 4, pp. 1-26, 2020, doi: 10.3390/cryst10040305.

[29] N. Fang et al., ‘Ultrasonic metamaterials with negative modulus’, Nat. Mater., vol. 5, no. 6, pp. 452–456, 2006, doi: 10.1038/nmat1644.

[30] D.-L. Yu, H.-J. Shen, J.-W. Liu, J.-F. Yin, Z.-F. Zhang, and J.-H. Wen, ‘Propagation of acoustic waves in a fluid-filled pipe with periodic elastic Helmholtz resonators’, Chinese Phys. B, vol. 27, no. 6, pp. 1-7, 2018, doi: 10.1088/1674-1056/27/6/064301.

[31] Z. Liu et al., ‘Locally Resonant Sonic Materials’, Science (80-.)., vol. 289, pp. 1734–1736, 2000, doi: 10.1126/science.289.5485.1734.

[32] G. Ma and P. Sheng, ‘Acoustic metamaterials: From local resonances to broad horizons’, Sci. Adv., vol. 2, no. 2, pp. 1-16, 2016, doi: 10.1126/sciadv.1501595.

[33] Z. Yang, J. Mei, M. Yang, N. H. Chan, and P. Sheng, ‘Membrane-Type Acoustic Metamaterial with Negative Dynamic Mass’, Phys. Rev. Lett., vol. 101, no. 20, pp. 1-4, 2008, doi: 10.1103/PhysRevLett.101.204301.

[34] J. Zhao et al., ‘A review of piezoelectric metamaterials for underwater equipment’, Front. Phys., vol. 10, pp. 1–10, 2022, doi: 10.3389/fphy.2022.1068838.

[35] B. S. Beck, K. A. Cunefare, and M. Collet, ‘The power output and efficiency of a negative capacitance shunt for vibration control of a flexural system’, Smart Mater. Struct., vol. 22, no. 6, pp. 1-10, 2013, doi: 10.1088/0964-1726/22/6/065009.

[36] J. Xu, H. Lu, W. Qin, P. Wang, and J. Bian, ‘Mechanical Shunt Resonators-Based Piezoelectric Metamaterial for Elastic Wave Attenuation’, Materials (Basel)., vol. 15, no. 3, pp. 1-14, 2022, doi: 10.3390/ma15030891.

[37] S. Dalela, P. S. Balaji, and D. P. Jena, ‘A review on application of mechanical metamaterials for vibration control’, Mech. Adv. Mater. Struct., vol. 29, no. 22, pp. 3237–3262, 2022, doi: 10.1080/15376494.2021.1892244.

[38] M. A. Nouh, O. J. Aldraihem, and A. Baz, ‘Periodic metamaterial plates with smart tunable local resonators’, J. Intell. Mater. Syst. Struct., vol. 27, no. 13, pp. 1829–1845, 2016, doi: 10.1177/1045389X15615965.

[39] G. Hu, J. Xu, L. Tang, C. Lan, and R. Das, ‘Tunable metamaterial beam using negative capacitor for local resonators coupling’, J. Intell. Mater. Syst. Struct., vol. 31, no. 3, pp. 389–407, 2020, doi: 10.1177/1045389X19891575.

[40] T. M. P. Silva, M. A. Clementino, V. C. De Sousa, and C. D. M. Junior, ‘An Experimental Study of a Piezoelectric Metastructure with Adaptive Resonant Shunt Circuits’, IEEE/ASME Trans. Mechatronics, vol. 25, no. 2, pp. 1076–1083, 2020, doi: 10.1109/TMECH.2020.2966463.

[41] L. P. R. de Oliveira, G. K. Rodrigues, ‘A multi-mode smart metamaterial for NVH control’, Proceedings of The 2024 Leuven Conference on Noise and Vibration Engineering, Leuven, 2024.

[42] K. RADULOVIĆ, Z. JAKŠIĆ, M. OBRADOV, and D. RADOVIĆ, 'ANALYSIS OF ACOUSTIC CLOAKS FOR ANTI-SONAR CAMOUFLAGE BASED ON LOCAL RESONANCE IN ACOUSTIC METAMATERIALS', Conf. Int. Sci. Technol. O N Defensive, pp. 1-5, 2014.

[43] Zou S., 'Analysis of the acoustic concealing from the underwater polymer matrix piezoelectric composites', Beijing, China Huazhong Univ. Sci. Technol., 2009.

[44] Y. Liao et al., 'Research on Low-Frequency Noise Control of Automobiles Based on Acoustic Metamaterial', Materials, vol. 15, no. 9, pp. 1-18, 2022, doi: 10.3390/ma15093261.

[45] A. Arjunan, A. Baroutaji, J. Robinson, A. Vance, and A. Arafat, 'Acoustic metamaterials for sound absorption and insulation in buildings', Build. Environ., vol. 251, pp. 1-20, 2024, doi: 10.1016/j.buildenv.2024.111250.

[46] S. Varanasi, J. S. Bolton, T. H. Siegmund, and R. J. Cipra, 'The low frequency performance of metamaterial barriers based on cellular structures', Appl. Acoust., vol. 74, no. 4, pp. 485–495, 2013, doi: 10.1016/j.apacoust.2012.09.008.

[47] Q. Lin, Q. Lin, Y. Wang, and G. Di, 'Sound insulation performance of sandwich structure compounded with a resonant acoustic metamaterial', Compos. Struct., vol. 273, pp. 1-16, 2021, doi: 10.1016/j.compstruct.2021.114312.

[48] F. Langfeldt and W. Gleine, 'Design of acoustic partitions with thin plate-like acoustic metamaterials', Proc. Int. Congr. Acoust., pp. 4870–4877, 2019, doi: 10.18154/RWTH-CONV-239261.

[49] S. Kim and S. Lee, 'Air transparent soundproof window', AIP Adv., vol. 4, no. 11, pp. 1-8, 2014, doi: 10.1063/1.4902155.

[50] K. Steijvers, C. Claeys, L. Van Belle, and E. Deckers, 'On the potential of injection moulding for the production of locally resonant metamaterials', in Proceedings of the 26th International Congress of Mechanical Engineering, ABCM, 2021, pp. 1-9. doi: 10.26678/ABCM.COBEM2021.COB2021-2334.

[51] K. Steijvers, C. Claeys, L. Van Belle, and E. Deckers, 'Incorporating Manufacturing Process Simulations to Enhance Performance Predictions of Injection Moulded Metamaterials', J. Vib. Eng. Technol., vol. 11, no. 6, pp. 2617–2629, 2023, doi: 10.1007/s42417-023-01159-1.

[52] K. Steijvers, N. Spelmans, E. Deckers, C. Claeys, and L. Van Belle, 'Mass-Manufacturable Compact Low-Frequency Locally Resonant Metamaterials Via Insert Injection Moulding', in Proceedings of the 29th International Congress on Sound and Vibration, Diepenbeek, 2023, pp. 1-8.

[53] R. Dangel, Injection Moulds for Beginners. München: Carl Hanser Verlag GmbH & Co. KG, 2016. doi: 10.3139/9781569906323.

[54] T. Vieten, D. Stahl, P. Schilling, F. Civelek, and A. Zimmermann, ‘Feasibility Study of Soft Tooling Inserts for Injection Molding with Integrated Automated Slides’, Micromachines, vol. 12, no. 7, pp. 1-13, 2021, doi: 10.3390/mi12070730.

[55] W.-R. Jong, T.-C. Li, Y.-W. Chen, and Y.-H. Ting, ‘Automatic Recognition and Construction of Draft Angle for Injection Mold Design’, J. Softw. Eng. Appl., vol. 10, no. 01, pp. 78–93, 2017, doi: 10.4236/jsea.2017.101005.

[56] F. Maciariello, G. Lucchetta, and M. Sorgato, ‘Analysis of the effect of draft angle and surface roughness on ejection forces in micro injection molding’, Mater. Res. Proc., vol. 41, pp. 2686–2694, 2024, doi: 10.21741/9781644903131-294.

[57] D. O. Kazmer, ‘Injection Mold Design Engineering’, in Injection Mold Design Engineering, München: Carl Hanser Verlag GmbH & Co. KG, 2007, pp. 38–77. doi: 10.3139/9783446434196.

[58] M. Studer and F. Ehrig, ‘Minimizing Part Warpage in Injection Molding by Optimizing Wall Thickness Distribution’, Adv. Polym. Technol., vol. 33, no. S1, pp. 1-15, 2014, doi: 10.1002/adv.21454.

[59] P. S. Minh and M. T. Le, ‘Improving the melt flow length of acrylonitrile butadiene styrene in thin-wall injection molding by external induction heating with the assistance of a rotation device’, Polymers, vol. 13, no. 14, pp. 1-18, 2021, doi: 10.3390/polym13142288.

[60] S. A. Dawale, ‘Modified Sprue Design for Reduction of Waste Material in Two Cavity Injection Mould’, Int. J. Adv. Res. Sci. Technol., vol. 5, no. 5, pp. 1-6, 2020.

[61] C.-C. Lin, T.-C. Wu, Y.-S. Chen, and B.-Y. Yang, ‘A Semi-Analytical Method for Designing a Runner System of a Multi-Cavity Mold for Injection Molding’, Polymers, vol. 14, no. 24, pp. 1-17, 2022, doi: 10.3390/polym14245442.

[62] P. D. Kale, P. D. Darade, and A. R. Sahu, ‘A literature review on injection moulding process based on runner system and process variables’, IOP Conf. Ser. Mater. Sci. Eng., vol. 1017, no. 1, pp. 1-8, 2021, doi: 10.1088/1757-899X/1017/1/012031.

[63] S. C. Goud and G. R. Prasad, ‘INTEGRAL ANALYSIS OF INJECTION MOULD WITH HOT RUNNERS FOR GATE’, Int. J. Eng. Sci. Res. Technol., vol. 6, no. 5, pp. 272–277, 2017, doi: 0.5281/zenodo.574455.

[64] M. Huszar, F. Belblidia, H. M. Davies, C. Arnold, D. Bould, and J. Sienz, ‘Sustainable injection moulding: The impact of materials selection and gate location on part warpage and injection pressure’, Sustain. Mater. Technol., vol. 5, pp. 8, 2015, doi: 10.1016/j.susmat.2015.07.001.

[65] M. Bakr, P. Bauwens, F. Bossuyt, J. Vanfleteren, I. Chtioui, and W. Christiaens, ‘Solar cells integration in over-molded printed electronics’, Proc. - 2020 IEEE 8th Electron. Syst. Technol. Conf. ESTC 2020, pp. 1-5, 2020, doi: 10.1109/ESTC48849.2020.9229822.

[66] C. Goument et al., ‘In-Mold Electronics on Poly(Lactic Acid): towards a more sustainable mass production of plastronic devices’, Int. J. Adv. Manuf. Technol., vol. 125, no. 5–6, pp. 2643–2660, 2023, doi: 10.1007/s00170-023-10878-4.

[67] M. Bakr, M. Hubmann, F. Bossuyt, and J. Vanfleteren, ‘A Study on Over-Molded Copper-Based Flexible Electronic Circuits’, Micromachines, vol. 13, no. 10, pp. 1-27, 2022, doi: 10.3390/mi13101751.

[68] M. Bakr, Y. Su, F. Bossuyt, and J. Vanfleteren, ‘Effect of overmolding process on the integrity of electronic circuits’, in 2019 22nd European Microelectronics and Packaging Conference & Exhibition (EMPC), IEEE, 2019, pp. 1-8. doi: 10.23919/EMPC44848.2019.8951797.

[69] J. Schirmer, M. Reichenberger, A. Wimmer, H. Reichel, S. Neermann, and J. Franke, ‘Evaluation of Mechanical Stress on Electronic Assemblies During Thermoforming and Injection Molding for Conformable Electronics’, in 2021 14th International Congress Molded Interconnect Devices (MID), IEEE, pp. 1-8, 2021, doi: 10.1109/MID50463.2021.9361624.

[70] C. Ott and D. Drummer, ‘Low-stress over-molding of media-tight electronics using thermoplastic foam injection molding’, Polym. Eng. Sci., vol. 61, no. 5, pp. 1518–1528, May 2021, doi: 10.1002/pen.25672.

[71] Kotadia, H.R.; Howes, P.D.; Mannan, S.H., ‘A Review: On the Development of Low Melting Temperature Pb-Free Solders’, Microelectron. Reliability., vol 54, no. 6-7, pp. 1253-1273, 2014, doi: 10.1016/j.microrel.2014.02.025.

[72] Zeng G, McDonald S, Nogita K, ‘Development of high-temperature solders: Review’, Microelectron. Reliability., vol 52, no.7, pp 1306-1322, 2012, doi: 10.1016/j.microrel.2012.02.018.

[73] Kumar N, Maurya A, ‘Development of lead free solder for electronic components based on thermal analysis’, Mater.Today Proc., vol 62, pp. 2163-2167, 2022, doi: 10.1016/j.matpr.2022.03.358.

[74] de Melo Filho NGR, Claeys C, Deckers E, Desmet W, ‘Realisation of a thermoformed vibro-acoustic metamaterial for increased STL in acoustic resonance driven environments’, Appl. Acousts., vol 156, pp. 78-82, 2019, doi: 10.1016/j.apacoust.2019.07.007.

[75] Bikkembergs, J., De Vloo, M., Janssen, S., Steijvers, K., Deckers, E.., ‘Ontwerp en massaproductie van modulaire paneelstructuren voor effectieve trillingsreductie door middel van spuitgieten’, Master thesis, Faculteit Industriële Ingenieurswetenschappen KU Leuven & UHasselt, 2024.

[76] Guo X-L, Sun B-H, ‘Assembly and disassembly mechanics of a spherical snap fit’, Theor. Appl. Mech. Lett., vol 13, no. 1, pp. 100403, 2023, doi: 10.1016/j.taml.2022.100403.

[77] Feng S, Kamat AM, Pei Y, 'Design and fabrication of conformal cooling channels in molds: Review and progress updates', Int. J. Heat Mass Transf., vol. 171, 2021, doi: 10.1016/j.ijheatmasstransfer.2021.121082.

[78] Ashby, M.F. and D. Cebon, 'Materials selection in mechanical design', Le Journal de Physique IV, vol. 3, no, C7, pp. C7-1-C7-9, 1993

[79] MatWeb. (2025). MatWeb Material Property Database. Retrieved August 13, 2025, from https://www.matweb.com

[80] BusinessAnalytiq. Trend indexes. 2025 Accessed 2025 11/09/2025]; Available from: https://businessanalytiq.com/index/.

[81] Trindade MA, Benjeddou A, 'Effective Electromechanical Coupling Coefficients of Piezoelectric Adaptive Structures: Critical Evaluation and Optimization', Mech. Adv. Mater. Struct., vol. 16, no. 3, pp. 210-223, 2009, doi: 10.1080/15376490902746863.

[82] Lustig S, Elata D., 'Ambiguous definitions of the piezoelectric coupling factor', J. Intell. Mat. Syst. Struct., vol. 31, no. 14, pp. 1689-1696, 2020, doi: 10.1177/1045389x20930104.

[83] Cadet G, Paredes M., 'Convergence analysis and mesh optimization of finite element analysis related to helical springs'. Mechanics & Industry, vol. 25, pp. 22, 2024, doi: 10.1051/meca/2024018.

[84] Janssen S, Schimidt CS, Oliveira LPR de, De Marqui Júnior C, Claeys C, Deckers E., 'On the stop band adaptivity range of locally resonant metamaterial resonators with piezoelectric patches: a case study', Proceedings, Leuven, Belgium, 2024

[85] S. Janssen, G. K. Rodrigues, L. P. R. De Oliveira, C. De Marqui Jr, C. Claeys, E. Deckers, 'Eigenfrequency adaptivity of locally resonant metamaterial resonators using piezoelectric elements with negative capacitance shunts', in ECCOMAS Thematic Conference on Smart Structures and Materials, Linz, Austria, 1-3 July 2025.

[86] Mohan, M., M.N.M. Ansari, and R.A. Shanks, 'Review on the Effects of Process Parameters on Strength, Shrinkage, and Warpage of Injection Molding Plastic Component', Polymer-Plastics Technology and Engineering, vol. 56, no. 1, pp. 1-12, 2017, doi: 2, 2017, doi: 10.1080/03602559.2015.1132466.

[87] Chen, S.-C., et al., 'Prediction of Part Shrinkage for Injection Molded Crystalline Polymer via Cavity Pressure and Melt Temperature Monitoring', Applied Sciences, vol. 13, no. 17, pp. 98-84, 2023, doi: 10.3390/app13179884.

[88] Bagalkot, A., et al., The Effects of Cooling and Shrinkage on the Life of Polymer 3D Printed Injection Moulds. Polymers,vol. 14, no. 3, pp. 520, 2022, doi: 10.3390/polym14030520

[89] Osswald, T. A., E. Baur, S. Brinkmann, K. Oberbach, and E. Schmachtenberg, "International Plastics Handbook," Int. Plast. Handb., Jun. 2006, doi: 10.3139/9783446407923.

[90] WeMould. Two-Shot Molding Process. Accessed in 11/09/2025; Available from: https://wemould.com/two-shot-molding-process/.

Declaration of Integrity

I declare that I conducted this academic work with integrity. I did not plagiarize or apply any form of misuse of information or falsification of results throughout the process that led to its preparation. I declare that the work presented in this document is original and my own and has not previously been used for any other purpose. I further declare that I am fully aware of the Code of Ethical Conduct of P.PORTO, ISEP.

NAME: David José Pereira Almeida

Porto, september 11, 2025

Annex A

INEOS STYROLUTION

NOVODUR P2H-AT

Acrylonitrile Butadiene Styrene (ABS)

TECHNICAL DATASHEET

DESCRIPTION

Novodur® P2H-AT is a general purpose injection molding grade providing high flowability and contains an antistatic additive. It is designed for best aesthetics: stable high gloss and smooth finish.

FEATURES

- Balanced properties
- Easy processing
- Good paintability
- High gloss

APPLICATIONS

- Housings for electrical & electronic devices
- Electrical and electronic components, switches, house automation
- Coffee machines
- Vacuum cleaner housings
- Cosmetic packaging

Property, Test Condition	Standard	Unit	Values
Rheological Properties			
Melt Volume Rate 220 °C/10 kg	ISO 1133	cm³/10 min	37
Mechanical Properties			
Charpy Notched Impact Strength, 23° C	ISO 179/1eA	kJ/m²	18
Charpy Notched Impact Strength, -30 °C	ISO 179/1eA	kJ/m²	8
Charpy Unnotched, 23 °C	ISO 179/1eU	kJ/m²	100
Charpy Unnotched, -30 °C	ISO 179/1eU	kJ/m²	80
Izod Notched Impact Strength, 23 °C	ISO 180/A	kJ/m²	18
Izod Notched Impact Strength, -30 °C	ISO 180/A	kJ/m²	9
Tensile Modulus	ISO 527	MPa	2500
Tensile Stress at Yield, 23 °C	ISO 527	MPa	44
Tensile Strain at Yield, 23 °C	ISO 527	%	2.1
Tensile Stress at Break, 23 °C	ISO 527	MPa	32
Nominal Strain at Break, 23 °C	ISO 527	%	> 18
Flexural Modulus, 23 °C	ISO 178	MPa	2400
Flexural Strength, 23 °C	ISO 178	MPa	70
Hardness, Shore D	ISO 868	-	110

Contact us:
INSTY.infopoint.emea@ineos.com
www.ineos-styrolution.com

Revision Date: 02/19/19

NOVODUR P2H-AT

Acrylonitrile Butadiene Styrene (ABS)

TECHNICAL DATASHEET

Property, Test Condition	Standard	Unit	Values
Thermal Properties			
Vicat Softening Temperature, VST/B/120 (50N, 120 °C/h)	ISO 306	°C	100
Vicat Softening Temperature VST/B/50 (50N, 50 °C/h)	ISO 306	°C	98
Heat Deflection Temperature A; (annealed 4 h/80 °C; 1.8 MPa)	ISO 75	°C	93
Heat Deflection Temperature B; (annealed 4 h/80 °C; 0.45 MPa)	ISO 75	°C	97
Coefficient of Linear Thermal Expansion	ISO 11359	10^{-6}/°C	90
Electrical Properties			
Dielectric Strength, Short Time, 1.0 mm	IEC 60243-1	kV/mm	34
Dielectric Strength, Short Time, 1.5 mm	IEC 60243-1	kV/mm	34
Comparative Tracking Index	IEC 60112	V	600
Other Properties			
Density	ISO 1183	kg/m³	1050
UL94 rating at 1.5 mm thickness	IEC 60695-11-10	-	HB
Glow wire test (GWFI), 2.0 mm	IEC 60695-2-12	°C	700
Processing			
Melt Temperature Range	ISO 294	°C	230 - 260
Mold Temperature Range	ISO 294	°C	60 - 80
Linear Mold Shrinkage	ISO 294-4	%	0.4 - 0.7
Drying Temperature	-	°C	80
Drying Time	-	h	2 - 4

Typical values for uncolored products
Please note that all processing data stated are only indicative and may vary depending on the individual processing complexities.
Please consult our local sales or technical representatives for details.

SUPPLY FORM

Novodur® is delivered in the form of cylindrical or spherical pellets. The bulk density of the pellets is from 0.55 to 0.65 g/cm³. Values may differ for special grades. Standard Packaging unit: 25 kg PE-bag on palette, shrunk or wrapped with PE film. In addition, delivery in larger units of up to 1000 kg (IBC = Intermediate Bulk Container) or silo trucks can be arranged. In dry areas with normal temperature control, Novodur pellets can be stored for relatively long periods of time without any change in mechanical properties. With unstable colors, however,

Contact us:
INSTY.infopoint.emea@ineos.com
www.ineos-styrolution.com

storage over a number of years can give rise to some change in color. Under poor storage conditions, Novodur absorbs moisture, but this can be removed by drying.

PRODUCT SAFETY

No adverse effects on the health of processing personnel have been observed where the products are correctly processed and the production areas are suitably ventilated. For styrene, alpha-methylstyrene, acrylonitrile, and butyl acrylate the maximum allowable workplace concentrations must be observed according to the pertaining national regulations. In Germany, the following limit values are valid TRGS 900 (Aug. 2004): styrene, MAK-value: 20 ml/m³; alpha-methylstyrene, MAK-value: 100 ml/m³; acrylonitrile, TRK-value: 3 ml/m³, and butyl acrylate, MAK-value: 2 ml/m³ (1.7.2004). According to EU directive 67/548/EEC, Annex I (2001), acrylonitrile is classified as carcinogenic, category 2 (´substances which should be regarded as if they are carcinogenic to man´). Experience has shown that when Novodur® is processed correctly with appropriate ventilation, the levels are far below the limits mentioned above. Inhalation of the vapors of degradation products which can arise on severe overheating of the materials or during purging out should be avoided. Further information can be found in the Novodur safety data sheets.

DISCLAIMER

The above mentioned data are accurate to the best of our knowledge. They are based upon reputable labs and industry standard testing methods. These are only typical values and actual product specification may deviate at industrial range. Therefore, no data in this technical data sheet shall constitute a warranty or representation regarding product features, fitness of the product for a specific purpose or application or its processability. INEOS Styrolution disclaims all liability in connection therewith. The customer himself is required to verify whether or not the product is suitable for the further processing or application intended and whether or not the product complies with the relevant statutory requirements. Unless explicitly and individually otherwise agreed in writing, INEOS Styrolution's sole and exclusive liability with respect to its products is set forth in INEOS Styrolution's General Terms and Conditions for Sale.

Contact us:
INSTY.infopoint.emea@ineos.com
www.ineos-styrolution.com

Annex B

Product Information **Ultradur®**

B 4040 G10

09/2016 **(PBT+PET)-GF50**

BASF We create chemistry

Product description

Injection molding grade with 50 % glass fibers for industrial parts with excellent surface quality, for example external door handles in vehicles, visible sunroof frames, oven door handles, toaster casings, external mirrors, rear screen wiper arms in vehicles and sunroof wind deflectors. Formerly called KR 4040 G10.

Abbreviated designation according to ISO 1043-1: PBT-PET-GF30

Product safety

Ultradur® melts are stable at temperatures up to 280°C and do not give rise to hazards due to molecular degradation or the evolution of gases and vapors. Like all thermoplastic polymers, however, Ultradur decomposes on exposure to excessive thermal stresses, e.g. when it is overheated or as a result of cleaning by burning off. At temperatures of > 290 °C can be emitted: carbon monoxide, tetrahydrofuran.
Under special fire conditions traces of other toxic substances are possible. Formation of further decomposition and oxidation products depends upon the fire conditions.
When Ultradur® is properly processed and there is adequate suction at the die no risks to health are to be expected.
Further safety information see safety data sheet of individual product.
Safety data sheet could be ask for at the Ultra-Infopoint under tel: 0621/60-78780 or fax:0621/60-78730.

Physical form and storage

Standard packaging includes the 25-kg-bag and the 1000 kg octabin (octagonal container). Other forms of packaging are possible subject to agreement. All containers are tightly sealed and should be opened only immediately prior to processing. Further precautions for preliminary treatment and drying are described in the processing section of the brochure. The bulk density is about 0,7 to 0,8g/cm³.
Ultradur® can be stored for a longer period of time in dry, well vented rooms without causing problems in processing.
Ultradur® should generally have a moisture content of less than 0,04% when being processed.
In order to ensure reliable production, therefore, pre-drying should generally be the rule and the machine should be loaded via a closed conveyor system. Appropriate equipment is commercially available. Pre-drying is also for the addition of batches, e.g. in the case of inhouse pigmentation.
In order to prevent the formation of condensed water, containers stored in unheated rooms must only be opened when they have attained the temperature prevailing in the processing area. This can possibly take a very long time.
Measurements have shown that the interior of a 25-kg bag originally at 5°C had reached the temperature of 20°C in the processing area only after 48 hours.

Note

The data contained in this publication are based on our current knowledge and experience. In view of the many factors that may affect processing and application of our product, these data do not relieve processors from carrying out their own investigations and tests; neither do these data imply any guarantee of certain properties, nor the suitability of the product for a specific purpose. Any descriptions, drawings, photographs, data, proportions, weights etc. given herein may change without prior information and do not constitute the agreed contractual quality of the product. It is the responsibility of the recipient of our products to ensure that any proprietary rights and existing laws and legislation are observed.
In order to check the availability of products please contact us or our sales agency.

BASF SE
67056 Ludwigshafen, Germany

Ultradur® B 4040 G10

We create chemistry

Product Information

Typical values for uncoloured product at 23 °C[1)]	Test method	Unit	Values[2)]
Properties			
Polymer abbreviation	-	-	**(PBT+PET)-GF50**
Density	ISO 1183	kg/m³	**1730**
Filler content: Glass fiber (GF), glass balls (GB), Mineral (M)	-	%	**GF50**
Viscosity number (solution 0,005 g/ml Phenole/1,2 Dichlorbenzol 1:1)	ISO 307, 1157, 1628	cm³/g	**90**
coloured	-	-	**+**
black	-	-	**+**
Water absorption, equilibrium in water at 23°C	similar to ISO 62	%	**0.4**
Moisture absorption, equilibrium 23°C/50% r.h.	similar to ISO 62	%	**0.20**
Processing			
Melt volume-flow rate MVR at 275 °C and 2.16 kg	ISO 1133	cm³/10min	**8.5**
Melting temperature, DSC	ISO 11357-1/-3	°C	**223**
Melt temperature, Injection moulding/Extrusion	-	°C	**250 - 280**
Mould temperature, Injection moulding	-	°C	**60 - 100**
Moulding shrinkage, free, longitudinal (plate with film gate 150*150*3 mm³)	-	%	**0.1**
Moulding shrinkage, free, transverse (plate with film gate 150*150*3 mm³)	-	%	**0.75**
Molding shrinkage (parallel)	ISO 294-4	%	**0.24**
Molding shrinkage (normal)	ISO 294-4	%	**0.77**
Flammability			
Burning Behav. at 1.6 mm nom. thickn.	IEC 60695-11-10	class	**HB**
Burning Behav. at thickness d = 0.75 mm	IEC 60695-11-10	class	**HB**
Automotive materials (thickness d>= 1mm) [3)]	FMVSS 302	-	**+**
Mechanical properties			
Tensile modulus	ISO 527-1/-2	MPa	**18000**
Stress at break	ISO 527-1/-2	MPa	**170**
Strain at break	ISO 527-1/-2	%	**1.6**
Charpy unnotched impact strength (23°C)	ISO 179/1eU	kJ/m²	**60**
Charpy unnotched impact strength (-30°C)	ISO 179/1eU	kJ/m²	**70**
Charpy notched impact strength (23°C)	ISO 179/1eA	kJ/m²	**10**
Flexural strength	ISO 178	MPa	**270**
Flexural modulus	ISO 178	MPa	**17700**
Thermal properties			
HDT A (1.80 MPa)	ISO 75-1/-2	°C	**205**
HDT B (0.45 MPa)	ISO 75-1/-2	°C	**221**
Max. service temperature (short cycle operation)	-	°C	**210**
Temperature index at 50% loss of tensile strength after 20000 h	IEC 60216	°C	**140**
Temperature index at 50% loss of tensile strength after 5000 h	IEC 60216	°C	**160**
Coefficient of linear thermal expansion, longitudinal (23-80)°C	ISO 11359-1/-2	E-6/K	**10 - 20**
Specific heat capacity	-	J/(kg*K)	**950**
Electrical properties			
Relative permittivity (100Hz)	IEC 60250	-	**4.7**
Relative permittivity (1 MHz)	IEC 60250	-	**4.5**
Dissipation factor (100 Hz)	IEC 60250	E-4	**20**
Dissipation factor (1 MHz)	IEC 60250	E-4	**150**
Volume resistivity	IEC 60093	Ohm*m	**1E14**
Surface resistivity	IEC 60093	Ohm	**1E13**
Comparative tracking index, CTI, test liquid A	IEC 60112	-	**225**

Footnotes
1) If product name or properties don't state otherwise.
2) The asterisk symbol '*' signifies inapplicable properties.
3) + = passed

BASF SE

67056 Ludwigshafen, Germany

Annex C

Ticona
Engineering Polymers

VECTRA® A115 | LCP | Glass Reinforced

Description

Provides easier flow than A130. Slightly tougher, but may warp slightly more than A130 in some parts. 15% glass reinforced.

Chemical abbreviation according to ISO 1043-1 : LCP
Inherently flame retardant
FDA compliant
UL-Listing V-0 in natural and black at 0.44mm thickness per UL 94 flame testing.
Relative-Temperature-Index (RTI) according to UL 746B: electricals 240°C, mechanicals 220°C at 0.85mm.

UL = Underwriters Laboratories (USA)

Physical properties	Value	Unit	Test Standard
Density	**1500**	kg/m³	ISO 1183
Mold shrinkage - parallel	**0.1**	%	ISO 294-4
Mold shrinkage - normal	**0.4**	%	ISO 294-4

Mechanical properties	Value	Unit	Test Standard
Tensile modulus (1mm/min)	**12000**	MPa	ISO 527-2/1A
Tensile stress at break (5mm/min)	**200**	MPa	ISO 527-2/1A
Tensile strain at break (5mm/min)	**3.1**	%	ISO 527-2/1A
Flexural modulus (23°C)	**12000**	MPa	ISO 178
Flexural strength (23°C)	**240**	MPa	ISO 178
Compressive stress @ 1% strain	**85**	MPa	ISO 604
Charpy impact strength @ 23°C	**48**	kJ/m²	ISO 179/1eU
Charpy notched impact strength @ 23°C	**42**	kJ/m²	ISO 179/1eA
Unnotched impact str (Izod) @ 23°C	**61**	kJ/m²	ISO 180/1U
Notched impact strength (Izod) @ 23°C	**45**	kJ/m²	ISO 180/1A
Compressive modulus	**10000**	MPa	ISO 604
Rockwell hardness	**80**	M-Scale	ISO 2039-2

Thermal properties	Value	Unit	Test Standard
Melting temperature (10°C/min)	**280**	°C	ISO 11357-1,-2,-3
DTUL @ 1.8 MPa	**230**	°C	ISO 75-1/-2
DTUL @ 0.45 MPa	**250**	°C	ISO 75-1/-2
DTUL @ 8.0 MPa	**157**	°C	ISO 75-1/-2
Vicat softening temperature B50 (50°C/h 50N)	**162**	°C	ISO 306
Coeff.of linear therm. expansion (parallel)	**0.1**	E-4/°C	ISO 11359-2
Coeff.of linear therm. expansion (normal)	**0.18**	E-4/°C	ISO 11359-2
Flammability at thickness h	**V-0**	class	UL94

Electrical properties	Value	Unit	Test Standard
Relative permittivity - 100 Hz	**3.5**	-	IEC 60250
Relative permittivity - 1 MHz	**3**	-	IEC 60250
Dissipation factor - 100 Hz	**200**	E-4	IEC 60250
Dissipation factor - 1 MHz	**180**	E-4	IEC 60250
Volume resistivity	**1E13**	Ohm*m	IEC 60093
Surface resistivity	**>1E15**	Ohm	IEC 60093
Electric strength	**34**	kV/mm	IEC 60243-1

VECTRA® A115 | LCP | Glass Reinforced

Electrical properties	Value	Unit	Test Standard
Comparative tracking index CTI	**200**	-	IEC 60112
Arc resistance	**135**	s	Internal

Test specimen production	Value	Unit	Test Standard
Injection molding melt temperature	**293**	°C	ISO 294
Injection molding mold temperature	**60**	°C	ISO 294
Injection molding flow front velocity	**150**	mm/s	ISO 294
Injection molding hold pressure	**48**	MPa	ISO 294

Stress-strain

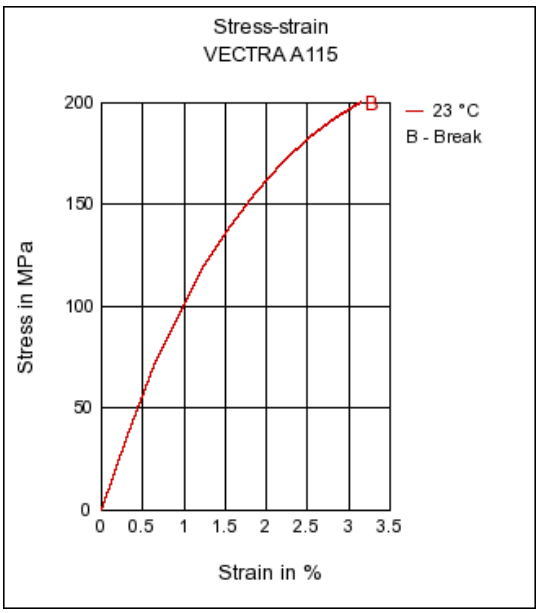

Secant modulus-strain

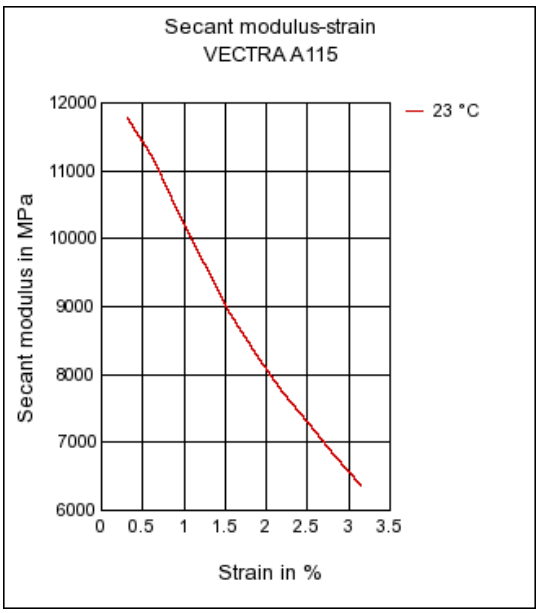

Typical injection moulding processing conditions

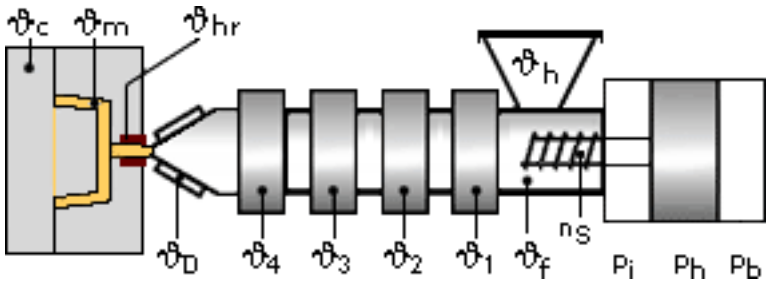

VECTRA® A115 | LCP | Glass Reinforced

Maximum residual moisture content: 0.0200%

Processing Temperatures:

	ϑ Cavity	ϑ Melt	ϑ Hot Runner	ϑ Die	ϑ 4	ϑ 3	ϑ 2	ϑ 1	ϑ Feeding	ϑ Hopper
min (°C)	80	285	285	290	285	280	275	270	60	20
max (°C)	120	295	295	300	295	290	285	280	80	30

Processing Pressures:

	Injection Pressure	Holding Pressure	Back Pressure
min (bar)	500	500	0
max (bar)	1500	1500	30

Injection speed: very fast

Screw speed:

Screw diameter (mm)	16	25	40
Screw speed (rpm)	200	140	80

Pre-drying conditions:

VECTRA should in principle be predried. Because of the necessary low maximum residual moisture content the use of dry air dryers is recommended. The dew point should be =< - 40° C. The time between drying and processing should be as short as possible.

For subsequent storage of the material in the dryer until processed the temperature does not need to be lowered for grades A, B, C, D and V (<= 24 h).

Drying time: 4 - 6 h

Drying temperature: 150 - 150 °C

Special information:

When using short metering strokes, an accumulator is recommended to achieve short injection times.

Injection Molding

A three-zone screw evenly divided into feed, compression, and metering zones is preferred. A higher percentage of feed flights may be needed for smaller machines: 1/2 feed, 1/4 compression, 1/4 metering.

```
Barrel temperature 270-295 C
Melt Temperature   285-295 C
Mold temperature    80-120 C
```

Vectra LCPs are shear thinning, their melt viscosity decreases quickly as shear rate increases. For parts that are difficult to fill, the molder can increase the injection velocity to improve melt flow.

Contact Information

Americas

Ticona
Product Information Service

Europe

Ticona GmbH
Information Service

VECTRA® A115 | LCP | Glass Reinforced

8040 Dixie Highway
Florence, KY 41042
USA
Tel.: +1-800-833-4882
Tel.: +1-859-372-3244
email: prodinfo@ticona.com
Ticona on the web: www.ticona.com

Customer Service
Tel.: +1-800-526-4960
Tel.: +1-859-372-3214
Fax: +1-859-372-3125

Tel.: +49 (0) 180-5842662 (Germany)*
+49 (0) 69-30516299 (Europe)
Fax: +49 (0) 180-2021202 (Germany & Europe)**
email: infoservice@ticona.de
Internet: www.ticona.com

*starting 01.01.2007 0,14€/minute + local landline rates
**0,06€/Call + local landline rates

General Disclaimer

NOTICE TO USERS: Values shown are based on testing of laboratory test specimens and represent data that fall within the standard range of properties for natural material. These values alone do not represent a sufficient basis for any part design and are not intended for use in establishing maximum, minimum, or ranges of values for specification purposes. Colorants or other additives may cause significant variations in data values.
Properties of molded parts can be influenced by a wide variety of factors including, but not limited to, material selection, additives, part design, processing conditions and environmental exposure. Any determination of the suitability of a particular material and part design for any use contemplated by the users and the manner of such use is the sole responsibility of the users, who must assure themselves that the material as subsequently processed meets the needs of their particular product or use.
To the best of our knowledge, the information contained in this publication is accurate; however, we do not assume any liability whatsoever for the accuracy and completeness of such information. The information contained in this publication should not be construed as a promise or guarantee of specific properties of our products. It is the sole responsibility of the users to investigate whether any existing patents are infringed by the use of the materials mentioned in this publication.
Moreover, there is a need to reduce human exposure to many materials to the lowest practical limits in view of possible adverse effects. To the extent that any hazards may have been mentioned in this publication, we neither suggest nor guarantee that such hazards are the only ones that exist. We recommend that persons intending to rely on any recommendation or to use any equipment, processing technique or material mentioned in this publication should satisfy themselves that they can meet all applicable safety and health standards.
We strongly recommend that users seek and adhere to the manufacturer's current instructions for handling each material they use, and entrust the handling of such material to adequately trained personnel only. Please call the telephone numbers listed (+49 (0) 69 30516299 for Europe and +1 859-372-3244 for the Americas) for additional technical information. Call Customer Services for the appropriate Materials Safety Data Sheets (MSDS) before attempting to process our products.
The products mentioned herein are not intended for use in medical or dental implants.

Annex D

Plexiglas® 8N

Polymethyl Methacrylate Acrylic

Evonik Industries AG

UL IDES | Prospector

ides.com/prospector

Technical Data

Product Description

Product Profile:
PLEXIGLAS® 8N is an amorphous thermoplastic molding compound (PMMA).

Typical properties of PLEXIGLAS® molding compounds are:
- good flow
- high mechanical strength, surface hardness and abrasion resistance
- high light transmission
- very good weather resistance
- free colorability due to crystal clarity

Special properties of PLEXIGLAS® 8N are:
- optimum mechanical properties
- maximum heat deflection temperature
- good flow / melt viscosity
- AMECA listing.

Application:
Used for injection molding optical and technical items.

Examples:
optical waveguides, luminaire covers, automotive lighting, instrument cluster covers, optical lenses, displays, etc.

Processing:
PLEXIGLAS® 8N can be processed on injection molding machines with 3-zone general purpose screws for engineering thermoplastics.

Physical Form / Packaging:
PLEXIGLAS® molding compounds are supplied as pellets of uniform size, packaged in 25kg polyethylene bags or in 500kg boxes with PE lining; other packaging on request.

General

Material Status	• Commercial: Active		
Literature [1]	• Technical Datasheet (English) • Processing - Injection (English)		
UL Yellow Card [2]	• E65495-100849262		
Search for UL Yellow Card	• Evonik Industries AG • Plexiglas®		
Availability	• Europe		
Features	• Amorphous • Good Abrasion Resistance • Good Colorability	• Good Flow • Good Weather Resistance • High Hardness	• High Strength
Uses	• Automotive Applications • Automotive Backlights	• Displays • Lenses	• Optical Applications • Protective Coverings
Forms	• Pellets		
Processing Method	• Injection Molding		
Multi-Point Data	• Creep Modulus vs. Time (ISO 11403-1) • Isochronous Stress vs. Strain (ISO 11403-1) • Isothermal Stress vs. Strain (ISO 11403-1)	• Secant Modulus vs. Strain (ISO 11403-1) • Shear Modulus vs. Temperature (ISO 11403-1) • Specific Volume vs Temperature (ISO 11403-2)	• Viscosity vs. Shear Rate (ISO 11403-2)

Physical	Nominal Value	Unit	Test Method
Density	1.19	g/cm³	ISO 1183
Melt Volume-Flow Rate (MVR) (230°C/3.8 kg)	3.00	cm³/10min	ISO 1133

Mechanical	Nominal Value	Unit	Test Method
Tensile Modulus	3300	MPa	ISO 527-2/1
Tensile Stress (Break)	77.0	MPa	ISO 527-2/5
Tensile Strain (Break)	5.5	%	ISO 527-2/5

Form No. TDS-33101-en

Document Created: Tuesday, May 07, 2013
Added to Prospector: August, 1998
Last Updated: 3/5/2013

Impact	Nominal Value	Unit	Test Method
Charpy Unnotched Impact Strength (23°C)	20	kJ/m²	ISO 179/1eU

Thermal	Nominal Value	Unit	Test Method
Heat Deflection Temperature			
0.45 MPa, Unannealed	103	°C	ISO 75-2/B
1.8 MPa, Unannealed	98.0	°C	ISO 75-2/A
Glass Transition Temperature	117	°C	IEC 1006
Vicat Softening Temperature	108	°C	ISO 306/B50
CLTE - Flow (0 to 50°C)	0.000080	cm/cm/°C	ISO 11359-2

Flammability	Nominal Value	Unit	Test Method
Flame Rating (1.60 mm)	HB		UL 94

Optical	Nominal Value	Unit	Test Method
Refractive Index	1.490		ISO 489
Transmittance [4]	92.0	%	ISO 13468-2
Haze	< 0.50	%	ASTM D1003

Additional Information	Nominal Value	Unit	Test Method
Fire Rating	B2		DIN 4102

Injection	Nominal Value	Unit
Drying Temperature	< 98.0	°C
Drying Time	2.0 to 3.0	hr
Processing (Melt) Temp	220 to 260	°C
Mold Temperature	60.0 to 90.0	°C

Notes

[1] These links provide you with access to supplier literature. We work hard to keep them up to date; however you may find the most current literature from the supplier.

[2] A UL Yellow Card contains UL-verified flammability and electrical characteristics. UL IDES continually works to link Yellow Cards to individual plastic materials in Prospector, however this list may not include all of the appropriate links. It is important that you verify the association between these Yellow Cards and the plastic material found in Prospector. For a complete listing of Yellow Cards, visit the UL Yellow Card Search.

[3] Typical properties: these are not to be construed as specifications.

[4] D65

Form No. TDS-33101-en
Document Created: Tuesday, May 07, 2013
Added to Prospector: August, 1998
Last Updated: 3/5/2013

Where to Buy

Supplier

Evonik Industries AG
Darmstadt, Germany
Telephone: 49-6151-18-3561
Web: http://www.plexiglas.de/

Distributor

Nexeo Solutions - Europe
Nexeo Solutions is a Pan European distribution company. Contact Nexeo for availability of individual products by country.
Telephone: +34-93-480-9125
Web: http://www.nexeosolutions.com/
Availability: Belgium, France, Ireland, Italy, Netherlands, Portugal, Spain, United Kingdom

Plastribution
Telephone: +44-845-345-4560
Web: http://www.plastribution.co.uk/
Availability: United Kingdom

Ultrapolymers
Ultrapolymers is a Pan European distribution company. Contact Ultrapolymers for availability of individual products by country.
Telephone: +32-11-57-95-57
Web: http://www.ultrapolymers.com/
Availability: Europe

Document Created: Tuesday, May 07, 2013
Added to Prospector: August, 1998
Last Updated: 3/5/2013

IDES

Founded in 1986 and based in Laramie, Wyoming, IDES is now part of the UL family of companies. UL is a premier global independent safety science company with more than a century of proven history. Employing nearly 10,000 professionals in over 100 countries, UL has five distinct business units -- Product Safety, Environment, Life & Health, Knowledge Services and Verification Services -- to meet the expanding needs of our customers and to deliver on our public safety mission.

Prospector Plastics Database - www.ides.com/prospector

Prospector is a searchable online database that includes 85,000 data sheets from 875 manufacturers and 44,000 UL yellow cards. Each data sheet includes property, processing and supplier contact information. Prospector is relied on by nearly 400,000 design engineers and plastics processors. Using Prospector, they save time with plastic material selection by quickly and easily referencing technical information critical to the success of their products.

"Prospector is absolutely the best and most well-known search engine for plastic raw materials in the world. We use Prospector every day – it's a real time saver!"
– Birgit Elvardt Bader, Production Manager, Micotron

Power Searches

- Property Search – select plastics by 500 key properties and design parameters.
- Alternative Resins Search – find replacement plastics within minutes.
- Automotive Plastics Search – easily locate automotive approved plastics.
- Curve Data – view, overlay and export curve data.

Material Data Management – www.ides.com/datasheets

With our data management services, plastic suppliers and distributors can have custom search interfaces available on their website for their customers, website visitors, sales and customer service teams. These provide intuitive ways to find and view technical data sheets for their products.

"With UL IDES data services, our website now displays the most current information on the products we distribute and links to our backend RFQ and sales order system, adding both value and service for our customers."
– Kevin Chase, Owner & President, Chase Plastics

Advertising – www.ides.com/advertise

Reach 365,000 pre-qualified plastics professionals and generate leads with proven techniques. Electronic newsletter insertions, sponsored webinars and powerful online ads are available to make the most of your lead-generation program.

For more information, call: 800.788.4668 or 307.742.9227 ext. 220